X-Ray Studies on Membrane Proteins

Submitted by

Yi-Lynn Liang

MSc Biotechnology

A thesis submitted in total fulfilment
of the requirements for the degree of
Doctor of Philosophy

School of Molecular Sciences
Faculty of Science, Technology and Engineering

La Trobe University
Bundoora, Victoria 3086
Australia

March 2012

Table of contents

List of Figures

List of Tables

Abbreviations

1D	one-dimensional
2D	two-dimensional
3D	three-dimensional
[^{35}S] GTPγS	guanosine 5'-*O*-(3-[^{35}S]thio)triphosphate
A2AR	A_{2A} adenosine receptor
B2AR	β_2-adrenergic receptor
B1AR	β_1-adrenergic receptor
Br	Bacteriorhodopsin
BRET	bioluminescence resonance energy transfer
A_{280}	Absorbance at 280 nm
cAMP	cyclic AMP
CMC	Critical micellar concentration
CXCR4	C-X-C chemokine receptor type 4
D3R	D_3 dopamine receptor
DAG	diacylglycerol
DDM	n-dodecyl-β-D-maltopyranoside
dNTP	deoxynucleoside triphosphate
DTAC	Dodecyltrimethylammonium chloride
ECL2	second extracellular cytoplasmic loop
EDTA	Ethylenediaminetetraacetic acid
FI	fluid isotropic
FRET	fluorescence resonance energy transfer
GαCT	peptide fragment from carboxyl terminus of G_T protein
GDP	guanosine diphosphate
GIRK	G protein-coupled regulated inwardly-rectifying potassium channels
GLP1	Glucagon-like peptide 1
GPCR	G Protein-Coupled Receptor
GR	Glucocorticoid receptor
GTP	guanosine triphosphate
H_{II}	Inverted hexagonal phase
H1R	H_1 histamine receptor
HA	hemagglutinin
HDAC	histone deacetylase
His-tag	Histidine tag
hr	hour
HRP	Horseradish peroxidase
ICL1	first intracellular cytoplasmic loop
ICL2	second intracellular cytoplasmic loop

ICL3	third intracellular cytoplasmic loop
IMAC	Immobilised metal affinity chromatography
IFN-γ	Interferon-γ
IP_3	inositol triphosphate
Lα	local lamellar liquid crystalline phase
LDAO	N-N-dimethyldodecylamine-N-oxide
LDS	Lithium dodecyl sulphate
LPR	lipid to protein ratio
M2R	M_2 musarinic receptor
Meta I	Metarhodopsin I
Meta II	Metarhodopsin II
M.O.I	Multiplicity of infection
MO	Monoolein
min	minute
MQH_2O	Milli-Q water
NF-κB	Nuclear factor *kappa*-light-chain-enhancer of activated *B* cells
Ni^{2+}-NTA	Ni^{2+}-nitrotriacetate
OD	Optical density
Ops	inactive opsin
Ops*	activated opsin
PCR	Polymerase chain reaction
PEG	Polyethylene glycol
pfu	plaque forming unit
PLL-g-PEG-NTA	Poly-(L-Lysine)-graft-Poly (ethylene glycol)-nitrolotriacetic acid group co-polymer
PPAR-γ	peroxisome proliferator-activated receptor-γ
PTX	Pertussis toxin
PYY	Peptide YY
Q_{II}^{D}	Diamond cubic phase
Q_{II}^{G}	Gyroid cubic phase
Q_{II}^{P}	Primitive cubic phase
QNB	3-quinuclidinyl-benzilate
RGS	Regulators of G protein signalling
SAXS	Small angle X-ray scattering
SCFA	short chain fatty acid
sec	second
SDS	sodium dodecyl sulphate
SDS-PAGE	sodium dodecyl sulphate polyacrylamide gel electrophoresis
Sf	*Spodoptera furgiperda*
siRNA	short interference RNA
S.O.C	Super Optimal Broth with Catabolite repression
SPR	Surface plasmon resonance
Talon	Co^{2+}-carboxymethylaspartate
TAE	Tris-acetate EDTA
TM	transmembrane
YT	Yeast extract tryptone broth
YTamp	Yeast extract tryptone broth with ampicillin

Summary

G protein-coupled receptors (GPCR) are a group of membrane proteins involved in major disease areas. GPR41 and GPR43 belong to class A (Rhodopsin-like receptors) of the GPCR family and they are activated by short chain fatty acids (SCFAs). Accumulation of SCFAs, in particular butyrate, has been found to be highly associated with colorectal cancer. Structures of these receptors have not been solved as large quantities of receptors are not easily available and crystallisation of membrane proteins remains as a major challenge. Cubic phase crystallisation has proven to be successful for a number of membrane proteins; however, the mechanism of crystal growth within this system is still unclear. This work was directed towards the production and crystallisation of GPR41 and GPR43.

GPR41 and GPR43 were expressed in a baculovirus insect cell expression system. The receptors were solubilised with Fos-Choline 12 detergent and the solubilised receptors were purified using immobilised metal affinity chromatography. Cubic phase characterisation studies were carried out in the presence of purified GPR41 and GPR43 with two cubic phase lipids, monoolein and phytantriol. GPR41 was found to destabilise the cubic phase of monoolein and phytantriol. By contrast, the cubic phase of both lipids was stable in the presence of GPR43 at high concentration.

In meso crystallisation trials have been carried out with purified GPR41 and GPR43. This project provides a good basis for further studies on GPR41 and GPR43.

Statement of Authorship

Except where reference is made in the text of the thesis, this thesis contains no material published elsewhere or extracted in whole or in part from a thesis submitted for the award of any other degree or diploma.

No other person's work has been used without due acknowledgment in the main text of the thesis.

This thesis has not been submitted for the award of any degree or diploma in any other tertiary institution.

27.03.2012

Yi-Lynn Liang

Acknowledgements

I would like to sincerely thank my supervisors Dr. Connie Darmanin and Prof. Leann Tilley without whom I would have never started my Ph.D. The valuable advice, guidance and assurance from Connie throughout this PhD had helped to shape me as a scientist and I will always be grateful for her encouragement.

I was very fortunate to have the opportunity to work in CSIRO, where I have met many scientists whom have helped me during the course of my PhD. I am grateful to Dr. Joanne Caine, Dr. Janelle Williams, Laura Castelli, Dr. Ross Fernly, Dr. Jenny Mckimm-Breshkin for their practical advices in various stages of this project. I would like to acknowledge members in the Fermentation group (CSIRO), Dr. Louis Lu, Nina Zuber and Tram Phan for performing the large-scale expression of GPCR. I also thank Dr. Janet Newman, Dr. Shane Seabrook and Tam Pham from Collaborative Crystallisation Centre (C3), whom have helped me set up all the samples for cubic phase characterization studies and *in meso* crystallisation trials. I would also like to acknowledge Dr. Lynne Waddington for her technical assistance and advice in electron microscopy, as well as in rock climbing.

Dr. Charlotte Conn has taught me everything in about small angle X-ray scattering and cubic phase characterisation; Chapter 4 would not exist without her. I thank her very much for all the time and patience in teaching me something, which I have absolutely no background on, as well as her company for all the sleepless night at the Australian Synchrotron. I would also like to thank Dr. Jacqui Gulbis for her advice in this project and her help with detergent solubilisation and purification of the receptors.

Special thanks to all my dear friends who have always been there to give me support, in particular, Wy Ching and Ginny who provided great support, understanding and encouragement when I most needed them. Finally, I owe my loving thanks to my family who have provided support and help throughout my life.

1 Literature review

1.1 G protein-coupled receptors

G protein-coupled receptors (GPCRs) belong to a large integral membrane protein family. They share a common topology comprising seven hydrophobic transmembrane (TM) alpha helices held together by six connecting loops; three on the extracellular side and three on the intracellular side. GPCRs are classified into three different families (Kolakowski, 1994):

- Class A, also known as the rhodopsin-like family is the largest family of GPCRs. This family is further subcategorised according to the types of ligands the receptor binds, which include amines, peptides, hormones, prostanoid and olfactory (Schiöth and Fredriksson, 2005).
- Class B members consist of receptors of secretin-like molecules, including secretin receptors, glucagon receptors, parathyroid hormone receptors and calcitonin receptors. These receptors have implicated roles in hypercalcaemia, hypoglycaemia and osteoporosis (Fredriksson et al., 2003; Schiöth and Fredriksson, 2005).
- Class C members include metabotropic glutamate receptors, calcium sensing receptors, GABA-B receptors, odorant and taste receptors (Schiöth and Fredriksson, 2005).

GPCRs transduce signals by coupling with the heterotrimeric G proteins and respond to a large range of molecules including amino acids, peptides, nucleotides, carbohydrates and lipids. They are located throughout the human body and have a broad range of physiological functions including metabolism, neurotransmission and immune modulation. GPCRs are thought to play an important role in various diseases including cancers, therefore they are strong targets for drug development. Currently, over 50% of the drugs with therapeutic efficacy target GPCRs, albeit that the structures of these proteins are largely unknown (Betz, 2005). The current

shotgun approach to drug development is faltering, as indicated by the 48% fall in registrations of new molecule entities with the Federal Drug Administration from 1996 to 2010 (US Food and Drug Administration, 2011). There is a critical need for structure based drug design in order to develop potential drugs that target GPCRs for treatment of different diseases.

1.2 G protein cycle

GPCRs mediate signalling pathways by activating the G protein cycle (Figure 1-1). When inactive, Gα, Gβ and Gγ subunits are bound together forming a heterotrimer. In this state, guanosine diphosphate (GDP) is associated with Gα subunits in a heterotrimeric complex. When an agonist binds to the GPCR, it acts as a guanine-nucleotide exchange factor by catalysing the dissociation of Gα from Gβγ subunits and GDP. Gα then binds to guanosine triphosphate (GTP), which is available in cells (Dupré et al., 2009). Both Gα bound GTP and Gβγ subunits are able to regulate downstream effectors and different subtypes of G proteins have different roles in effector regulation, resulting in a range of biological responses (Dorsam and Gutkind, 2007; Johnston and Siderovski, 2007). The signal is terminated when GTP is hydrolysed to GDP, either by the intrinsic GTP hydrolysing activity of the Gα subunit, or by regulators of G protein signalling (RGS), which enhance the GTP-hydrolysing activity (Benians et al., 2005; Malbon, 2005). The Gα bound GDP subunit then reverts back to its inactive state by re-association with Gβγ subunits.

Figure 1-1 G protein cycle

In its inactive state (R*), the G protein heterotrimer complex consists of GDP bound Gα (α, blue), Gβ (β, green) and Gγ (γ, yellow) subunits. The agonist (brown) binds to the extracellular domain, which activates the GPCR and results in disassociation of Gβγ subunits and binding of GTP to Gα, both of which can regulate downstream effector molecules (E, purple). The G protein cycle returns to the inactive state upon hydrolysis of GTP to GDP. This inactivation step may be catalysed by the regulators of G protein signalling (RGS, red). Diagram adapted from Oldham and Hamm (2006).

20 unique Gα, 5 Gβ and 12 Gγ subunits have been identified in humans (Malbon, 2005). Subtypes of Gα protein can be divided into four classes: $G\alpha_s$, $G\alpha_{i/o}$, $G\alpha_q$ and $G\alpha_{12/13}$ as follows:

- $G\alpha_s$ stimulates adenylate cyclase, which results in an increase in the level of cyclic AMP (cAMP).
- $G\alpha_{i/o}$, on the other hand, inhibits adenylate cyclase and activates potassium channels.
- $G\alpha_q$ stimulates phospholipase C resulting in hydrolysis of phosphotidylinositol biphosphate to inositol triphosphate (IP_3) and diacylglycerol (DAG), both of which are secondary messengers (Malbon, 2005).

- $G\alpha_{12/13}$ are primarily involved in small G protein and Rho-mediated responses (Malbon, 2005).

The $G\beta\gamma$ subunit pair was initially believed to function as a stabilising factor for the inactive form of $G\alpha$, but was later found to also be capable of regulating a variety of downstream effectors. The $G\beta\gamma$ subunits do not dissociate and they function as a dimer complex. They are known to regulate G protein-coupled inwardly-rectifying potassium channels (GIRK), and to inhibit adenylyl cyclase and calcium channels (Dupré et al., 2009). The complex was also found to mediate chemotaxis and the immune response by interacting directly with chemokine receptors such as IL-8 receptor and CXCR4 receptor (Kuang et al., 1996; Littman, 1998). The $G\beta\gamma$ dimer has also been shown to be involved in gene transcription regulation by interacting with the glucocorticoid receptor (GR) and down-regulating GR transcriptional activity in the nucleus (Kino et al., 2005). The diverse roles of $G\beta\gamma$ in various physiological functions are extensive and new roles continue to be discovered (Smrcka, 2008).

1.3 Structural knowledge of GPCRs

To date only eight GPCRs have had their structures solved to atomic resolution. The rhodopsin structure was first solved in the year 2000; only seven years later, β_2-adrenergic receptor had its structure solved. The T4 lysozyme fusion strategy and lipidic cubic phase method were successful in solving the β_2-adrenergic receptor structure and this approach has since been applied to other GPCRs, leading to recent successes in structure determination. The A_2 adenosine receptor, D_3 dopamine receptor, H_1 histamine receptor, CXCR4 chemokine receptor and M_2 muscarinic receptor structures have all been solved using this approach (Jaakola et al., 2008; Chien et al., 2010; Wu et al., 2010; Shimamura et al., 2011; Haga et al., 2012). These structures provide valuable information in understanding the structure and mechanisms involved in GPCR activation and are described in the following paragraphs.

Rhodopsin

The first solved GPCR structure was bovine rhodopsin, which is the photoreceptor found abundantly in the retinal rod cell of the eye (Palczewski et al., 2000; Park et al., 2008b). Rhodopsin comprises a 40 kDa protein, opsin, that is covalently linked to an 11-cis-retinal chromophore through Lys296 in TM7 (Palczewski et al., 2000). Light activation causes the 11-cis-retinal chromophore to isomerise to all-trans-retinal, which leads to the formation of different states, including bathorhodopsin, lumirhodopsin, Metarhodopsin (Meta I) and finally, the fully activated state - Metarhodopsin II (Meta II) (Salom et al., 2006). From Meta II, all-trans-retinal is then hydrolysed from the binding pocket to produce ligand-free opsin, which can be in an active form (Ops*) or an inactive form (Ops) (Scheerer et al., 2008). This leads to the activation of a signal transduction cascade via the G protein, transducin G_T (Scheerer et al., 2008). Currently, crystal structures are available for rhodopsin in various states. These include inactive forms, Meta I, Meta II, Meta II bound to a peptide fragment from the carboxyl terminus of G_T protein (GαCT), ligand-free opsin, and the active form, opsin, bound to GαCT (Palczewski et al., 2000; Ruprecht et al., 2004; Salom et al., 2006; Scheerer et al., 2008; Park et al., 2008a; Choe et al., 2011).

The first rhodopsin structure was solved in its ground (dark) state to a resolution of 2.8 Å (Palczewski et al., 2000) showing the topology of seven TM alpha helices. In addition, the 8^{th} α-helix was also observed lying along the cytoplasmic surface of the membrane at the C-terminal end of the receptor (Figure 1-2). The ligand-binding pocket of rhodopsin showed covalently bound 11-cis-retinal stabilising the inactive conformation. It is shielded by a buried β sheet in the second extracellular cytoplasmic loop (ECL2), preventing the binding of other ligands from the extracellular compartment. A hallmark of the rhodopsin structure is known as the 'ionic lock', which is a salt bridge between Arg135 in the D(E)RY motif of TM3 and Glu247 in TM6 (Palczewski et al., 2000). This 'ionic lock' arrangement is suggested to stabilise the inactive conformation or 'dark state' of rhodopsin.

A

B

Figure 1-2 Overall structure of rhodopsin and changes observed in opsin

(A) Rhodopsin structure showing the TM segments and the 8th α-helix segment at the C-terminal end, adapted from (Palczewski et al., 2000). (B) Ligand free opsin showing movement of TM6 outwards and TM5 inwards closer to TM6. Green represents inactivated rhodopsin and orange represents opsin (Park et al., 2008a).

Structures of intermediate states of rhodopsin allow us to further understand the changes in protein conformation upon activation. The Meta I structure was solved at low resolution (to 5.5 Å), using electron microscopy (Ruprecht et al., 2004). The electron density map showed that Meta I formation did not result in large movements of the TM helices, however, there is a rearrangement close to the bend of TM6. The Meta II structure was solved with and without a G_T peptide fragment (to a resolution of 2.85 Å and 3 Å, respectively). These two structures were found to be quite similar to previously solved structures of Ops* and Ops* bound GαCT (Scheerer et al., 2008; Park et al., 2008a). The structure of Ops* bound to G_t fragment was the first fully activated GPCR structure and showed major differences compared to previously solved structures. There is an outward tilt (~ 6-7 Å) of TM6 allowing the binding of the G_t peptide

and the cytoplasmic end of TM5 is shifted 2-3 Å closer to TM6, as shown in Figure 1-2B (Scheerer et al., 2008).

β_2-adrenergic receptor (B2AR)

The second unique GPCR structure solved was the human β_2-adrenergic receptor (B2AR) (Cherezov et al., 2007; Rasmussen et al., 2007). It plays an important role in cardiovascular and pulmonary function (Moran, 1963). It is found in smooth muscle throughout the body and is activated by adrenaline (Moran, 1963). B2AR had its structure solved using two different approaches. In the first approach, B2AR was crystallised with an antibody (Fab) fragment specifically bound to the third intracellular cytoplasmic loop (ICL3) of the receptor, referred to as B2AR-Fab (Rasmussen et al., 2007). ICL3 is known to be highly flexible; hence the conformational stability was achieved by the addition of the Fab fragment. The crystal structure of this construct diffracted to a resolution of 3.7 Å (Rasmussen et al., 2007) and provided an insight into the positioning of the helices and loops. In the second approach, ICL3 was replaced by a highly soluble and readily crystallised protein, T4 lysozyme, and the construct is referred to herein as B2AR-T4 (Cherezov et al., 2007). The crystals of this construct diffracted to a resolution of 2.4 Å (Cherezov et al., 2007). These two B2AR constructs were crystallised in the presence of a high-affinity partial inverse agonist, carozolol. B2AR-Fab crystals were grown in DMPC bicelles, whereas the B2AR-T4 crystals were grown in the lipidic cubic phase of monoolein.

Similar to rhodopsin, B2AR was found to have an additional α-helix that runs along the cytoplasmic side of the membrane. In the middle of ECL2, a short α-helical segment was observed, which was not found in rhodopsin (Cherezov et al., 2007). The presence of this short α-helical fragment in ECL2 enables the extracellular ligand to access the ligand binding pocket (Lefkowitz et al., 2008). Several differences are apparent in the TM segment when rhodopsin is compared with B2AR. A major difference is in TM1. There is a kink in rhodopsin TM1 which is a result of a proline residue. However, this kink was not observed in the B2AR TM1 (Cherezov et al., 2007). The structure of B2AR-T4L revealed cholesterol

mediated crystallisation packing, with three molecules of cholesterol bound to each monomer of B2AR-T4. This suggests that cholesterol plays an important role in stabilising the B2AR conformation.

A

B

Figure 1-3 Comparison of the overall structures of agonist-Nb80 bound B2AR (orange) active state and inverse agonist bound B2AR (green), inactive state

(A) Side view comparison of the crystal structures showing movement of TM5 and TM6. (B) Cytoplasmic view of the structures showing outward movement of TM6 by approximately 11.4 Å and movement of TM5 towards TM6. TM3 and TM7 in the activated B2AR were also found to move towards the core. The active B2AR structure was observed with a short α-helical segment in the ICL2, that was not observed in the inactive B2AR bound to carolol (Cz). Diagram adapted from Rasmussen et al., (2011a).

Subsequently, other structures of B2AR bound with other partial inverse agonists or antagonists were solved (Hanson et al., 2008; Wacker et al., 2010). Recently, two new structures were solved for the active conformation of B2AR. One structure of agonist-bound B2AR was obtained in complex with the Gs heterotrimer. The other made use of a nano-body, that exhibits G protein like behaviour, to stabilise the active conformation of B2AR (Rasmussen et al., 2011a; 2011b). Both activated B2AR structures revealed conformational changes when compared to the inactive B2AR structures as shown in Figure 1-3. The largest conformational change was an outward movement at the cytoplasmic end of TM6

(Rasmussen et al., 2011b). An extension on the cytoplasmic end of TM5 was observed in the activated B2AR and Gs complex. A short α-helix segment was observed in the second intracellular cytoplasmic loop (ICL2) of the activated B2AR, but not in the inactive B2AR structures. This feature is not restricted to the active state of GPCRs, as it was also observed in the inactive states of β_1-adrenergic receptor, A_2 adenosine receptor, dopamine D_3 receptor and M_2 muscarinic receptor (the structures of which are discussed in a later section) (Jaakola et al., 2008; Warne et al., 2008; Chien et al., 2010; Haga et al., 2012). Another notable observation in the structure of active B2AR-Gs complex is the absence of a direct interaction between the B2AR and Gβγ subunits. This was not predicted, as all three subunits of G protein are required for receptor activation and the Gβγ pair was thought to interact directly with the GPCR polypeptide (Smrcka, 2008).

A_2 Adenosine receptor (A2AR)

Adenosine receptors consist of four subtypes – A1, A2a (A2AR), A2b and A3. These receptors are all activated by adenosine and the receptors are classified based on their affinities (Olah and Stiles, 1995). The first crystal structure of A2AR was solved to a resolution of 2.6 Å in complex with an antagonist (Jaakola et al., 2008). Other than the presence of a short α-helix in the ICL2 of inactive A2AR, as mentioned previously, the noticeable helical secondary structure present in ECL2 of inactive rhodopsin, B1AR and B2AR was not observed in A2AR. The ECL2 of A2AR was found to adopt a random coil structure. Three disulphide bonds were observed linking ECL2 and ELC1, one of which is conserved among class A GPCRs, while two are unique to A2AR (Jaakola et al., 2008).

Figure 1-4 Structures of A2AR

A2AR in complex with a synthetic agonist (NECA, yellow) and comparison with A2AR bound to inverse agonist ZM241385 (blue). Adapted from Lebon et al. (2011).

The inactive form of A2AR had most of its ICL3 replaced with T4-lysozyme and crystals were grown in lipidic cubic phase. A more recent structure of agonist-bound A2AR was achieved using several point mutations to generate a thermostable construct for crystallisation (Lebon et al., 2011). Thermostable constructs were first generated for the B1AR, as discussed in a later section. The agonist-bound A2AR was crystallised with its natural ligand, adenosine, or a synthetic agonist, NECA. Both agonists bind to the receptor in a similar fashion (shown in Figure 1-4) and it was noted the cytoplasmic end of TM6 remained partially closed, thereby obstructing the G protein binding cleft (Lebon et al., 2011). Therefore, it was suggested that binding of the G protein to the receptor is required for stabilisation of the fully activated conformation and the structure presented was described as an intermediate state between active and inactive conformations.

Dopamine D_3 receptor (D3R)

Dopamine receptors can be classified into two subtypes, D1-like and D2-like. The D1-like subfamily consists of D1 and D5 receptors, whereas the D2-like subfamily consists of D2, D3 and D4 receptors (Missale et al., 1998). D1-like receptors couple to G_s protein and stimulate adenyl cyclase activity, whereas D2-like receptors inhibit adenyl cyclase activity by coupling to $G_{i/o}$ protein (Missale et al., 1998). D2R and D3R receptors have been implicated in schizophrenia and Parkinson's disease (Sokoloff et al., 1990). The D3R structure was solved to a resolution of 3.15 Å in complex with an antagonist, eticlopride (Chien et al., 2010). Compared to the B2AR stucture, the ECL2 of D3R is much shorter while it also lacks the α-helical structure observed in B2AR, as shown in Figure 1-5 (Chien et al., 2010). The structure of D3R also shows subtle changes in the TM helices. For example the extracellular ends of TM6 and TM7 are tilted by 3 Å and 2 Å, respectively, and the extracellular ends of TM3 and TM5 are closer to each other than they are in the B2AR structures (Chien et al., 2010). In addition, a short α-helical segment, which is absent in the B2AR structure, was observed in ICL2 of D3R. The D3R structure was also observed with the "ionic-lock" arrangement, which was found in the inactive rhodopsin structure (Palczewski et al., 2000). The structure of D3R was used to create a homology model of D2R, which is highly homologous to D3R. Docking studies of D3R and D2R with D3R-selective antagonist, R-22, revealed differences in the ligand binding pockets of D2R and D3R (Chien et al., 2010). Such information can aid in novel drug design for improving drug specificity in the treatment of the neurological diseases that D2R and D3R are associated with.

Figure 1-5 D3R structure

D3R in complex with an agonist (eticlopride). ECL2 lacks the α-helical segment that was found in B2AR and other GPCR structures. Instead, a short alpha helix was observed in ICL2 (purple). Diagram adapted from Chien et al. (2010).

C-X-C Chemokine receptor type 4 (CXCR4)

CXCR4 is a subtype of chemokine receptors commonly found in tumour cells and has been associated with lung, brain, breast, ovary and prostate cancer (Woodard and Nimmagadda, 2011). CXCR4 also functions as a co-receptor involved in binding and entry of HIV-1 virus (Carter et al., 2011). The CXCR4 structure was solved with a small molecule antagonist, isothiourea derivate (IT1t) (shown in Figure 1-6) or a cyclic peptide inhibitor, CVX15 (Wu et al., 2010). The CVX15-bound structure represents the first GPCR structure bound to a peptide ligand. The major differences observed within the TM helices of the structures when compared with other known GPCR structures may reflect the class of smaller ligands they bind. For example the extracellular end of TM1 is shifted towards the

central axis by 9 Å when compared with B2AR. The extracellular end of TM5 and TM7 are different to those of other GPCR structures, as they are one and two turns longer, respectively (Wu et al., 2010). When compared with other GPCR structures, the intracellular and extracellular ends of TM5 were observed to be approximately 5 Å and 3 Å away from the expected position (Wu et al., 2010). Bound IT1t occupies only part of the pocket, making interactions with side chains from TM1, 2, 3 and 7; however CVX15 was shown to occupy the entire ligand-binding pocket. CXCR4 structures revealed the absence of several features commonly observed in the structures of other GPCRs. This suggests that additional chemokine structures with bound agonists might provide new insights into the mechanism for GPCR activation at a molecular level.

Figure 1-6 Structure of CXCR4

Model showing the inactive form of CXCR4 structure in complex with a small molecule antagonist (IT1t). Red spheres indicate conserved water molecules. Diagram adapted from Wu et al. (2010).

H_1 Histamine receptor (H1R)

The histamine receptor family consists of four subtypes, H_1, H_2, H_3 and H_4 (Hill, 1990). H_1 receptor (H1R) has a major role in allergic inflammatory

responses as it is expressed on a variety of immune cells, including mast cells, dendritic cells, T cells, B cells and macrophages (Cameron et al., 1986; Gutzmer et al., 2002; Triggiani et al., 2007; Forward et al., 2009). While anti-histamines have been in clinical use for many years, the structure of H1R in complex with anti-histamine, doxepin, solved to a resolution of 3.1 Å, was only made available recently (Shimamura et al., 2011). The overall structure of H1R was found to be similar to B2AR, B1AR and D3R; however, it was quite different when compared to rhodopsin, A2AR and CXCR4 (Figure 1-7) (Palczewski et al., 2000; Rasmussen et al., 2007; Warne et al., 2008; Chien et al., 2010; Wu et al., 2010; Shimamura et al., 2011). In addition, the salt bridge that forms the 'ionic lock' arrangement in inactive rhodopsin and D3R structures was not observed in the H1R structure. Instead, the conserved residue, Arg125 was found to form a hydrogen bond to Gln416 in TM6 (Shimamura et al., 2011). It was found that the antagonist, doxepin, binds deeper in the ligand-binding pocket than antagonists in other known GPCR structures. Moreover, doxepin in the structure did not make any interaction with ECL2, which is generally thought to control the specificity of ligand binding in GPCRs.

Figure 1-7 Structure of HIR

H1R in complex with antagonist, dopexin. Dopexin is shown in yellow, while the blue ribbon highlights three conserved motifs: D(E)RY, CWxP and NPxxY. Diagram adapted from Shimamura et al. (2011).

M_2 muscarinic receptor (M2R)

The muscarinic receptors family consists of five members; M1, M2, M3, M4 and M5. This family of receptors regulates the function of the central nervous system and M2R is a potential target for the treatment of Alzheimer's disease and schizophrenia (Eglen, 2005). The latest addition to the GPCR structure database is the structure of M2R bound to its antagonist, 3-quinuclidinyl-benzilate (QNB), shown in Figure 1-8 (Haga et al., 2012). The T4-lysozyome and lipid cubic phase crystallisation approach was applied and the M2R structure was solved to a resolution of 3.0 Å. The structure of M2R bound to QNB is similar to other inactive GPCR structures and it displays an α-helical conformation in the ICL2 as observed in the inactive B1AR, D3R and A2AR structures (Jaakola et al., 2008; Warne et al., 2008; Chien et al., 2010). A notable difference in this structure is the aqueous channel located at the ligand-binding pocket. This channel is present in other GPCR structures; however, in the M2R structure, it extends from the extracellular surface into the TM core and beyond the QNB molecule. The length of this channel, from ECL2 to the TM core, was found to be approximately 33 Å.

Figure 1-8 Structure of M2R

M2R in complex with antagonist, QNB. Diagram adapted from Haga et al. (2012).

β_1-adrenergic receptor (B1AR)

The turkey B_1-adrenergic receptor (B1AR) is the third GPCR that has had its structure solved (up to 2.7 Å) (Warne et al., 2008). To date, this is one of the few structures where the crystal was obtained without using the T4-lysozyme fusion and lipidic cubic phase crystallisation approach. Six mutation points were introduced to obtain a thermostable mutant for crystallisation and the vapour diffusion method was used to obtain high quality diffracting crystals in complex with an antagonist, cyanopindolol (shown in Figure 1-9A) (Warne et al., 2003; 2008).

The structures of B1AR bound to two full agonists, i.e carmoterol and isoprenaline, and two partial agonists, i.e salbutamol and dobutamine, were recently solved (Warne et al., 2011). All four compounds bound to B1AR in a similar fashion, though the full agonists form hydrogen bonds to the side chain of Ser212 and Ser215 in TM5, whereas the partial agonists only interact with Ser215. When compared with antagonist-bound B1AR, the major differences are the hydrogen bonds formed by the agonist with the two serine residues, and the contraction of the ligand binding pocket by ~1 Å (shown in Figure 1-9B) (Warne et al., 2011).

A B

Figure 1-9 Structure of antagonist bound B1AR and changes relative to agonist bound B1AR. (A) Model showing the inactive form of B1AR. Adapted from Warne et al. (2008). (B) Antagonist bound B1AR is shown in grey and agonist bound B1AR is shown in orange. The interaction of agonist between TM5 and TM7 resulted in both TMs moving towards the core. Diagram adapted from Warne et al. (2011).

The GPCR structures that have recently become available have shed some lights on the understanding of the conformational changes that occur upon receptor activation. Although they all belong to Family A GPCRs, these receptors have low sequence homology. Several conserved characteristics such as the "ionic lock" arrangement, which were thought to be in all Family A GPCR members, were not found in some of the recently solved GPCR structures. In light of this, using existing structures as homology models for other unknown GPCR structures is risky. In addition, knowledge of G protein binding sites is very limited. Therefore, increasing the number of known GPCR structures will allow us to further understand the mechanisms involved in activation of different receptors and in allosteric modulation. This will contribute to efforts to undertake structure-based drug design.

1.4 GPR41 and GPR43 – Short chain fatty acid (SCFA) receptors

The GPR40 family consists of a small number of members; GPR40, GPR41, GPR42 and GPR43 were originally identified as orphan receptors encoded by genes located on the human chromosome 19q13.1 (Sawzdargo et al., 1997). GPR40 is activated by medium to long chain fatty acids, with carbon chain lengths greater than six (Briscoe et al., 2003). GPR41 and GPR43 were recently identified as short chain fatty acid (SCFA) receptors (Brown et al., 2003; Le Poul et al., 2003; Nilsson et al., 2003). The protein sequence of GPR42 shares more than 92% amino acid identity with GPR41; however, GPR42 is not activated by any of the short chain fatty acids (Brown et al., 2003). This led to the suggestion that GPR42 is a pseudo-gene derived from gene duplication of GPR41. This is supported by the fact that it was not possible to detect GPR42 mRNA expression in human tissues using GPR42 specific primers (Brown et al., 2003).

Calcium immobilisation and [^{35}S] GTPγS binding assays have been used to measure the concentrations of SCFAs required to activate both receptors. SCFAs found to activate GPR41 and GPR43 at different affinities are acetate, propionate, butyrate and pentanoate. GPR41 is activated by SCFAs in the order of butyrate = propionate = pentanoate > acetate. For GPR43, the order is butyrate = acetate = propionate > pentanoate (Brown et al., 2003). Treatment with pertussis toxin (PTX) abolished the GPR41 signal induced by SCFA activation, indicating that the receptor specifically couples to $G_{i/o}$ protein (Le Poul et al., 2003). GPR43, on the other hand, appears to couple to both $G_{i/o}$ and $G_{q/11}$ proteins since the signal was reduced but not completely eliminated when treated with PTX (Le Poul et al., 2003). SCFAs are not highly potent activators of GPR41 and GPR43. The concentrations required to activate the receptors are in the high micromolar to low millimolar range (Le Poul et al., 2003; Nilsson et al., 2003). Nonetheless, these concentrations fall within the physiological ranges found in the human colon, where an abundant supply of SCFAs is present.

Following the deorphanisation of GPR41 and GPR43, no synthetic agonist or antagonist was identified for some time thereafter. Recently, a series of branched, cyclic or unsaturated carboxylic acids have been shown to activate the receptors at approximately the same potencies as SCFAs (Schmidt et al., 2011). Phenylacetamide derivatives were found to also activate GPR43 and the signal was detected by calcium mobilisation, [^{35}S] GTPγS binding and lipolysis (Lee et al., 2008). This group of compounds was found to be 100-fold more potent than the endogenous ligands as an activator of GPR43. The phenylacetamide derivatives bind at a site distinct from the orthosteric site of GPR43, suggesting that they have positive co-operativity with acetate and propionate (Lee et al., 2008). The side chain of phenylacetamide was further modified to create a series of compounds which exhibit allosteric modulation of GPR43 activity (Wang et al., 2010).

Early studies suggested that Arg174, found in the second extracellular loop of GPR41, is an important residue for ligand binding; this was shown with regained ligand binding ability by mutation of W174R in GPR42 (Brown et al., 2003). Conserved polar residues in GPR41 and GPR43 were proposed to be critical for SCFA binding, in particular forming ionic interactions with the carboxyl head-group of SCFA (Stoddart et al., 2008). For GPR41, these residues are His146, Arg185, His245 and Arg258. For GPR43, they are His140, Arg180, His242 and Arg255. Mutation studies with GPR41 have shown that the substitution of any of these residues to alanine completely abolishes the ability to respond to propionate (Stoddart et al., 2008; Swaminath et al., 2010). Similar results were obtained for GPR43, with the exception that ligand-induced activation was retained with construct H140A. This group also showed that the ECL2 of GPR43 is required for the transmission of allosterism between propionate and phenylacetamide. Site mutagenesis of residues in ECL2 was performed and ECL2 of GPR43 was replaced with ECL2 of GPR41 (Smith et al., 2011). The D(E)RY motif is a conserved region at the bottom of TM3 of GPR43 found in other members of Family A GPCRs. The structure of rhodopsin and other GPCRs revealed that this motif is important for stabilising the receptor conformation. Similarly, mutation of the glutamic acid (E) residue or the tyrosine (Y) residue to alanine (A) resulted in orthosteric agonist

binding activity or phenylacetamide binding activity being abolished (Swaminath et al., 2010).

1.4.1 Production of SCFAs in humans

Fatty acids are classified according to the number of carbons in their chain and SCFA are generally one to six carbons in length. Carbohydrates, fats and proteins that are not digested in the intestine undergo breakdown by bacterial fermentation upon reaching the colon and the end products of this process are SCFAs, as shown in Figure 1-10. The three main SCFAs found in human intestine are acetate, propionate and butyrate (Roy et al., 2006). The molar ratio of SCFAs produced are approximately 60:20:18 for acetate: propionate: butyrate, but the ratio varies in relation to the type of bacteria present in the gut, dietary intake, and gut transit time (Wong et al., 2006). Concentration of SCFAs found in the colon range from 20 mM to 140 mM (Topping and Clifton, 2001).

Figure 1-10 Overview of SCFAs production

Production of SCFAs from carbohydrates and other nutrients in the human gastrointestinal tract. Diagram adapted from Roy et al. (2006).

Daily production of SCFAs in humans is approximately 100 to 200 mM (Cook, 1998). SCFAs are rapidly taken up by epithelial cells in the colon and the mechanisms for absorption are either by a) diffusion through the membrane or b) counter-ion transport with bicarbonate and anion exchange (Cook, 1998; Scheppach and Weiler, 2004; Sengupta et al., 2006). Depending on the pH, SCFAs

can be charged or de-protonated; de-protonated SCFAs are absorbed by cells through diffusion while charged SCFAs are absorbed by cells through a counter-ion transport mechanism.

1.4.2 Roles of SCFAs

SCFAs are thought to have a wide range of effects on colonic health and the human immune system. They act as an energy source for colon cells and they are also transported to other organs for use as energy substrates. There has been a rising interest in SCFAs over the last decade due to their potential for improving overall colonic health and they have been implicated in various diseases including inflammatory bowel disease, cardiovascular disease and colorectal cancer (Cook, 1998; Wong et al., 2006; Tang et al., 2011).

Butyrate is the major energy source for colonocyte metabolism. Once it is absorbed, 70-90% is used by colon epithelial cells in preference to acetate and propionate (Wong et al., 2006). The remaining butyrate and propionate and 50-70% of the acetate are transported to the liver for use in gluconeogensis. Propionate has an inhibitory effect on cholesterol synthesis in liver cells and was also found to increase leptin production in adipocytes (Cook, 1998; Xiong et al., 2004). Residual acetate is used for synthesis of long chain fatty acids, glutamine, glutamate and beta-hydroxybutyrate; it is also oxidised to produce energy for muscle cells (Roberfroid, 2007).

Apart from being an important respiratory fuel, butyrate also plays a role in modulating the immune response. Nuclear factor *kappa*-light-chain-enhancer of activated *B* cells (NF-κB) is a transcription factor that regulates the expression of pro-inflammatory molecules including cytokines, cell adhesion molecules, growth factors, and immune receptors (Jobin and Sartor, 2000). Dimerisation of NF-κB is required for NF-κB activation and it was found to be inhibited by butyrate; therefore, butyrate may exert an anti-inflammatory effect by suppressing NF-κB activation (Inan et al., 2000). Bowel inflammatory diseases such as ulcerative

colitis and Crohn's disease have an important inflammatory component as part of their pathology (Williams et al., 2003). As these diseases have been linked to reduced SCFA metabolism, butyrate has been used as an adjuvant in the treatment of these diseases (Steinhart et al., 1996; Segain et al., 2000). Interferon-γ (IFN-γ) is an important regulator of the human immune response (Schroder et al., 2004) and peroxisome proliferator-activated receptor-γ (PPAR-γ) is another transcription factor that regulates expression of genes involved in lipid metabolism, inflammation and cell proliferation (Dubuquoy et al., 2006). In addition to acting on NF-κB, butyrate was also found to inhibit production of IFN-γ and to increase the activation of PPAR-γ (Kinoshita et al., 2002; Klampfer et al., 2003). Therefore, it was suggested that the anti-inflammatory effects of butyrate might involve the regulation of IFN-γ and PPAR-γ.

Butyrate also has diverse roles in colorectal cell proliferation, differentiation and apoptosis; these effects are implicated in colorectal carcinogenesis. Scheppach et al. studied the effects of SCFAs, in particular of butyrate, on different stages of adenoma-carcinoma colon cells (Scheppach et al., 1995). On normal mucosa cell lines, acetate, propionate and butyrate all increased proliferation in the basal crypt and butyrate inhibited proliferation in the upper crypt (Scheppach et al., 1992). Butyrate treatment of a colon adenoma cell line showed a dose-dependent inhibition on proliferation and up-regulation of cell differentiation (Menzel et al., 2004). These effects were also observed in a colon carcinoma cell line. In addition, butyrate has been shown to induce apoptosis and to inhibit histone deacetylase (HDAC) (Scheppach et al., 1995).

The mechanisms and pathways that underlie SCFAs mediated effects are still not well understood, however it is possible that some of the effects may be due to their ability to interact with GPR41 and GPR43, as discussed in the next section.

1.4.3 Physiological roles of GPR41 and GPR43 – SCFA mediated effects

GPR41 is predominantly expressed in adipose tissues with lower expression levels in lymph node, spleen, bone marrow, lung, colon, pancreas and liver (Le Poul et al., 2003; Brown et al., 2005; Tazoe et al., 2009). The mRNA of GPR43 can be detected in spleen, bone marrow, human colonocytes, skeletal muscle, and the heart, with the highest expression level found in immune cells, including monocytes and neutrophils (Brown et al., 2003; Le Poul et al., 2003; Nilsson et al., 2003; Karaki et al., 2006).

Leptin and insulin are anorexigenic hormones that regulate a wide range of physiological functions, including food intake. GPR41 was first shown to mediate SCFA-stimulated leptin production in adipose tissues and in mouse models (Xiong et al., 2004). In this study, treatment with short interference RNA (siRNA) targeting GPR41 mRNA decreased leptin gene expression. However, two later studies showed that GPR41 was not expressed in adipocytes and concluded that GPR43 is responsible for (i) SCFAs mediated adipogenesis, (ii) a reduction in both lipolysis activity and plasma free fatty acid levels (Hong et al., 2005; Ge et al., 2008). These results have been further confirmed by a more recent study showing that leptin production stimulated by SCFAs in adipose tissue is mediated by GPR43 (Zaibi et al., 2010). Although debate continues on the role of GPR41 in leptin production, both of these studies showed that leptin production is signalled through a $G\alpha_{i/o}$ pathway, as evidenced by an observed reduction in leptin levels when cells were treated with PTX. Understanding the mechanism of GPR41 and GPR43 in leptin production could provide beneficial information for the treatment of obesity and type 2 diabetes.

Glucagon-like peptide 1 (GLP1) is another anorexigenic hormone. Its activation has an inhibitory effect on food intake, gastrointestinal secretion and mobility (Holst, 2007). Together with peptide YY (PYY), which has the same effects on the gastrointestinal tract and on regulation of food intake, they are able

to completely inhibit gastrin-stimulated secretion, resulting in relaxation at the level of the proximal stomach (Holst, 2007; Taylor, 2008; Karra et al., 2009). It has been reported that SCFAs up-regulate the expression of both PYY and GLP1 (Zhou et al., 2006). Further studies showed that increased levels of PYY and GLP1 by SCFAs could be mediated by GPR43, as proven by the reduced level of GLP1 in GPR43 knockout mice (Tolhurst et al., 2011). In addition, GPR43 was abundantly expressed in PYY-containing enteroendocrine cells (Karaki et al., 2006). Along with demonstrating the relevance of GPR43 in PYY release, the author also showed that GPR43 was abundantly expressed in serotonin-containing mucosal mast cells in mice, thus implying that SCFA-induced serotonin release was mediated by GPR43 (Karaki et al., 2006). Serotonin has an effect on increased upper gastrointestinal tract mobility and contraction, and has also been implicated in inflammatory bowel diseases, where changes in content, release and uptake of serotonin in inflammatory models were observed (Costedio et al., 2007). In a recent report, colitis induced in GPR43 knockout mice showed an increased inflammatory component when compared to the response of wild type mice (Maslowski et al., 2009). This suggests that the anti-inflammatory effect of SCFAs is mediated by GPR43.

The effects of SCFAs on colorectal cancer cells have been discussed previously. Expression of GPR43 was found to be significantly reduced in most colorectal adenocarcinoma tissues and transfection of GPR43 construct in colorectal cancer cell lines showed inhibition on cell proliferation and increased apoptosis upon treatment of SCFA (Tang et al., 2011). This suggests GPR43 acts as a tumour suppressor with the anti-tumour effects of SCFA being mediated by GPR43. This is in contradiction with another study where it was shown that GPR43 is an oncogene and an increase in GPR43 expression was observed in gastric cancer and colorectal cancer tissue specimens (Hatanaka et al., 2010). In order to verify the role of GPR43 in colorectal cancer, more research into this area is required.

Extensive research has shown that SCFAs play a key role in colonic function and may be an important regulator of the immune system. The mechanisms and

pathways involved however still remain to be elucidated. The discoveries of GPR41 and GPR43 as SCFA receptors have raised interest in this field. Basic molecular and structural studies of these receptors will provide key information regarding the involvement of these receptors in effects exerted by SCFAs and may lead to the development of novel drugs.

1.5 Heterologous expression of GPCRs

Studies on structure-function relationships and the characterisation of GPCRs require substantial amounts of purified functional receptors. Over-expression of functional GPCRs is a major bottleneck in obtaining crystal structures. Furthermore, the folding pathways and stability requirements of the membrane protein are not well understood. Endogenous GPCRs are typically expressed at low levels and many GPCRs have been expressed in heterologous systems to achieve high expression levels. Bacteria, insect cells and mammalian cells have been used successfully to express functional GPCRs.

Production of recombinant proteins in *E. coli* has major advantages such as low cost, short doubling time and the availability of different strains, which explains why this system is often used to express soluble proteins recombinantly. However, recombinant membrane protein expression in this system has limitations, such as the inability of *E. coli* to perform post-translational modification and the fact that the composition of the bacterial membranes are significantly different to the mammalian cell membranes, which could affect the folding and functionality of recombinant receptors. Expression of membrane proteins in *E. coli* is usually toxic to the cells, resulting in expression of receptors in inclusion bodies, and therefore they often require a re-folding process. Despite these drawbacks, several GPCRs have been functionally expressed in *E. coli.* Attril et al. expressed the rat neurotensin receptor type I using the BL21 strain, generating 0.2 mg of ligand-binding receptor per litre of culture (Attrill et al., 2009). Another group established high-throughput production of GPCRs as inclusion bodies, where 40 out of the 100 selected GPCRs were able to be expressed under optimal conditions (Michalke et al., 2009). Although high expression levels were demonstrated, assays were not conducted to determine the functionality of the receptors. Four members of the chemokine receptor family, CCR5, CCR3, CXCR4 and CX3CR1, were also expressed in *E. coli* at a level of mg/L (Ren et al., 2009). Similarly, no functional assay was conducted for these receptors

but circular dichroism analyses showed that the purified receptors adopted a reasonable level of secondary structure.

In the early 1980s, baculovirus expression of recombinant proteins production became popular and is now made easy by the commercially available baculovirus expression kits (Bernard et al., 2001). This system utilises recombinant fusions of baculovirus encoding genes and the target protein in insect cells infections. Insect cells have the advantage of being an eukaryotic system that is capable of performing post-translational modifications similar to mammalian cells, though with less complexity (Richardson and Hosey, 1992; Massotte, 2003). There is also evidence for the presence of endogenousG proteins such as $G\alpha_{i/o}$, $G\alpha_s$ and $G\alpha_q$ in insect cells. Human substance P receptor, μ-opioid receptor and bradykin 2 receptor have shown G protein coupling activity when they are expressed in this system (Nishimura et al., 1998; Wei et al., 2000; Arun Kumar et al., 2006). In fact most of the GPCRs that have been crystallised to date have been expressed in insect cells (Warne et al., 2003; Rasmussen et al., 2007; Jaakola et al., 2008; Chien et al., 2010; Wu et al., 2010).

Mammalian cells have been frequently used to express GPCRs due to their ability to express the recombinant protein in a native environment. They have the ideal lipid composition in the membrane bilayer and are able to carry out post-translational modifications that facilitate expression and folding of the receptor. The presence of endogenous co-factor molecules allows functional studies, including signalling, activation, ligand screening and oligomerisation studies, to be conducted in this system (Salahpour et al., 2003; Wang et al., 2009; Stoddart, 2007). Baby hamster kidney (BHK21), Chinese hamster ovary (CHO) and human embryonic kidney (HEK293) cell lines are commonly used for GPCR expressions (Sen et al., 2003; Lundstrom et al., 2006). However, the levels of recombinant GPCR expressed in this system are often low, thus they are not commonly used for large-scale expression. Moreover, the costs for large-scale purification using mammalian culture are extremely high, while difficulties also arise in the transition from adherent mammalian cell cultures to suspension cultures (Prashen et al., 2006; McCusker et al., 2007).

As there is no one universal expression system available for optimal expression of all membrane proteins, the advantages and disadvantages of each expression system should be carefully evaluated to maximise the production yield as well as achieving the functionality of the target protein.

1.6 Solubilisation and purification of GPCRs

GPCRs are integral membrane proteins, hence isolation of GPCRs requires solubilisation, which is usually achieved using mild detergents to stabilise the hydrophobic regions of the receptor. Detergents are amphipathic compounds comprised of a polar head-group and a hydrophobic tail. They can be classified into three types; ionic, non-ionic and zwitterionic based on the nature of their head-group. Ionic detergents have a charged head-group, which can be positively or negatively charged. Sodium dodecyl-sulphate (SDS) is an extremely harsh ionic detergent commonly used as a denaturant for membrane proteins as it breaks the electrostatic interactions in protein leading to complete denaturation. Non-ionic detergents have an uncharged hydrophilic head-group and they preferentially disrupt lipid-lipid or lipid-protein hydrophobic interactions. Consequently, they are found to be suitable for membrane protein solubilisation (Seddon et al., 2004). Zwitterionic detergents have both a positive and negative charge in their head-group, giving them zero net charge; they are also found to be milder than ionic detergents.

The choice of the detergent and the concentration of the detergent used for solubilisation are critical to ensure optimal extraction without disrupting the 3-dimensional structure of membrane proteins. The concentration of detergent to be used is dependent on the critical micellar concentration (CMC), which is different for each detergent. CMC is defined as the lowest concentration at which detergent micelle forms, and the number of detergent monomers in each micelle is known as the aggregation number (le Maire et al., 2000). Detergents are usually used at concentrations above the CMC for effective solubilisation. However,

excessive detergent in a purified sample may not be beneficial for further studies and needs to be removed either by dialysis or by absorption to a hydrophobic resin (Rigaud et al., 1997).

A classical detergent, n-dodecyl-β-D-maltopyranoside (DDM) is used to solubilise GPCRs for structural studies. This detergent has been used effectively in the solubilisation of A2AR, B2AR, H1R, B1AR, Urotensin-II receptor, human parathyroid hormone 1 receptor, smoothened receptor and muscarinic acetylcholine receptor (Warne et al., 2003; Venkata et al., 2004; Gan et al., 2006; Rosenbaum et al., 2007; Jaakola et al., 2008; Ma et al., 2008; Du et al., 2010; Nehmé et al., 2010). A mixture of detergents can also be applied for solubilisation of GPCRs. M2R was solubilised using a combination of digitonin and sodium cholate (Rinken et al., 1994; Hayashi and Haga, 1996). A group of zwitterionic detergents, the Fos-choline® series was found to be efficient in solubilising a family of chemokine receptors CCR5, CCR3, CXCR4 and CX3CR1 (Mirzabekov et al., 1999; Ren et al., 2009).

Once the target protein is solubilised, it can be purified using conventional methods. These methods include affinity tag, gel filtration, ion exchange, receptor specific ligand chromatography and others. Following solubilisation, GPCRs are often purified via an affinity tag introduced during the cloning step and it can be situated on the N- or C- terminus of the receptor. Affinity tags like FLAG, c-Myc, hemagglutinin (HA) and histidine tag (His-tag) are commonly used for protein purification (Reiländer et al., 1991; Park and Wells, 2003; Warne et al., 2003). A subsequent purification step is often, but not always, required to improve the purity of membrane proteins. This can be achieved with gel filtration chromatography, which separates proteins according to size. Most of the GPCRs used to obtain crystal structures were obtained by combination purification methods that provide samples of high purity.

1.7 Crystallisation

A crystal is a material consisting of an orderly arrangement of molecules, comprising unit cells in two- (2D) or three-dimensional (3D) form. Examples of common 3D crystal lattices are depicted in Figure 1-11. The unit cell is defined by its lattice parameters, which are the length of the edges of lattice (a, b and c) and the angles between them (α, β and γ) (Rhodes, 1993). Protein crystallisation occurs when protein solutions become supersaturated in the presence of precipitants. Structure determination of proteins requires well-ordered protein crystals that are of sufficient size to generate diffraction patterns when exposed to X-rays. Traditional and newly developed methods for 2D and 3D crystallisations are discussed in the following sections.

Figure 1-11 Examples of 7 lattice classes

Lattice classes commonly observed with in three-dimensional crystals (Amar, 2010).

1.7.1 3D crystallisation

A 3D crystal is a material made of an orderly arrangement of molecules in three-dimensional form. The traditional way to obtain 3D crystals is by vapour diffusion, which can be set up using the hanging drop or sitting drop methods (Figure 1-13 A and B, respectively). In the schematic diagram, P is the protein solution and R is the reservoir solution; both solutions consist of buffer, salt and precipitant. Generally, the concentration of the precipitant in the protein drop is lower than in the reservoir. Diffusion occurs over time in the vapour phase between the reservoir and the protein drop, such that the water migrates from the protein drop to reservoir until the system reaches an equilibrium (Sutton and Sohi, 1993). This results in an increasing concentration of the precipitant and supersaturation of protein in the drop, which leads to crystal growth.

Figure 1-12 A schematic diagram of two crystallisation setup.
(A) Hanging drop method and (B) sitting drop method. P and R in both figures refer to protein sample solution and reservoir solution, respectively. Adapted from Sutton and Sohi (1993).

Although the vapour diffusion method has produced several GPCR crystals for structure determination, *in meso* crystallisatio has proven to be more robust for growing diffracting quality crystals of GPCRs. This method involves the addition of lipids to the vapour diffusion set-up. *In meso* crystallisation is a novel method developed for crystallisation of membrane proteins, which relies on the cubic phase formation by lipids (Landau and Rosenbusch, 1996). Lipids can exist in different phases in aqueous solution due to their hydrophobicity. A variety of phases can be formed depending on parameters such as temperature, pH, the shape of the lipid, and other components in the aqueous solution (Hacker et al.,

2009). Lipids with a head-group wider than the hydrophobic tail will have a cone shape and tend to form micelles, whereas lipids with larger hydrophobic tails and a smaller head-group form inverted micelle. The packing of these inverted micelles leads to another phase, which is known as inverted hexagonal (H_{II}) phase. The cubic phase used in *in meso* crystallisation consists of a highly curved lipid bilayer, extending in three dimension with two interpenetrating but unconnected water channels (Cherezov et al., 2002). Figure 1-14 illustrates how a membrane protein resides within the cubic phase where the hydrophobic TM segments are located within the lipid bilayer with the cytoplasmic region facing the water channels.

Figure 1-13 A schematic diagram of a bicontinuous cubic phase

A cartoon showing the bicontinuous cubic phase used for *in meso* crystallisation and enlarged section of the system with a model membrane protein inserted into the lipid bilayer (Landau and Rosenbusch, 1996).

The exact mechanism of *in meso* crystallisation is not well understood. It is suggested that upon mixing protein with lipids such as monoolein (MO) at a protein to lipid ratio of 60:40, the hydrated lipid forms a cubic phase, and that the protein is incorporated within the curved lipid bilayer. Subsequent addition of precipitant results in phase separation, with the formation of local lamellar liquid crystalline phase (Lα) (Caffrey and Cherezov, 2009), and it is hypothesised that crystal nucleation occurs within this local Lα phase (Nollert et al., 2001; Qutub et al., 2004).

1.8 Phase behaviour of cubic phase lipids

SAXS can be applied on a wide range of samples, including metals, plastics, polymers, lipids, proteins, DNA, and RNA (Koch, 2006; Petoukhov and Svergun, 2007). It has proven very useful for characterisating the microstructure of lipids. There are many components present in buffers that can have large impact on the phase behaviour of cubic phase lipids and as mentioned above, the *in meso* crystallisation method requires cubic phase protein incorporation and crystal growth. Therefore, SAXS can be used to study the effect of different buffer components or the target proteins on the lipid phase, to determine if the conditions are favourable to begin with for *in meso* crystallisation.

The effects of water and temperature on the phase behaviour of MO have been well characterised by SAXS. Figure 1-15 shows a temperature composition phase diagram of MO/water (Qiu and Caffrey, 2000). In this study, the phases identified are L_c lamellar crystal phase, $L\alpha$ phase, fluid isotropic (FI) phase, inverted hexagonal (H_{II}) and two cubic phases, diamond and gyroid. The phase diagram shows that the L_c phase was found at low water concentration (<15%) and at temperatures below 37°C. An increase in temperature resulted in the formation of FI phase. At low temperatures, increasing the water content was associated with a phase transition from $L\alpha$ to the gyroid cubic phase, and a further increase in water content resulted in the formation of the diamond cubic phase. The diamond cubic phase was identified in excess water (up to 50%).

Figure 1-14 Temperature composition phase diagram of MO/water system.

MO/water phase diagram was observed with L_c lamellar crystal phase, Lα phase, fluid isotropic (FI) phase, inverted hexagonal (H_{II}) phase, diamond cubic phase (Pn3m) and gyroid cubic phase (Ia3d). Diagram adapted from (Qiu and Caffrey, 2000).

The presence of detergent in a purified membrane protein sample is inevitable, and Caffrey's group have studied the effect of DDM on phase behaviour of MO (Ai and Caffrey, 2000). They found that a low concentration of DDM induced a phase transition from diamond cubic to gyroid cubic, while at high concentration the cubic phase gave way to Lα phase. Similar effects were also observed with alky glucoside detergents (Misquitta and Caffrey, 2003). Additives such as cholesterol were also found to increase the stability of GPCRs and in most cases crystals of GPCRs were obtained in the presence of cholesterol in the buffer. As cholesterol is a lipid naturally present in the lipid bilayer of cell membranes, it might stabilise the folding of GPCRs by direct interaction as shown in the B2AR structure (Hanson et al., 2008). In addition, cholesterol was observed to have a swelling effect on the cubic phase of MO, which results in formation of the sponge phase (Cherezov et al.,

2006). This sponge phase was proposed to improve the crystallisation process of membrane proteins with its enlarged water channel to increase the mobility of membrane proteins, thereby accelerating self-association of the protein and promoting crystal growth (Cherezov et al., 2006). Therefore, the sponge phase could be an alternative phase suitable for crystallisation of large membrane proteins.

Crystallisation screens are often made up of buffer components that have a dehydrating effect, which further concentrates the protein for crystal nucleation, though it is unclear how these components affect the phase behaviour of cubic phase lipids. The Hampton screen kit is commercially available and its components include various salts, buffer and precipitants. This kit is commonly used for crystallisation trials of soluble proteins and membrane proteins. The compatibility of the Hampton screen for *in meso* crystallisation was studied using undiluted and half-strength screens (Cherezov et al., 2001). It was found that at 20°C, half of the screens used at undiluted concentration destroyed the cubic phase of MO and 90% of the screens used at half strength retained the cubic phase. This shows that the majority of crystallisation screens in the Hampton screen kit are incompatible with *in meso* crystallisation as cubic phase is required as a starting point. The above studies were carried out in the absence of membrane protein and the effects observed were solely caused by the components present in the screens.

The different effects of membrane proteins on the phase behaviour of lipids are attributed to the size of the hydrophobic and hydrophilic domains, and the degree of penetration into the lipid bilayer, together with their ability to alter the membrane curvature (Yaghmur et al., 2007). Several studies carried out with specially designed TM peptides have shown that they have different effects on the phase behaviour of MO (Chupin et al., 2003; Yaghmur et al., 2007). These studies provide limited information with regards to GPCRs, as GPCRs are much larger than the single TM peptides. Recent publications by Conn et al., report the effects of incorporation of dopamine D2L receptor and bacteriorhodopsin within the cubic phase (Conn et al., 2010b; 2010a). These two receptors exerted different effects on MO. An increase in the concentration of D2L receptor was observed with an

increase in the lattice parameter of the cubic phase, while this effect was not observed with bacteriorhodopsin (Conn et al., 2010a). Two other lipid surfactants known to form cubic phase were included in the same study, i.e anadaminde and H-farnesoyl monoethanolamide and it was found that the cubic phases of both lipids were retained in the presence of up to 18 mg/mL of bacteriorhodopsin (Conn et al., 2010b). Although MO is currently the preferred lipid for *in meso* crystallisation of membrane proteins, it might not be a universal lipid compatible with all membrane proteins. Development of other cubic phase lipids would provide valuable insight into the endeavour of obtaining more crystal structures.

1.9 Project aims

The work described in this PhD thesis aimed to achieve the following objectives:

1) Generation of different constructs of GPR41 and GPR43 fused with histidine tag on either the C or N terminus
2) Expression of at least one construct
3) Solubilisation and purification of the expressed receptor
4) Phase characterisation of cubic phase lipids using SAXS
5) Development of crystallisation methods for purified receptor

2 Cloning and expression of GPR41 and GPR43

2.1 Introduction

The level of expressions of GPCRs in native tissues is often low and they have to be heterologously expressed in order to obtain sufficient material for crystallisation trials. Despite the availability of many expression systems, structural studies have been hindered by the low yields of GPCRs in these systems. The baculovirus expression system has proven to be the most useful for expressing GPCRs in amounts sufficient for cell signalling and structural studies. A number of GPCRs with known structures have been obtained with this system; these include B2AR (Cherezov et al., 2007), B1AR (Warne et al., 2008), A2AR (Jaakola et al., 2008), CXCR4 chemokine receptor (Wu et al., 2010), D3R (Chien et al., 2010) and M2R (Haga et al., 2012).

A strong promoter drives the expression of the polyhedrin protein in baculoviruses (*Autographa californica),* however polyhedrin is not essential for virus replication. The baculovirus expression system takes advantage of this by replacing the polyhedrin gene with a gene of interest permitting its over-expression as a recombinant protein. There are several commercially available kits that can be used to generate recombinant baculovirus for protein expression, one of which is the Bac-to-bac™ Baculovirus expression system (Invitrogen, 2004). This system utilises a special strain of *E. coli* (DH_{10Bac}™) containing a helper plasmid and a baculovirus shuttle vector (bacmid), which allow site-specific transposition of the gene of interest into the vector (Ciccarone et al., 1997). After cloning of the gene into DH_{10Bac}™, the recombinant bacmid DNA is used for transfection of insect cells to generate recombinant viruses, as shown in Figure 2-1. Insect cells that are commonly used for heterologous protein expression are derived from *Spodoptera frugiperda (Sf)* cell lines; typically *Sf21* and *Sf9* cells are used. They have similar characteristics in protein expression, however *Sf9* cells are found to be overall smaller in size and have slower growth rates compared to

Sf21 cells. Recombinant viruses generated from transfection are subsequently used to infect more insect cells to scale up the volume and infectivity of recombinant virus stocks. Compared to mammalian cells, insect cells are considered to be easier and cheaper in terms of maintenance and up-scaling. As the polyhedrin promoter is a 'late' promoter, the recombinant protein is only expressed in the late cycle of infection, usually between 24 to 96 hrs after infection (Massotte, 2003).

Figure 2-1 A diagram of the Bac-to-Bac™ - Baculovirus expression system.
The recombinant plasmid is transformed into DH10Bac E. coli cells, a special strain of cell line that contains baculovirus DNA to generate recombinant bacmid. Recombinant bacmid can then be used for transfection into insect cells to produce recombinant virus. The recombinant virus is then amplified and used for expression. Diagram modified from Invitrogen (2004).

This chapter describes the cloning and expression of GPR41 and GPR43 constructs in *Sf9* and *Sf21* cells using the baculovirus expression system. To date, there has not been any report on expression of GPR41 and GPR43 in insect cells. Expressions of these two receptors has only been reported in mammalian cells, yeast cells and oocytes (Brown et al., 2003; Stoddart, 2007). Studies in these other cell types were not conducted for purification and structural studies; instead they were performed to investigate cell-based signalling. Since the majority of the

known GPCR structures have been generated from proteins expressed in insect cells, this system is a promising tool for expressing functional GPCRs in high yield. In addition, GPR40, which belongs to the same family as GPR41 and GPR43, has been expressed in insect cells and retained functionality (Hara et al., 2009). Therefore, the baculovirus/insect cells expression system was used in this project with the aim of achieving high expression yields of GPR41 and GPR43 for structural studies.

2.2 Materials and methods

2.2.1 Materials

Primers used to generate GPR41 and GPR43 constructs were ordered from GeneWorks. [^{35}S] GTPγS was purchased from Perkin Elmer at a concentration of 1 mCi/ml and specific activity of 1250 Ci/mmol. Unless otherwise stated, all buffers and chemicals were purchased from Sigma Aldrich.

2.2.2 Methods

2.2.2.1 Preparation of competent *E. coli* cells ($DH_5\alpha$ and DH_{10Bac}™)

Competent cells were prepared by inoculating 2.5 mL of overnight culture into 250 mL of 2 x yeast extract tryptone broth (YT) media supplemented with 10 μg/mL of tetracycline and 50 μg/mL of kanamycin. The cell culture was grown at 37 °C until the optical density (O.D) reached 0.375 at 590 nm. Cells were kept on ice for 5 mins, followed by centrifugation at 3,500 rpm (5147R, Eppendorf) at 4 °C for 15 mins. The cell pellets were then resuspended in 10 mL of chilled 100 mM $CaCl_2$ and incubated on ice for 30 minutes. At the end of incubation, cells were re-centrifuged at 3,500 rpm at 4 °C for 15 mins. The $CaCl_2$ competent cells were resuspended in 9 mL of 100 mM $CaCl_2$. Competent cells were then stored at -80 °C as glycerol stocks (10% glycerol) until required. Two strains of *E. coli* cells ($DH_5\alpha$ and DH_{10Bac}™) were used to prepare competent cells using the procedures described above.

2.2.2.2 *E. coli* transformation

$DH_5\alpha$ *E. coli* was used for all plasmid amplification in this study. Plasmid vectors (pCMV6-ex14) containing the cDNA encoding GPR41 (accession no. NM_005304.2) and GPR43 (accession no. NM_005306.1) were purchased from

Origene Technologies. An aliquot of competent *E. coli* generated from section 2.2.2.1 was thawed on ice for transformation. For each transformation, 5 ng of DNA (pFastBac1™ vector or cDNA encoding GPR41 or GPR43) was mixed with 50 μL of competent cells; the mixture was then incubated on ice for 30 mins. At the end of incubation, the cells were subjected to heat shock for 45 secs in a 42 °C water bath, followed by incubation at 37 °C for 1 min. The cells were then added to 200 μL of Super Optimal Broth with Catabolite repression (S.O.C) media (Invitrogen) and incubated at 37 °C for 1 hr (for cDNA) or 4 hrs (for pFastBac1™ vector). The transformed cells were then plated on YT plates containing 100 μg/mL of ampicillin (YTamp). Plates were incubated overnight at 37 °C and an overnight culture was prepared by inoculating a single colony from this plate into 40 mL of 2xYT media supplemented with 100 μg/mL of ampicillin (2YTamp).

2.2.2.3 Generation of histidine tagged constructs

Plasmid DNA was extracted from the overnight culture using a QIAGEN plasmid mini kit as per manufacturer's instructions. The histidine tags (His-tag) on GPR41 and GPR43 constructs were generated and amplified by polymerase chain reaction (PCR) with specifically designed forward and reverse primers, shown in Figure 2-2. The PCR was carried out by adding forward and reverse primers (0.5 μg of each) to 0.2 mM of dNTP, 5 units/μL of *Taq* polymerase (New England Biolabs), 2.5 μL of 10x PCR buffer (New England Biolabs) and 50 ng of template DNA. The final volume was made up to 50 μL with sterile water. The PCR was initiated by denaturing the template DNA at 93 °C for 3 mins. The template was then amplified using 35 cycles of: DNA denaturation (94 °C, 45 secs), primer annealing (55 °C, 45 secs) and polymerase extension (72 °C, 5 mins). A single cycle of final extension was carried out at 72 °C for 7 mins to complete the amplification process. PCR products were then loaded on a gel consisting of 1% w/v agarose in Tris-acetate EDTA (TAE) buffer made of 40 mM Trizma® Base, 20 mM acetic acid and 1.27 mM ethylenediaminetetraacetic acid (EDTA) and electrophoresis was carried out at 100 V until the dye line was approximately 70% of the way down the gel. DNA gel was stained in ethidium bromide/TAE buffer

and visualised by exposure to UV light. The size of each fragment was assessed by comparison with DNA molecular markers (New England Biolabs). GPR41 and GPR43 constructs incorporated with a deca His-tag on the N terminus are referred to as His_{10}-GPR41 and His_{10}-GPR43, respectively. GPR41-His_{10} and GPR43-His_{10} refer to 10 His-tag fused to C-terminus of GPR41 and GPR43, respectively. Wild type constructs without incorporation of any His-tag were generated; they are referred to herein as GPR41 and GPR43.

2.2.2.4 Cloning of GPR41 and GPR43 constructs into pFastBac1™ vector

Figure 2-3 shows the restriction enzyme cut sites that are available for cloning within the pFastBac1™ vector. The PCR products were cloned within XhoI and HindIII cut sites. PCR products generated from section 2.2.2.3 and the pFastBac1™ vector were digested with XhoI and HindIII restriction enzymes. The digested DNA was separated using DNA electrophoresis and the desired DNA fragments on the gel were excised from the agarose and extracted using a QIAQUICK Gel Extraction Kit (QIAGEN). Digested GPCR cDNA was combined with digested pFastBac1™ vector (100 ng) at 1:3 molar ratio of vector:insert. DNA mixture was added to 1 μL of ligase buffer (New England Biolabs) and 1μL T4 DNA ligase (New England Biolabs) and the final volume was made up to 10 μL with sterile water. The ligation reaction was carried out at 4 °C overnight and on the following day the reaction mixture was transformed into chemically competent *E. coli* cells. Transformation was carried out by heat shock method described in section 2.2.2.2. The transformed cells were plated on YTamp plates to isolate single colonies. A single colony was used to set up the overnight culture by inoculating into 2YTamp media.

GPR41

Forward:
5' gggcccactcgagatggatacaggccccgaccagtcctacttctccggcaatc 3'

Reverse:
5'ctgcaagcttctagctttcagcacaggccacctggccaccagttccgcagcc 3'

His_{10}- GPR41

Forward:
5'gggcccactcgagatgcatcaccatcaccatcaccatcaccatcacgatacaggccccgaccagtcctacttctccggcaatc 3'

Reverse:
5'ctgcaagcttctagctttcagcacaggccacctggccaccagttccgcagcc 3'

GPR41-His_{10}

Forward:
5' gggcccactcgagatggatacaggccccgaccagtcctacttctccggcaatc 3'

Reverse:
5'ctgcaagcttctagtgatggtgatggtgatggtgatggctttcagcacaggccacctggccaccagttccgcagcc 3'

GPR43

Forward:
5' gggcccactcgagatgctgccggactggaagagctccttgatcctcatggctt 3'

Reverse:
5' ctgcaagcttctactctgtagtgaagtccgaacttggcatcccttctcct 3'

His_{10}-GPR43

Forward:
5'gggcccactcgagatgcatcaccatcaccatcaccatcacctgccggactggaagag ctccttgatcctcatggctt 3'

Reverse:
5' ctgcaagcttctactctgtagtgaagtccgaacttggcatcccttctcct 3'

GPR43-His_{10}

Forward:
5' gggcccactcgagatgctgccggactggaagagctccttgatcctcatggctt 3'

Reverse:
5' ctgcaagcttctagtgatggtgatggtgatggtgatgctctgtagtgaagtccgaacttggcatcccttctcct 3'

Figure 2-2 Primers used to generate His-tag constructs of GPR41 and GPR43.

These sets of primers were used to generate a deca His-tag on N or C-terminus of GPR41 and GPR43 constructs

Figure 2-3 Schematic diagram of the pFastBac1™ vector used in this study.
Diagram adapted from Invitrogen (2004).

Recombinant vector were extracted from the overnight culture using a QIAGEN plasmid mini kit. The extracted vector DNA was subjected to restriction enzyme digestion and the size of each fragment was analysed by DNA gel electrophoresis. Clones that generated DNA of the expected size were selected and confirmed by DNA sequencing (SUPAMAC, Sydney University Prince Alfred Molecular Analysis Centre).

2.2.2.5 Constructions of recombinant baculovirus DNA (bacmid)

Constructs in pFastBac1™ vector confirmed by DNA sequencing were used to generate recombinant bacmid DNA by transformation into a special strain of *E. coli*, DH_{10Bac}™. Transformation procedures were carried out as described in section 2.2.2.2 by adding 1 ng of recombinant vector into 100 μL of DH_{10Bac}™ cells. The cells were added to 900 μL of S.O.C medium and incubated in a shaking incubator for 4 hrs at 37 °C. At the end of incubation, 100 μL of culture was plated onto Luria Bertani (LB) agar plate (1% w/v Tryptone, 0.5% w/v yeast extract, 1.0% w/v NaCl pH 7.0) containing 50 μg/mL kanamycin, 7 μg/mL gentamicin and

10 μg/mL tetracycline for DH_{10Bac}™ selection; 100 μg/mL of Bluo-gal and 40 μg/mL of IPTG were added for detecting *LacZ* interrupted clones. Plates were incubated for 48 hrs at 37 °C. A single white colony of DH_{10Bac}™ cells was isolated and re-streaked onto a fresh LB agar plate to verify the colony phenotype.

Once the colony was verified, it was inoculated into 2 mL of LB media supplemented with antibiotics as described above. The cell culture was incubated at 37 °C, shaking at 250 rpm until the cells reached stationary phase. The culture was then centrifuged for 1 min at 14, 000 x g to pellet cells and the cell pellet was suspended in 0.3 mL of Solution I (15 mM Tris-HCl pH8.0, 10 mM EDTA, 100 μg/mL RNase A). The mixture was vortexed and mixed with 0.3 mL of Solution II (0.2 N NaOH and 1% SDS). After 5 mins incubation at room temperature, 0.3 mL of 3 M potassium acetate at pH 5.5 was added. The sample was then incubated on ice for 10 mins and followed by centrifugation at 14, 000 x g for 10 mins. The supernatant, containing bacmid DNA, was transferred to 0.8 mL of isopropanol and incubated on ice for 10 mins. The sample was re-centrifuged at 14, 000 x g for 15 mins to isolate the pellet. Ethanol (0.5mL of 70% stock) was added to the pellet and was centrifuged at 14, 000 x g for 5 mins. The DNA pellet was air-dried at room temperature to evaporate the ethanol and then dissolved in 40 μL of 1x TE buffer at pH 8.0. The method above was used to isolate bacmid DNA for all constructs used in this study.

The recombinant bacmid DNA was verified by PCR analysis. Gene and bacmid specific primers were used. The bacmid specific primers were designed as follows; M13 forward (-40) (5'd [GTTTTCCCAGTCACGAC] 3') and M13 reverse (5'd [CAGGAAACAGCTATGAC] 3'). These sequences were provided in the Bac-to-bac Expression kit manual (Invitrogen, 2004). DNA gel electrophoresis was used to verify the PCR products and verified bacmid DNA stocks were stored at 4 °C until required.

2.2.2.6 Transfection of insect cells with recombinant bacmid DNA to generate recombinant baculoviruses

Insect cells (*Sf21*) were seeded in a 6-well tissue culture plate (Nunc, Thermo Scientific) at 9 x 10^5 cells per well. The bacmid (1 μg) was diluted in 194 μL of Sf900-II serum free insect culture media (Invitrogen) and 6 μL of Cellfectin® reagent (Invitrogen) was added to the mix. DNA/lipid complex formation was promoted by room temperature incubation for 45 mins. After incubation, the mixture was made up to 1 mL with Sf-900 II media and added to each well containing insect cells. Cells were incubated at 27 °C for 5 hrs, followed by replacement of the media with 2 mL of fresh Sf900-II media. The cells were then incubated in a 27 °C humidified incubator and monitored every 24 hrs. Cell morphology changes and a decrease in cell viability generally become noticeable within 72 hrs post infection. Cell culture were analysed for signs of bacmid infection by light microscopy and staining with trypan blue (0.05% in PBS, diluted 1:1 with cells). At 72 hrs post infection, the culture was harvested and was centrifuged at 750 x g for 10 mins. The supernatant was then collected and filtered (0.2 μm). The supernatant represents the P0 viral stock. The P0 viral stock was used for plaque purification (as described in section 2.2.2.7) to obtain purified P1 viral stock and subsequently used for viral stock amplification to P2, P3 and P4 viral stocks.

2.2.2.7 Insect cell culture

Suspension cultures of *Sf9* or *Sf21* cells were grown routinely in our lab using Sf-900 II media in sterilised Schott bottles with a loosened lid to allow for airflow. Culture volumes were usually no more than a quarter of the total bottle volume. Both cell lines were maintained at cell density of 1 x 10^6 cells/mL to 3 x 10^6 cells/mL. Cell density of 1 x 10^6 cells/mL was used for virus amplification and 2 x 10^6 cells/mL was used for protein expression in this study. Cell cultures were incubated at 27 °C with shaking at 130 rpm. Cells were routinely split every 3-4 days.

2.2.2.8 Plaque assay

A plaque assay was carried out for plaque purification of P0 viral stock to obtain purified P1 viral stock and was also used to determine viral titres for P2, P3 and P4 viral stocks. The assay was carried out by seeding 5 x 10^5 cells/well in a 6-well tissue culture plate. Cells were incubated overnight in a 27 °C humidified incubator. On the following day, serial dilutions (10^{-1} to 10^{-6}) of virus stock were prepared in Sf-900 II media to a final volume of 200 µL. In the 6-well tissue culture plate, the media in each well was replaced with 0.5 mL of Sf-900 II media and 100 µL of each diluted virus was added to each well. Cells were then incubated for 1 hr at 27 °C. During incubation, plaquing medium (1% low-melting agarose gel) was heated in a microwave oven with the melted agarose and Sf-900 II media kept at 37 °C until required. After cell incubation, 1% agarose was diluted to 0.5% in the Sf-900 II media. The cell media was aspirated off from each well and immediately replaced with 2 mL of the diluted agarose. The agarose was allowed to set by incubating at room temperature for 15 mins and 1 mL of Sf-900 II media was added on top of the agar to prevent it from drying out during the subsequent incubation period. The tissue culture plate was then incubated at 27 °C for 7 days in a humidified incubator. After incubation, the culture plate was examined for presence of plaques. The number of plaques were counted to determine the plaque titre and/or isolated for plaque purification prior to staining of the plate.

Plaque purification

A plastic pipette tip was used to penetrate and extract the agarose and viral plaque. The agarose/plaque was then dispensed into a new well of a 6-well tissue culture plate that was seeded with cells at 5 x 10^5 cells/well for virus amplification. This plate was then incubated at 27 °C in a humidified incubator and the supernatant was collected at 72 hrs post infection or when signs of viral infection were visible. The supernatant represents the purified P1 viral stock from which virus DNA were isolated using Easy DNA kit (Invitrogen) for verification of purity by PCR with specific primers outlined in section 2.2.2.5.

Plaque staining

For virus titre determination, identified plaques were stained with freshly diluted 0.05% neutral red in PBS (2 mL) and incubated for 6 hrs at room temperature, followed by overnight incubation with fixer solution (2mL of 0.15 M NaCl/ 1% formalin). On the following day, the tissue culture plate was washed under the tap to remove the stain and agarose. The virus titre is expressed in plaque forming unit per mL (pfu/mL). The number of plaques in each well was counted and the virus titre was calculated using Equation 1.

$$\text{Virus titre (pfu/mL)} = \text{number of plaques} \times \text{dilution factor} \times \frac{1}{1\ \text{mL of inoculum/well}}$$

Equation 1 Calculation of virus titre from plaque assay

2.2.2.9 Virus stock amplification

The virus titres were used to determine the volume of inoculum for generating P2, P3 and P4 virus stocks of all constructs in this study. Baculovirus P1 stocks of $G\alpha_i$, $G\beta$ and $G\gamma$ fused with His-tag on C-terminal ($G\gamma$-His) were generously supplied by Dr. Richard Glatz from SARDI. Each virus stock was amplified using a Multiplicity of Infection (M.O.I) of 0.1. The volume of inoculum for viral amplification was determined by Equation 2.

$$\text{Volume of inoculum required (mL)} = \frac{(\text{M.O.I} \times \text{number of cells}) \times \text{virus titre (pfu/mL)}}{}$$

Equation 2 Calculation of virus inoculum (mL) for viral amplification

2.2.2.10 Insect cells expression of GPR41 and GPR43 constructs

Insect cells, *Sf9* and *Sf21,* at cell density of $2x10^6$ cells/mL were set up for small-scale expression studies. A 50 mL culture was infected with GPR41-His_{10} or GPR43-His_{10} viruses at M.O.I of 1, 3, 5 or 10. Four 50 mL cultures were set up for each M.O.I and each culture was harvested at intervals of 24 hrs and up to 96 hrs by low speed centrifugation at 750 x g for 10 mins (Allegra6R, Beckman). Infected insect cell membrane fractions were prepared as described in the following section 2.2.2.11.

2.2.2.11 Insect cell membrane preparation

All membrane preparation steps were carried out with ice-cold buffers at 4 °C with the inclusion of fresh protease inhibitors: 0.1 mM phenylmethylsulfonyl fluoride (PMSF), 2 μg/μL aprotinin, 4 mM leupeptin and 10 μM E64. Infected cells were subjected to low speed centrifugation and the cell pellet was washed twice with PBS buffer. The cell pellet was then suspended at a cell density of 4 x 10^7 cells/mL in buffer A (20 mM HEPES pH 8.0, 150mM NaCl and 5% glycerol). Cells were disrupted by Ultrasonic liquid processor S-4000 (Misonix) for 15 secs with an amplitude of 40 and then returned to ice for 30 secs; these steps were repeated 10 times. The suspension was then centrifuged at 500 x g for 15 mins to remove unbroken cells and nuclear material. The supernatant was then re-centrifuged at 80,000 x g (Optima™ L-90K, Beckman) for 1 hr at 4 °C to pellet the membrane fractions. The membrane pellet was washed and resuspended in buffer A at a final protein concentration of 5 mg/mL. Protein concentrations were determined by modified Bradford method (Reisner et al., 1975; Spector, 1977). The suspension was stored at -80 °C until required.

2.2.2.12 Measurement of receptor expression by ELISA

Total protein concentration of membrane fractions prepared in 2.2.2.11 was adjusted to 1 mg/mL and dispensed into each well of a 96 well plate (100 μL/well; Maxisorp, Nunc). The plate was incubated at 37 °C for 1 hr to allow attachment of membrane to the surface of the well. The excess solution from each well was then aspirated off and the surface of the well was blocked in 1 % casein in PBS for 1 hr at room temperature with gentle shaking. Subsequently, the blocking solution was replaced with primary anti-His antibody at 1:1,000 (PentaHis, QIAGEN) and incubated for 1 hr at 37 °C with gentle shaking. Bound primary anti-His antibody was detected by incubation with secondary goat anti-mouse horseradish peroxidase (HRP) conjugated antibody (Biorad, Australia) at 1:5,000 for 1 hr with gently shaking. Each well was washed 5 times with 150 μL of TBST (Tris buffered saline with 0.05% Tween-20) after primary and secondary antibody incubation. A final wash was performed with citrate-EDTA (pH 5.5) buffer and followed by the addition of 100 μL TMB solution (0.1 mg/mL of 3,3',5,5'-tetramethylbenzidine, 1% dextran sulphate, 10 mM citrate-EDTA and 0.0002% hydrogen peroxide). Plates were incubated at room temperature for 5 mins and 100 μL of stop solution (0.5 M sulphuric acid) was added to each well. The absorbance of the reactants in the wells of the 96-well plate was read at 450 nm in a plate reader (Labsystem Multiskan MS, Thermo Fisher Scientific).

2.2.2.13 Sodium dodecyl sulphate polyacrylamide gel electrophoresis (SDS-PAGE) and Western blot

SDS-PAGE

Membrane samples were analysed by SDS-PAGE based on a method developed by Laemmli (Laemmli, 1970). The NuPAGE® Gel system was used in combination with 4-12% Bis Tris Pre-Cast NuPAGE gels in MOPS or MES running buffer (Invitrogen, Australia). Protein samples were added to lithium dodecyl sulphate (LDS) loading buffer (Invitrogen, Australia) supplemented with 1 mM

DTT. BenchMark Pre-stained protein ladder or SeeBlue Plus 2 Pre-stained standard marker (Invitrogen, Australia) was also loaded onto the gel. Samples were incubated at 50 °C for 5 mins prior to loading and the gel was run under constant voltage (200 V) for 45 mins.

Western Blot detection

For Western blot detection of GPR41 and GPR43, several primary antibodies were trialled to optimise the conditions for detection. Receptor-specific antibody for GPR41 (sc-98332) and GPR43 (sc-32906) were purchased from Santa Cruz Biotechnology. His-tag antibody (QIAGEN) was used to detect His-tag constructs. The protocol below describes the conditions for Western Blot detection using the anti-His antibody.

Proteins from SDS-PAGE were transferred to a 0.45 μm nitrocellulose membrane using a wet transfer system (Biorad, Australia). The transfer was carried out for 1 hr at 200 mA in a cold transfer buffer (20 mM Tris Base, 160 mM glycerine and 20% methanol). The nitrocellulose membrane was then blocked for 1 hr in 1% casein in TBST, followed by incubation overnight with primary anti-His mouse antibody at 1:1,000. Subsequently, the membrane was incubated with goat anti-mouse HRP conjugated secondary antibody (1:20,000, Biorad) for 1 hr. Washing was carried out with 3 washes of 15 mins each of TBST, after incubation with the primary and secondary antibodies. Protein bands were visualised using a chemiluminescent HRP substrate (GE Health, Australia) according to the manufacturer's instructions. The blots were scanned on a VersaDoc Molecular Imager system (Biorad, Australia).

2.2.2.14 Co-expression of GPR41-His_{10} or GPR43-His_{10} with G protein subunits

Insect cells *Sf9* were seeded in a 25 cm tissue culture flask (Nunc, Thermo Scientific) at 6 x 10^6 cells/flask in a final volume of 10 mL. The cells were infected with GPR41-His_{10} or GPR43-His_{10} virus at M.O.I of 1, 3, 5 or 10, while keeping G protein subunits M.O.I constant at 2:2:1 for $G\alpha_i$: $G\beta$: $G\gamma$-His viruses. The infected cells were harvested at 48 hrs, 72 hrs and 96 hrs post infection and cell pellets were used to prepare membrane fractions as described in section 2.2.2.11.

2.2.2.15 Fluorescence ligand binding assay

Control (uninfected *Sf9*) insect cells and GPR43-His_{10} infected *Sf9* cells were used to set up a fluorescence assay with 4-methylumbelliferyl butyrate. Briefly, 10 μg of sample was added to 100 mM of 4-methylumbelliferyl butyrate in an eppendorf tube and incubated for 1 hr at 27 °C. At the end of incubation, each tube was centrifuged at 20,000 x g for 30 mins to pellet the sample and to remove any unbound ligand. The pellet was washed and suspended in Buffer A and transferred to a black 96-well plate (Greiner Bio-One). Porcine esterase (9 μg) was added to each well and fluorescence measurement was carried out on a FLUOstar OPTIMA (BMGLab) fluorometer at 330 nm excitation and 450 nm emission wavelengths.

2.2.2.16 [^{35}S] GTPγS binding assay

Interactions between GPR41/GPR43 and G protein were measured using a modified method of the [^{35}S] GTPγS binding assay (Windh and Manning, 2002). Two samples were trialled in this assay i) insect cell membranes expressing GPR41-His_{10}/GPR43-His_{10} were prepared as described in section 2.2.2.10 and G proteins were added individually to the assay and ii) insect cell membranes

expressing GPR41-His_{10}/GPR43-His_{10} and G protein subunits prepared as described in section 2.2.2.14.

For both samples, the assays were prepared in a 96-well plate (Nunc v-well, Thermo Scientific). Total assay volume of 75 µL was made up with TMN buffer (50 mM Trizma® pH 7.6, 10 mM $MgCl_2$, 100mM NaCl). Reactions were initiated by addition of buffer (basal) or 166 mM propionic acid (agonist) to the sample mix. The 96-well plate containing samples was incubated at 27 °C with shaking (250 rpm) for 90 mins (TITRAMAX 101, Heidolph Instruments). At the end of incubation, 75 µL of the samples were transferred to a MultiScreen™ 96 well filter plate (MHVBN45, Millipore) and the assay was terminated by rapid filtration using Multiscreen™ Vacuum manifold system (Millipore). The excess unbound [^{35}S] GTPγS was removed by thoroughly washing the samples with 5 x 200 µL of buffer and filtering it through the wells. The filter plate was then air-dried overnight. Ultima Gold™ (Perkin Elmer) liquid scintillant (75 µL) was added to each well and [^{35}S] was detected in a Wallac MicroBeta TriLux 1450LSC Counter (Perkin Elmer). The plates were sealed with adhesive clear film and each well was counted for 20 secs. The level of [^{35}S] GTPγS (pmoles) bound per mg of proteins was calculated based on Equation 3.

$$\text{pmol/mg} = \frac{\text{(cpm total – cpm non-specific) x pmol [35S] GTPγS}}{\text{cpm added x mg proteins}}$$

Equation 3 Calculation of agonist-induced [^{35}S] GTPγS binding activity (Wieland and Seifert, 2006).

2.2.2.16.1 [^{35}S] GTPγS binding assay on cell membranes containing GPR41-His_{10} /GPR43-His_{10}

GPR41-His_{10} or GPR43-His_{10} containing membranes were used for optimisation of [^{35}S] GTPγS binding assay. This project was fortunate to inherit a small amount of purified $G\alpha_i$-His from a previous project carried out in the lab

(expressed and purified by Dr. Amanda Aloia) and Gβγ subunits were sourced from Calbiochem. The assay conditions were first trialled with 0.2 nM of [^{35}S] GTPγS, 6.75 μM GDP, 10 μg sample, and 2.5 nM purifiedG proteins in TMN buffer. Subsequently, different concentrations of propionic acid, [^{35}S] GTPγS, GDP and purified $G\alpha_i$-His, Gβγ subunits were trialled for optimisation of the binding assay.

2.2.2.16.2 [^{35}S] GTPγS binding assay on cell membranes containing GPR41-His-$_{10}$/GPR43-His$_{10}$ co-expressed withG proteins

An assay mix consisting of 10 μg membrane (GPR41-His$_{10}$/GPR43-His$_{10}$ andG proteins) sample prepared from section 2.2.2.14, 5 μM GDP and 0.4 nM [^{35}S] GTPγS was added to TMN buffer. The assays were prepared in a 96 well plate and reaction was initiated by addition of either buffer (basal) or 166 mM propionic acid to the mix. Non-receptor induced [^{35}S] GTPγS was determined with cell membrane fractions expressed withG proteins only. Incubation and reading of [^{35}S] GTPγS binding were carried out as described in section 2.2.2.16.

2.3 Results

2.3.1 Cloning and generation of recombinant viruses for GPR41 and GPR43 constructs

Plasmid vectors consisting of cDNA encoding human GPR41 and GPR43 receptors were used to generate constructs with a His-tag fused to either the C or N-terminus (shown in Figure 2-4). Wild type constructs without any modification were also generated. PCR products, generated with a set of specific primers, were analysed by agarose gel electrophoresis, as shown in Figure 2-5. The estimated size of the major PCR product was 1 kb, although several bands between 2 kb and 1 kb were also noted. These bands were considered to be due to non-specific binding of primers, generating different size DNA products.

Figure 2-4 Schematic diagram of GPR41 and GPR43 constructs used in this project.
Constructs consist of wild type, N-terminal His-tag and C-terminal His-tag receptors.

Figure 2-5 1% agarose gel showing GPR41 and GPR43 constructs.

PCR products generated with a set of primers designed to incorporate a His-tag fused at the C or N terminus of the receptors; reactions were set up in duplicate. Lane description: 1 and 2 – GPR43, 3 and 4 – His_{10}-GPR43, 5 and 6 – GPR43-His_{10}, 7 and 8 – GPR41, 9 and 10 – His_{10}-GPR41, 11 and 12 – GPR41-His_{10}. Arrow indicates the 1 kb expected size of the PCR products.

The PCR products were cloned into pFastBac1™ vector via *Xho*I and *Hind*III restriction enzyme cut sites, followed by transformation into $DH_5\alpha$ cells. Colonies containing of recombinant pFastBac1™ plasmid were isolated and confirmed by DNA sequencing. They were then transformed into DH_{10Bac} cells to generate recombinant bacmid.

Selectively grown DH_{10Bac} colonies containing recombinant bacmid were isolated and the bacmids were extracted. Recombinant bacmids were verified by PCR and analysed by agarose gel electrophoresis. Two bands were seen at 3.3 kb and 1.7 kb, as shown in Figure 2-6. The expected size of the PCR product generated with the bacmid specific primers is 3.3 kb and the 1.7 kb bands were considered to be PCR products resulting from non-specific binding of primers. The recombinant bacmids were then used to transfect *Sf21* cells for recombinant virus production.

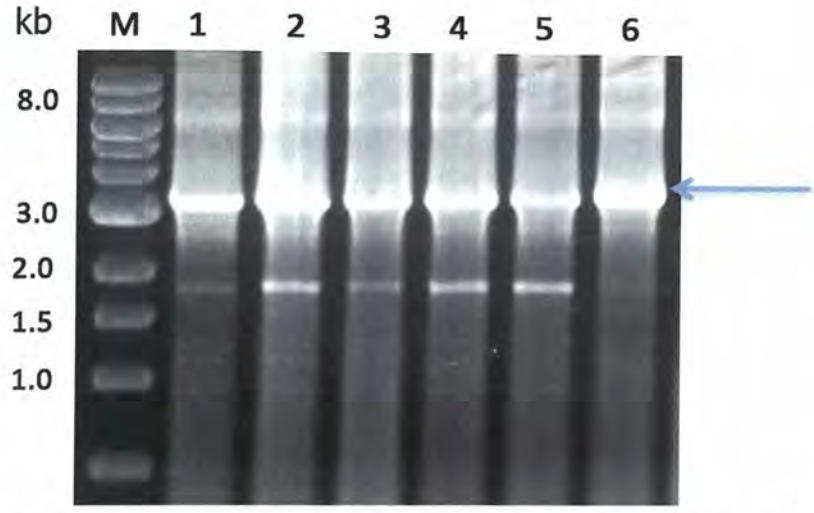

Figure 2-6 1% agarose gel verifying recombinant bacmid by PCR with M13 forward and M13 primers.

Lane description: 1 – GPR41, 2 – His_{10}GPR41, 3 – GPR41-His_{10}, 4 – GPR43, 5 – His_{10}GPR43 and 6 – GPR43-His_{10}. Arrow indicates the expected size (3.3 kb) of PCR products.

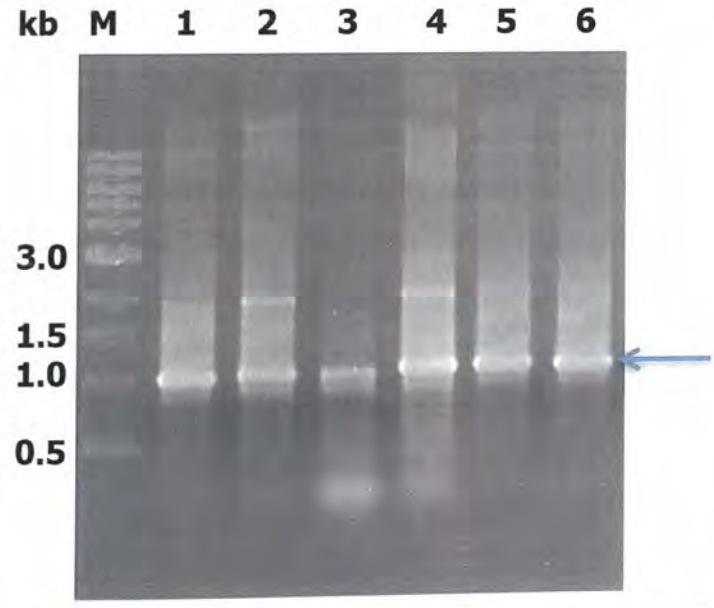

Figure 2-7 1% agarose gel verifying the presence of recombinant viruses by GPR41 or GPR43 specific primers.

Lane description: 1 – GPR41, 2 – His_{10}GPR41, 3 – GPR41-His_{10}, 4 – GPR43, 5 – His_{10}GPR43 and 6 – GPR43-His_{10}. Arrow indicates expected size (1 kb) of PCR products.

Recombinant viruses were plaque purified and the viral DNA was extracted. PCR reactions carried out with GPR41 or GPR43 specific primers generated a band at the expected size of 1 kb, as shown in Figure 2-7. It was noted that in some of

the lanes there were faint bands at approximately 2 kb; these were also observed in previous PCR reactions carried out to generate GPR41 and GPR43 constructs, as shown in Figure 2-5.

Recombinant viruses from plaque purification were used to upscale virus stocks. *Sf21* cells were infected at $1x10^6$ cells/mL for 3 rounds to generate high titre virus stocks. Titres for each passage of virus were determined by plaque assay and virus titres were achieved at approximately 1×10^8 pfu/mL to 3×10^8 pfu/mL. The virus stocks were then used to infect *Sf21* or *Sf9* insect cells for small-scale protein expression studies.

2.3.2 Optimisation of Western blot conditions for detection of GPR41 and GPR43 constructs.

Western blots using the commercially available GPR41 and GPR43 primary antibodies did not yield specific bands. Optimisation of the primary antibody incubation time from 1 hr to overnight still did not result in any signal. Dilutions ranging from 1:100 to 1:1,000 were attempted for both antibodies. None of the conditions attempted was able to produce a convincing signal (data not shown).

Since the constructs were generated with a His-tag fused to either the N- or C- terminus, His-tag antibodies were employed as an alternative means to detect the expressed receptors. A His-tag antibody was sourced from QIAGEN (penta-His antibody), and as shown in Figure 2-8A, this antibody was able to detect GPR41-His_{10} and GPR43-His_{10}. No signal was observed for the negative controls, which were uninfected *Sf21* cells, GPR41 infected cells and GPR43 infected cells. Both GPR41-His_{10} and GPR43-His_{10} were detected as a ladder of bands with polypeptides with apparent molecular masses of with approximately 32 kDa, 51 kDa, 64 kDa and 97 kDa. These bands are considered to be GPR41-His_{10} and GPR43-His_{10}, as they are not seen with the control samples. At approximately 32 kDa, a doublet band was observed for GPR41-His_{10} and three faint bands were observed for GPR43-His_{10} (indicated by black arrow). These are most likely the

monomeric forms of both receptors. The lowest band at 32 kDa could be the non-glycosylated form of the monomer and the bands above it may be the glycosylated forms. The 64 kDa and 97 kDa bands may correspond to the dimer and trimer, respectively. The 51 kDa band and several higher molecular mass species were also detected. Since these bands were not observed in the negative control samples, they may be other forms of GPR41-His_{10} and GPR43-His_{10}.

Expression of His_{10}-GPR41 and His_{10}-GPR43 in *Sf21* were analysed using the same anti-His antibody from QIAGEN. As shown in Figure 2-8B, the antibody was unable to detect His_{10}-GPR41 and His_{10}-GPR43. This is unlikely to be caused by the Western blot condition or the sensitivity of the antibody, as it was able to detect the C-terminal His-tag receptors and the positive control that generated a signal at the expected size. This is further discussed in section 2.4.1.

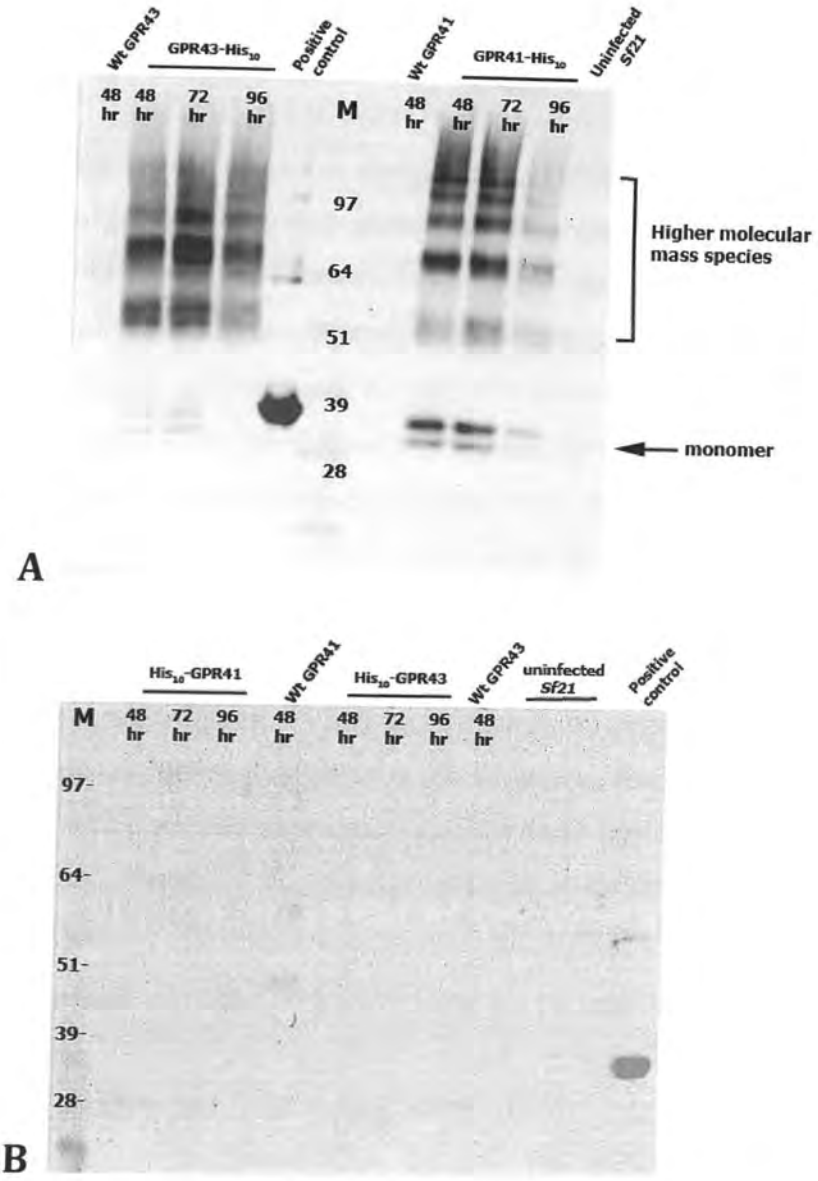

Figure 2-8 Western blot results showing expression of GPR41 and GPR43 constructs in *Sf21* insect cells probed with anti-His antibody.

Expression of (A) C-termini His-tag or (B) N-termini His-tag GPR41 and GPR43 in *Sf21* cells. Cells were infected at M.O.I 3 and harvested at different time points post-infection (48, 72 and 96 hrs). Uninfected *Sf21* cells were used as negative control and positive control consists of a purified His-tag protein (35 kDa). Pre-stained molecular marker (M) was run in parallel.

2.3.3 Optimisation of GPR41-His_{10} and GPR43-His_{10} expressions

Expressions of the receptors were optimised by varying a few parameters: (i) harvesting time, (ii) multiplicity of infection (M.O.I), which is the ratio of virus to target cells and (iii) choice of insect cell lines *Sf21* or *Sf9*. Expression levels of GPR41-His_{10} and GPR43-His_{10} were quantified by ELISA using the anti-His antibody, which was shown to detect these receptors (refer to section 2.3.2). The polyhedrin promoter of baculovirus drives expression of the protein between 24 hrs and 96 hrs post infection. Therefore, it is important to determine the best harvesting time where the highest level of recombinant protein is expressed. The amount of virus used to infect cells is critical, as all cells should be infected simultaneously to achieve the optimal expression level. An M.O.I of 1 or higher is commonly used to infect cells for protein expression. In this study, four M.O.I values were tested (1, 3, 5 and 10) to determine the least amount of virus required to achieve highest level of protein expression. Most of the attempts to express GPCRs in baculovirus have been carried out in *Sf9* cells (Schneider and Seifert, 2010). However, expression patterns of different proteins can vary considerably in different cell lines (Akermoun et al., 2005). Expression trials of GPR41-His_{10} and GPR43-His_{10} in the two cell lines were carried out in this study.

Different harvesting time points appeared to have an effect on the expression of GPR41-His_{10} in *Sf9* and *Sf21* cells. In *Sf9* cells, GPR41-His_{10} expression peaked at 48 hrs for all M.O.I studied. As for *Sf21* cells, the optimal harvesting time varied with M.O.I. For M.O.I values of 1 and 10, the highest level of expression was achieved as late as 96 hrs. In both cell lines, increasing M.O.I did not result in increased level of expression or GPR41-His_{10} being expressed earlier. These results suggest that all the cells were infected simultaneously even at an M.O.I of 1. By comparing the absorbance values at 450 nm (y-axis) in Figure 2-9A and B, *Sf9* cells are shown to have higher a level of expression of GPR41-His_{10} when compared to *Sf21* cells.

The level of expression of GPR43-His_{10} in *Sf9* and *Sf21* was affected by the harvesting time. The highest level of expression of GPR43-His_{10} in *Sf9* was

achieved with an M.O.I of 1 at 48 hrs post infection, no further increase in expression level was attained by increasing the M.O.I. This suggests that an M.O.I of 1 was sufficient for optimal expression of GPR43-His_{10} in *Sf9* cells (Figure 2-9C). By contrast, the M.O.I value was observed to exert a different effect in *Sf21* for GPR43-His_{10}. In this case a higher level of expression was observed in *Sf21* compared with the *Sf9* cells. Increasing protein expression and earlier harvesting time were observed with increasing M.O.I, as shown in Figure 2-9D. The highest expression of GPR43-His_{10} in *Sf21* cells was observed with M.O.I of 10 at 48 hrs.

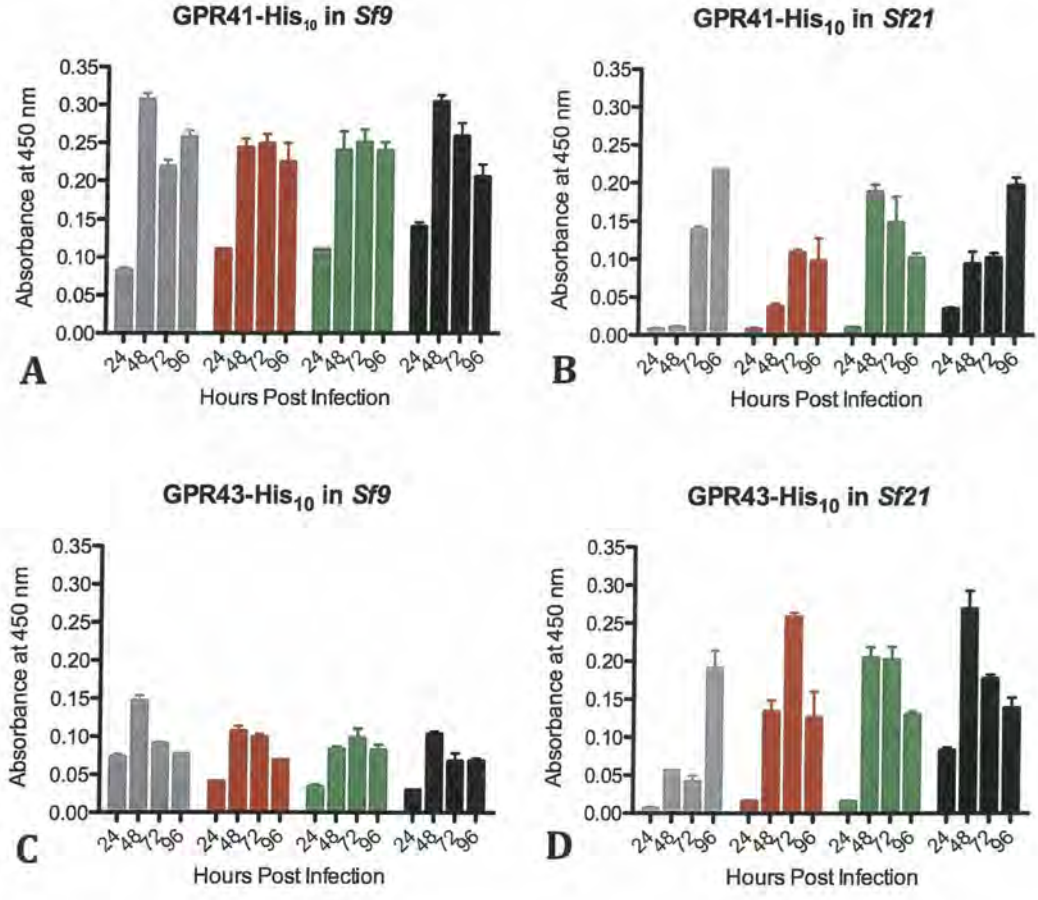

Figure 2-9 ELISA results showing expression of GPR41-His_{10} and GPR43-His_{10} in *Sf9* and *Sf21* insect cells.

(A) GPR41-His_{10} in *Sf9*, (B) GPR41-His_{10} in *Sf21*, (C) GPR43-His_{10} in *Sf9* and (D) GPR43-His_{10} in *Sf21*. Harvesting times and M.O.I were varied. M.O.I of 1 (grey), 3 (red), 5 (green) and 10 (black) were trialled and infected cells were harvested at 24 hrs, 48 hrs, 72 hrs and 96 hrs for analysis. Expression of receptors was detected by anti-His antibody. Each column shows mean ± SD of data from three replicates.

The Western blots of both receptors expressed in *Sf21* cells revealed the presence of higher molecular mass species. In order to determine if these higher molecular mass species were also expressed in *Sf9*, they were analysed by Western blot. As depicted in Figure 2-10, monomeric and higher molecular mass species were also observed in *Sf9* cells. In *Sf21,* GPR43-His_{10} was mainly expressed as higher molecular mass species with a low level of monomeric species. A similar result was also observed for GPR41-His_{10} in *Sf21* cells. Previous results in the laboratory on other GPCRs have found that sample consists mainly of the monomeric form have a higher ligand binding activity. Based on these data, *Sf9* cells were chosen for large-scale expression because the level of monomeric species was more abundant. Expressions of the receptors were carried out under optimal conditions as determined by ELISA, which was at an M.O.I of 1 with harvesting time at 48 hrs post infection.

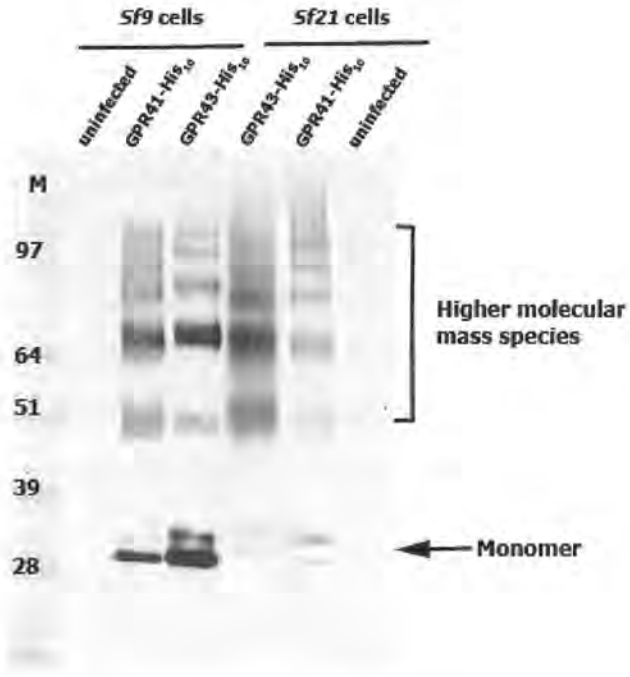

Figure 2-10 Western blot showing different expression profiles of GPR41-His_{10} and GPR43-His_{10} in *Sf9* and *Sf21* cells.

Expression of GPR41-His_{10} and GPR43-His_{10} in two cell lines were detected by anti-His antibody. Signal was not generated with negative controls (uninfected *Sf21* and *Sf9* cells). Pre-stained molecular weight marker (M) was run in parallel.

2.3.4 [^{35}S] GTPγS binding assay

2.3.4.1 Reconstitution of GPR43-His$_{10}$ with purified G protein subunits

The functionalities of GPR41-His$_{10}$ and GPR43-His$_{10}$ could not be determined by fluorescence ligand binding assay or radiolabelled ligand binding assays due to the low affinity of the agonists. An alternative method for assessing GPCR functionality is the [^{35}S] GTPγS assay (Cooper et al., 2009). This assay is routinely used to study GPCR and G protein signalling. It mimics the G protein cycle (shown in Figure 1-1) with the addition of a GPCR agonist resulting in the activation of the G protein cycle, and is followed by an exchange of GDP to GTP. In this assay, GTP was substituted with [^{35}S] GTPγS, which is a hydrolysis-resistant analogue of GTP. Therefore the accumulated [^{35}S] GTPγS is measured by the radioactivity.

This assay is routinely performed in mammalian cells for signalling studies. Unlike mammalian cells, insect cells may not express the appropriate subtype ofG proteins. It has previously been reported that GPR41 specifically couples to $G\alpha_i$ and that GPR43 may couple to either $G\alpha_i$ or $G\alpha_q$ (Brown et al., 2003). In this study, a preparation of insect cell membranes expressing GPR43-His$_{10}$ were reconstituted with purified $G\alpha_i$-His and $G\beta\gamma$. Initial experiments showed high basal binding activity of [^{35}S] GTPγS in the absence of agonist (propionic acid) and attempts were made to optimise the assay.

In the inactive state of the G protein cycle, the heterotrimeric G proteins are bound together with GDP, while GDP has been reported to decrease the basal binding level in the [^{35}S] GTPγS assay (Keen, 1998; Harrison and Traynor, 2003). As shown in Figure 2-11A, increasing the GDP concentration did reduce basal binding in the assay, however it did not improve the agonist-induced signal. The agonist-induced binding of [^{35}S] GTPγS was also not observed at any of the concentrations of GDP studied.

The amount of membrane material was also varied to determine if lower or higher levels of the membranes would improve the agonist-induced binding signal. As shown in Figure 2-11B, basal binding increased with increasing amount of the membrane sample, however, agonist-induced binding was not observed. The uninfected *Sf9* cell membrane sample showed a similar level of basal binding.

Subsequently, [^{35}S] GTPγS concentration was varied between 0.1 nM to 1 nM. Typically, 0.2 nM of [^{35}S] GTPγS is used in a GPCR and G protein reconstitution assay (Cooper et al., 2009). As shown in Figure 2-11C, increasing [^{35}S] GTPγS did not result in increasing specific binding of [^{35}S] GTPγS in the assay.

Finally, the [^{35}S] GTPγS binding assay was attempted with increased concentrations of purified G protein subunits. As shown in Figure 2-11D, increasing the G protein subunits concentration to 10 nM resulted in a slight increase in agonist-induced binding of [^{35}S] GTPγS; however, the increase is too low (approximately 200 cpm). A four-fold (2.5 nM to 10 nM) increase in G protein subunits should have led to a higher increase in [^{35}S] GTPγS binding, and as such, the increase was considered to be insignificant.

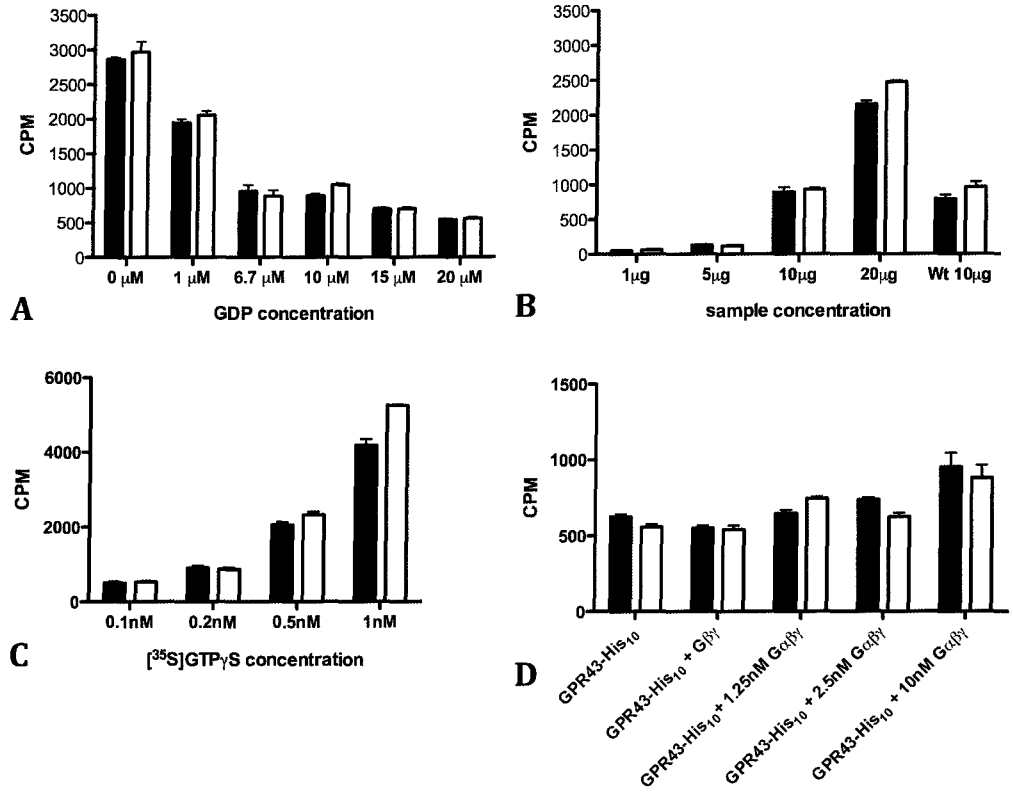

Figure 2-11 Optimisation of [^{35}S] GTPγS binding assay.

The assay was initially carried out for detection of GPR43-$His_{10}$with 10 μg of GPR43-His_{10} infected cell membrane samples in the presence of 0.2 nM of [^{35}S] GTPγS, 6.75 μM of GDP, 2.5 nM of purified Gαi-His and Gβγ subunits and the following conditions were altered to optimise the assay (A) varying GDP concentration or (B) varying sample concentration or (C) varying [^{35}S] GTPγS concentration or (D) varying G protein subunits concentrations. Basal binding was determined by the absence of agonist (propionic acid), shown by white bar and agonist-induced binding was determined by the addition of propionic acid, shown by black bar.

2.3.4.2 Co-expression of GPR43-His_{10} or GPR41-His_{10} with G protein subunits

Low titre virus stocks encoding $G\alpha_i$, Gβ and Gγ-His were used for virus amplification to obtain high titre virus stocks for expression. High titre virus stocks of Gαi-His and Gγ-His were obtained but virus amplification for Gβ was problematic, and as a consequence, G protein expression could not be carried out further. This is further discussed in section 2.4.1.

To determine if *Sf9* insect cells could express functional GPR41-His_{10} and GPR43-His_{10}, each receptor was co-infected with G protein viruses in a small scale (10 mL) culture and the cell membrane fractions were used for the [^{35}S] GTPγS assay. The signal to noise ratio of the [^{35}S] GTPγS assay was remarkably improved with these samples. The agonist-induced [^{35}S] GTPγS binding activities were expressed in pmol/mg using Equation 2-3. Results for GPR41-His_{10} co-expressed with theG proteins are shown in Figure 2-12A. Cells infected with GPR41-His_{10} at all M.O.I displayed [^{35}S] GTPγS binding activity as early as 48 hrs, with a gradual decline over time. The M.O.I did not appear to affect the level of activity for GPR41-His_{10}. The highest level of activity for GPR41-His_{10} was at 0.3 pmol of [^{35}S] GTPγS bound/mg of membrane sample protein. Figure 2-12B shows that the overall activity of GPR43-His_{10} was lower than GPR41-His_{10}. The highest activity observed for GPR43-His_{10} was approximately 0.35 pmol/mg with M.O.I of 3 at 72 hrs.

The aim of conducting this co-expression study with G proteins was to determine if *Sf9* cells could express GPR41-His_{10} and GPR43-His_{10} in a functional form, as determined by the [^{35}S] GTPγS assay. These results show that both GPR41-His_{10} and GPR43-His_{10} are expressed in a functional form in insect cell membranes.

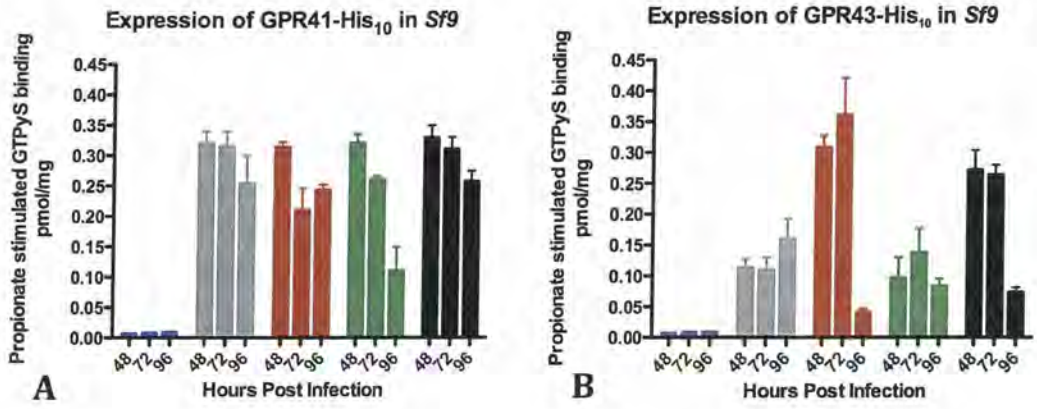

Figure 2-12 Assays of [^{35}S] GTPγS binding assays for GPR41-His$_{10}$ and GPR43-His$_{10}$ expressed in *Sf9* insect cells with co-expression of G proteins (Gαβγ).

(A) GPR41-His$_{10}$ or (B) GPR43-His$_{10}$ co-expressed with G proteins in *Sf9* cells. Cells were infected with G protein viruses at constant M.O.I (2:2:1 for Gα:Gβ:Gγ-His) and varying M.O.I for GPR41-His$_{10}$ or GPR43-His$_{10}$ viruses as indicated on the graph. M.O.I of 0 (control) (blue), 1 (grey), 3 (red), 5 (green) and 10 black) were trialled and infected cells were harvested at 48 hrs, 72 hrs and 96 hrs for analysis.

2.4 Discussion

2.4.1 Cloning and expression

Specific sets of primers were designed to amplify the GPR41 and GPR43 genes ready for expression with the incorporation of 10 histidine residues at either the N- or C-terminus. PCR products of expected size (1 kb) were observed along with small amounts of non-specific products that were larger than 1 kb. Non-specific binding of primers is not uncommon in PCR reaction and can be caused by non-specific annealing at the start of the reaction or when the concentration of primers is too high. The 1 kb bands encoding GPR41 and GPR43 constructs were excised from the gel, purified and used for ligation and transformation. The transformed clones were verified by DNA sequencing.

High titre virus stocks are essential for recombinant protein expression in insect cells because the virus titre is inversely related to the volume required for insect cell infection. Ideally, the virus titre should be of the order of 10^8 pfu/mL. For example, 20 mL of 1 x 10^8 pfu/mL of virus is required to infect 1 L of cells at an M.O.I of 1; however, if the titre is at 10^7 pfu/mL, 200 mL of virus will be required. Using a large volume of virus for expression is not practical as it increases the cost. In addition, large volumes of virus stocks reduce the amount of fresh media added to the suspension culture and result in nutrient depletion during expression, which is undesirable and can result in poor expression levels.

In this study, four rounds (P4) of virus amplification were required to achieve high titre virus stocks. On several occasions, amplified (P4) virus stocks had low virus titre. These virus stocks had to be discarded and the amplification step was repeated starting at P0. Low virus titre generally arise from transfecting insect cells with bacmid DNA of low purity, which consists of a mixture of empty and recombinant bacmid DNA. To overcome this issue, plaque purification of P0 virus stock was performed to isolate a plaque consisting only of the recombinant virus as verified by PCR.

A further problem arose in that; expression of G protein subunits was unsuccessful due to the Gβ virus remaining in 10^6 to 10^7 pfu/mL range after several rounds of virus amplification. Several attempts were made to plaque purify and amplify the virus but after substantial effort the titre remained low and was unsuitable for large-scale expression.

Several antibodies were trialled for detection of GPR41 and GPR43 on Western blots. The commercially available GPR41 and GPR43 antibodies used in this study were unable to detect the expressed receptors. These could be due the levels of expressions of the receptors were too low to be detected by the antibodies. To date, there is no publication on the use of the antibodies for detection of GPR41 and GPR43.

Western blots were probed with antibody targeting the His-tag on the receptor. The monomeric and higher molecular mass species of the C-terminal His-tag constructs were detected by anti-His antibody sourced from QIAGEN. GPR41 and GPR43 have predicted molecular masses of 38 and 37 kDa, respectively. However, the monomeric species of both receptors migrated with an apparent molecular mass of approximately 32 kDa. It is common for GPCRs and other membrane proteins to migrate slightly faster than the predicted size (Bane et al., 2007; Rath et al., 2009). The higher molecular mass species ranged from 49 to 98 kDa. These unlikely to be due to non-specific binding of the antibodies because they were not observed in the control samples. Since crude membrane preparations was used, different post-translational forms of these receptors could have been isolated from different compartments including Golgi apparatus, endoplasmic reticulum and plasma membrane. Therefore, it is possible that these high molecular species represent different post-translational and oligomeric forms of the receptors. Deglycosylation of the receptors was attempted using PNGase and endoglycosidases (generously supplied by Dr. Bill McKinstry from CSIRO). However, there was no significant difference observed between treated and non-treated samples. However, the lack of a positive control for the enzymatic deglycosylation reaction prevents us from drawing any conclusions from the result.

SDS and reducing agent-resistant higher molecular mass species have been reported for other GPCRs including B2AR (Salahpour et al., 2003) and the D_2 dopamine receptor (Guo et al., 2008). The formation of oligomers of GPR41-His_{10} and GPR43-His_{10} is unlikely to be an artefact due to expression in insect cells as they have also been observed in mammalian cells (Stoddart, 2007). It has also been suggested that GPCRs function as dimers or oligomers, and are capable of forming hetero-dimers with other subtypes (Issafras et al., 2002; Wang et al., 2005; Panetta and Greenwood, 2008; Hara et al., 2009; Jockers and Kamal, 2011).

Sf21 and *Sf9* cell lines are derived from *Spodoptera frugiperda*. These two cell lines are routinely used in our lab for protein expression and therefore were used for expression studies of GPR41 and GPR43. Although there are no major differences between *Sf21* and *Sf9* cells, this study showed that the expression profiles for GPR41 and GPR43 are different in these two cell lines. Multiple species of both receptors were observed in *Sf9* cells, including monomeric and high molecular mass species; expression in *Sf21* cells resulted in mainly oligomeric species. Varying expression efficiencies between *Sf21* and *Sf9* insect cells has been observed with different GPCRs (Akermoun et al., 2005). Our results support the suggestion that testing of different cell lines is useful to obtain optimal expression of GPCRs. The High-Five™ cell line derived from *Trichopulsia ni* species, has been reported to give highly efficient expression for certain recombinant proteins; an example is the thermo-stabilised construct of B1AR used for crystallisation (Warne et al., 2003). A small volume of High-Five™ was obtained and attempts were made to maintain the cell line (These cells were a generous gift from Dr. Matthew Chung; St. Vincent Institute). However, up-scaling the cell culture in suspension following the standard protocols was unsuccessful. This problem was also reported in other studies (Wickham and Nemerow, 2002), where a majority of the cells formed aggregates (cell-clumping) and adaptation of cell to suspension culture could not be achieved. Therefore, expression trials with the High-Five™ cell line were not attempted.

The N-terminus of GPCRs is crucial for protein processing and transportation to the cell surface; the detrimental effect of N-terminus tagging has been demonstrated for Dopamine D_2 receptor (Cho et al., 2011). It was also shown that no expression was detected when a construct of GPR43 with a c-Myc tag located on the N-terminus was transfected in mammalian HEK293T cells (Stoddart, 2007). This was again proven in this study with N-terminus His-tagged GPR41 and GPR43 receptors, where no signal was observed with Western blot when probed with anti-His antibody. The N-terminal region of the receptors may be associated with integration of receptor into the plasma membrane, and modifications to this region may impair the conformational and signalling properties of the receptors. For this reason, N-terminal His-tag GPR41 and GPR43 constructs were not used in further studies.

2.4.2 Ligand binding/Functional assay

Many difficulties are encountered in studying recently deorphanised GPCRs. These difficulties are exacerbated for SCFA-binding GPCRs as the natural agonists for these receptors binds with low affinity (μM to mM), this makes it challenging to develop binding assays using radiolabelled ligands. As an alternative, [^{35}S] GTPγS-binding assay was developed in attempt to measure the level of agonist-induced [^{35}S] GTPγS binding. GPR41-His_{10} or GPR43-His_{10} was co-expressed with G proteins in *Sf9* cells and both receptors appeared to be functional. We concluded that the receptor is also likely to be in a functional conformation when it is expressing in the absence of G proteins. By contrast, when *Sf9* cell membranes expressing GPR43-His_{10} were reconstituted with purified Gαβγ subunits, no agonist-induced binding was observed. The assay was attempted with different concentrations of GDP, sample, [^{35}S] GTPγS, and G proteins; however, specific agonist-induced [^{35}S] GTPγS binding was not detected. We believe that this is likely due to inefficient reconstitution of the G protein interactions rather than any problem with the receptors themselves.

The [^{35}S] GTPγS binding assays has been used previously to determined functionality of other GPCRs with exogenous G proteins used to reconstitute the system (Cooper et al., 2009). However, agonist-dependent binding of [^{35}S] GTPγS for GPR41 and GPR43 has only been reported when the proteins are expressed in mammalian cells, which have endogenous G proteins and do not require reconstitution (Brown et al., 2003; Stoddart, 2007). Although the presence of endogenous G proteins in *Sf9* cells has been reported and its coupling activity was demonstrated with human substance P receptor (Nishimura et al., 1998) and human μ-opioid receptor (Wei et al., 2000), these findings remain controversial as there are also other reports suggesting the absence of endogenous G proteins in *Sf9* cells (Heitz et al., 1995; Wehmeyer and Schulz, 1997).

We considered the possibility of co-expressing GPR41/GPR43 with G proteins during up scaling of protein production for crystallisation trials; this was to ensure the production of functional receptor. However, co-infecting insect cells with four different viruses could potentially impair the expression efficiency of GPR41/GPR43. Therefore, subsequent experiments were carried out by infecting *Sf9* cells with only GPR41-His_{10} or GPR43-His_{10} virus under the conditions determined in section 2.3.3.

2.5 Conclusion

Recombinant baculoviruses were produced for GPR41 or GPR43 constructs fused with His-tag at the either N- or C-termini for insect cell expression. Receptor-specific antibodies for GPR41 and GPR43 obtained from commercial sources were not able to detect the expressed receptors. By contrast, the C-terminal His-tag constructs (GPR41-His_{10} and GPR43-His_{10}) were detected by Western blot with an anti-His antibody. The expressions of GPR41 and GPR43 were not detected when the His-tag was fused with the N-terminus of the receptors.

Small-scale expression studies were carried out for both GPR41-His_{10} and GPR43-His_{10}. The optimal conditions for the receptors were found to be an M.O.I of 1 at 48 hrs in *Sf9* cells. SCFA-induced [^{35}S] GTPγS binding was shown when either receptor was co-expressed with G protein subunits in *Sf9* insect cells, confirming the functionalities of the expressed GPR41-His_{10} and GPR43-His_{10} in this system.

3 Solubilisation and purification of GPR41-His_{10} and GPR43-His_{10}

3.1 Introduction

Solubilisation of GPCRs with detergent is essential in the process of extracting the receptor from its native membrane environment. The choice of detergent for solubilisation is critical in maintaining the solubility while retaining its structural conformation. Once solubilised, the receptor can then be purified using conventional methods such as affinity tagging, size exclusion, ion-exchange and other forms of chromatography. During the generation of GPR41 and GPR43 constructs described in Chapter 2, 10 histidine residues were incorporated onto the C-termini of the receptors. This allowed both GPR41-His_{10} and GPR43-His_{10} to be purified via immobilised metal affinity chromatography (IMAC). IMAC utilises metal charged resin to isolate His-tag receptors and subsequently, imidazole can be used to elute the bound receptors for further studies. There are many commercially available resins for this purpose; in this study Ni^{2+} nitrotriacetate (Ni^{2+}-NTA) resin from QIAGEN and Co^{2+}-carboxymethylaspartate (Talon) resin from Clontech were used. Depending on the protein and expression host, a high level of purity is often achieved by following a limited number of purification steps. Gel filtration is routinely used to improve the purity of GPCRs. As gel filtration chromatography separates protein according to size, it is often performed to evaluate the monodispersity of purified proteins. This chapter describes the solubilisation and purification of GPR41-His_{10} and GPR43-His_{10} expressed in *Sf*9 insect cells.

3.2 Materials and methods

3.2.1 Materials

All detergents were purchased from Anatrace, except digitonin, which was sourced from Wako, Japan. Ni^{2+} chelating (Ni^{2+}-NTA) resin was purchased from QIAGEN and Co^{2+} chelating (Talon) resin was from Clontech. Unless otherwise stated, all buffers and protease inhibitors were purchased from Sigma Aldrich.

3.2.2 Methods

3.2.2.1 Detergent screens for solubilisation of GPR41-His_{10} and GPR43-His_{10}

Insect cells membrane fractions were prepared from *Sf9* cells infected with GPR41-His_{10} or GPR43-His_{10} virus as described in 2.2.2.11. Small-scale detergent solubilisations with twelve different detergents were carried out in 1.5 mL eppendorf tubes. Briefly, the detergents were weighed out at 2 μg in each tube. Membrane samples at 5 mg/mL were aliquoted (100 μL) into each tube and samples were allowed to equilibrate for 10 mins at room temperature with gentle shaking. The suspensions were then rotated for 2 hrs at 4 °C, followed by centrifugation at 20,000 x g for 1 hr (5147R, Eppendorf). The supernatant (containing detergent solubilised proteins) was isolated and analysed by SDS-PAGE followed by Coomassie staining or Western blot analysis as described in section 2.2.2.13. Detergents and their properties (type and CMC) used for screening are presented in Table 3-1.

Table 3-1 List of detergents, types and their respective critical micelle concentration (CMC)

Detergents	Type	Critical micelle concentration (CMC)
Anzergent® 3-12	Zwitter-ionic	0.094%
n-decyl-β-D-maltopyranoside (DM)	Non-ionic	0.087%
n-octyl-β-D-glucopyranoside (OG)	Non-ionic	0.53%
n-dodecy-β-D-maltopyranoside (DDM)	Non-ionic	0.0087%
Fos-Choline® 12	Zwitter-ionic	0.047%
Cymal® 5	Non-ionic	0.12%
Mega 10	Non-ionic	0.21%
Hega 10	Non-ionic	0.26%
Dimethyloctyl phosphine oxide	Non-ionic	0.76%
Digitonin	Non-ionic	0.01 – 0.1%
CHAPS	Zwitter-ionic	0.49%
N-N-dimethyldodecylamine-N-oxide (LDAO)	Zwitter-ionic	0.023%

3.2.2.2 Immobilised Metal Affinity Chromatography (IMAC)

Membrane fractions prepared as described in 2.2.2.11 were thawed from -80 °C; 50 mL of 5 mg/mL membrane fractions were used for each purification preparation. All purification steps were carried out with iced-cold buffer A (20 mM HEPES pH 8.0, 150 mM NaCl, 5% glycerol and 100 mM propionic acid) supplemented with protease inhibitors (0.1 mM PMSF, 2 μg/μL aprotinin, 4 mM leupeptin and 10 μM E64) prior to use. Detergent solubilisation was carried out in the presence of 2% w/v detergent with rotation for 2 hrs at 4 °C. The suspension was then subjected to ultracentrifugation at 80, 000 x g for 1 hr at 4 °C (Optima™ L-90K, Beckmand Coulter). The supernatant (containing detergent solubilised proteins) was then incubated with 0.5 mL of Talon resin (equilibrated with buffer A) in the presence of 10 mM imidazole with rotation for 1 hr at room temperature. After incubation, the resin was packed into a Poly-prep column (0.8 x 4 cm, Biorad). The column was washed with 20 mL of buffer A supplemented with 20 mM imidazole to remove any non-specific binding proteins. GPR41-His_{10} or GPR43-

His_{10} was eluted with a step gradient of imidazole (50, 150, 250 and 500 mM) in buffer A and 8 mL were used for each imidazole concentration. Eluted fractions were collected in 2 mL aliquots and analysed by SDS-PAGE, followed by silver staining or Western blot. Fractions containing GPR41-His_{10} or GPR43-His_{10} were collected and concentrated using a MW 30, 000 cut off concentrator (Amicon Ultra, Millipore) to a final volume of 0.5 mL in Buffer B (20 mM HEPES pH 8.0, 300 mM NaCl, 10% glycerol, 100 mM propionic acid and 0.05% Fos-Choline 12). Protein concentrations were determined by measuring the absorbances at 280 nm (NanoDrop 200, Thermo Scientific).

3.2.2.3 Preparative gel filtration chromatography

Fractions eluted from IMAC containing GPR41-His_{10} or GPR43-His_{10} were concentrated and further purified using a Superdex 200 10/300 gel filtration column (GE Healthcare). HPLC was carried out using a Biological HR Workstation and Fraction Collector (2128, Biorad). The column was equilibrated with Buffer B at a flow rate of 0.4 mL/mL before loading 0.5 mL of each concentrated sample. The first 5 mL of flowthrough was discarded and the remaining samples were collected in 0.5 mL aliquots. The collected fractions were analysed by SDS-PAGE, followed by silver staining. The absorbance reading at 280 nm and the conductivity profile were collected for each HPLC run.

3.2.2.4 Analytical gel filtration chromatography

Analytical gel filtration chromatography was carried out to exchange detergent present in the IMAC purified GPR43-His_{10} samples using Superdex 200 5/150 gel filtration column (GE Healthcare) on an AKTA basic FPLC system. The column equilibrated with Buffer B supplemented with detergent at the concentration listed in Table 3-2. The concentrated sample (0.1 mL) from IMAC purification was loaded and the flow rate was at 0.15 mL/min. The first 0.9 mL of flowthrough was discarded and the remaining samples were collected in 0.2 mL

aliquots. The collected fractions were analysed by SDS-PAGE, followed by silver staining. An absorbance reading at 280 nm profile was collected for each run.

Table 3-2 Detergents used in analytical size exclusion chromatography for GPR43-His_{10}

Detergents	Type	CMC	Concentration used
n-dodecy-β-D-maltopyranoside (DDM)	Non-ionic	0.0087%	0.03%
Cymal® 5	Non-ionic	0.12%	0.2%
Anzergent® 3-12	Zwitter-ionic	0.094%	0.1%
N-N-dimethyldodecylamine-N-oxide (LDAO)	Zwitter-ionic	0.023%	0.05%
Fos-Choline 12	Zwitter-ionic	0.047%	0.15%

3.2.2.5 SDS-PAGE – Coomassie and Silver staining

Coomassie staining

SDS-PAGE gel was stained with a solution composed of 45% methanol, 10% acetic acid, and Coomassie Brilliant Blue R250 (2.5 g/L) overnight at room temperature. The gel was then de-stained in 20% ethanol and 10% acetic acid solution until bands were visible.

Silver staining

Silver staining of SDS-PAGE gel was carried out at room temperature with gentle rocking. The gel was incubated in fixer solution (40% ethanol and 10% acetic acid) for 25 mins and the solution was replaced 3 times. The gel was then rinsed with 20% ethanol for 10 mins, followed by a rinse with Milli-Q water (MQH_2O). The gel was sensitised by incubating in pre-treatment solution (0.02% w/v sodium thiosulphate) for 1 min, followed by 3 washes with MQH_2O (20 sec each wash). After the washes, the gel was stained with silver stain solution (0.1% w/v silver nitrate and 0.075% w/v formaldehyde) for 20 mins. To remove the excess silver, the gel was washed twice with MQH_2O (20 sec each wash).

Developer solution (4% w/v Na_2CO_3, 0.05% w/v formaldehyde and 0.0005% w/v sodium thiosulphate) was then added to the gel until the desired level of staining was observed and the reaction was terminated by 5% acetic acid for 10-20 mins. The gel was scanned to produce a digital image and then discarded.

3.3 Results

3.3.1 Solubilisation and purification of GPR41-His_{10}

Solubilisation

Detergent solubilised fractions from detergent screening were analysed by SDS-PAGE, followed by Coomassie staining (Figure 3-1A) or Western Blot analysis using His-antibody (Figure 3-1B). Coomassie stained gel showed the total protein present in the solubilised sample. Due to low expression of GPR41-His_{10}, the expected bands of GPR41-His_{10} were difficult to visualise in the Coomassie stained gel. Western blot with anti-His antibody was carried out to determine which samples contained solubilised GPR41-His_{10}. Out of the 12 detergents chosen for this screen, only samples solubilised with Anzergent 3-12 and Fos-Choline 12 were found to contain GPR41-His_{10}. In the Anzergent 3-12™ detergent (Lane 1 in the Figure 3-1B), a faint monomer band is apparent on the Western blot (arrow). A higher molecular mass species that did not reproduce well was also observed in the original blot (indicate with *). Fos-Choline 12 appeared to be the most efficient detergent for solubilising GPR41-His_{10} and procedures were carried out with Fos-Choline 12.

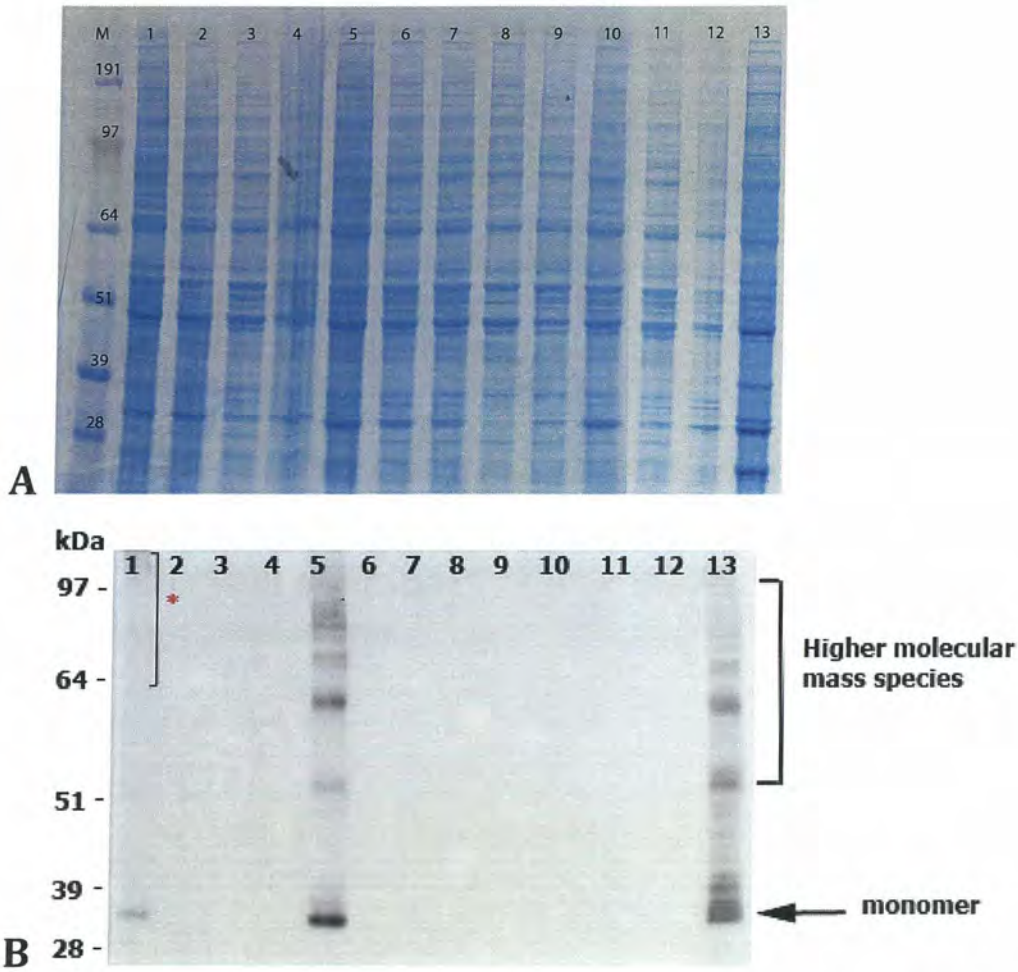

Figure 3-1 Coomassie-stained gel and Western blot of GPR41-His_{10} detergent screen samples.

Detergent solubilised fractions were analysed by SDS-PAGE followed by (A) Coomassie-staining or (B) Western Blot. Lane description: 1 – Anzergent 3-12, 2 – n-decyl-β-D maltopyranoside, 3 – n-ocytl- β-D- glucopyranoside, 4 – n-dodecyl-β-D-maltopyranoside, 5 –, Fos-Choline 12, 6 – Cymal 5, 7 – MEGA 10, 8 – HEGA 10, 9 – Dimethyloctyl phosphine oxide, 10 – digitonin, 11 – CHAPS, 12 – n-dodecyl dimethylamine-N-oxide and 13 – untreated GPR41-His_{10} membrane.

Purification of GPR41-His_{10} – IMAC

Ni^{2+}-NTA resin is routinely used in our laboratory to purify other GPCRs; hence, it was used for initial purification trials of GPR41-His_{10}. Detergent solubilised GPR41-His_{10} fraction was incubated with Ni^{2+}-NTA resin and eluted with a concentration gradient of imidazole ranging from 50 mM to 500 mM. Eluted fractions were collected and analysed by SDS-PAGE followed by silver staining (Figure 3-2). The eluted fractions contained a large amount of contaminating proteins eluted along with GPR41-His_{10}. Increasing the number of washes prior to elution, and reducing the incubation time of samples with the resin did not improve the purification profile (results not shown).

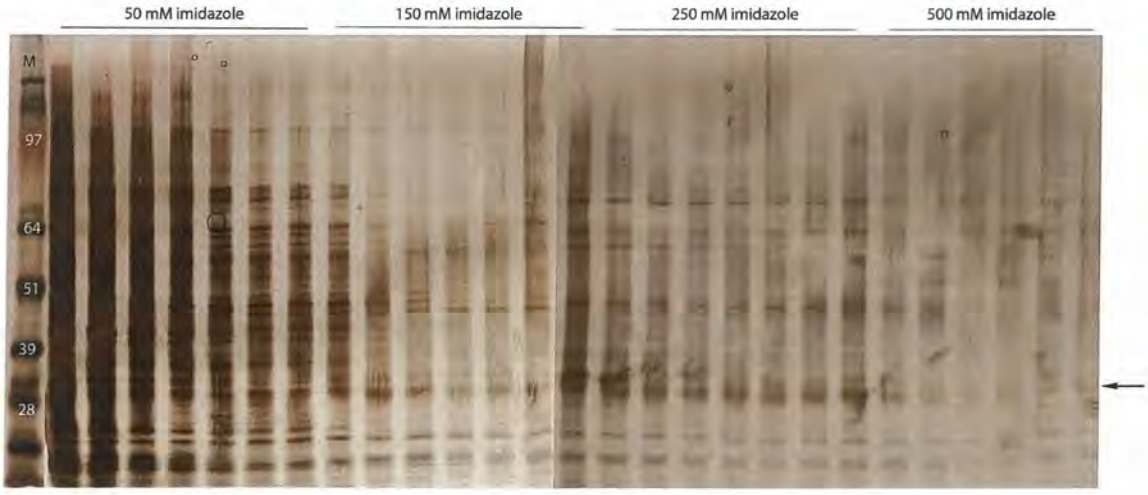

Figure 3-2 Silver-stained gels showing step gradient purification of GPR41-His_{10}

The Fos-Choline 12 detergent solubilised GPR41-His_{10} was run on a Ni^{2+}-NTA resin column and was eluted with a step gradient of imidazole (50 mM, 150 mM, 250 mM and 500 mM). The eluted fractions were analysed by SDS-PAGE followed by silver staining. Molecular marker (M) was run in parallel. Arrow points to presumed monomeric GPR41-His_{10}.

Due to the low purity of GPR41-His_{10} obtained from Ni^{2+}-NTA resin, purification was carried out with Talon resin. The fractions collected were analysed by SDS-PAGE, followed by silver staining (Figure 3-3A) or Western blot (Figure 3-3B). Although a small amount of contaminating proteins were still observed in the fractions eluted with 50 mM imidazole, the purities of fractions

eluted with higher concentration of imidazole were significantly improved. Monomer and higher molecular mass species of GPR41-His_{10} eluted with 150 mM and 250 mM imidazole were confirmed by Western blot. This result shows that 250 mM imidazole is sufficient to elute all GPR41-His_{10}, as no proteins were observed in 500 mM imidazole-eluted fractions.

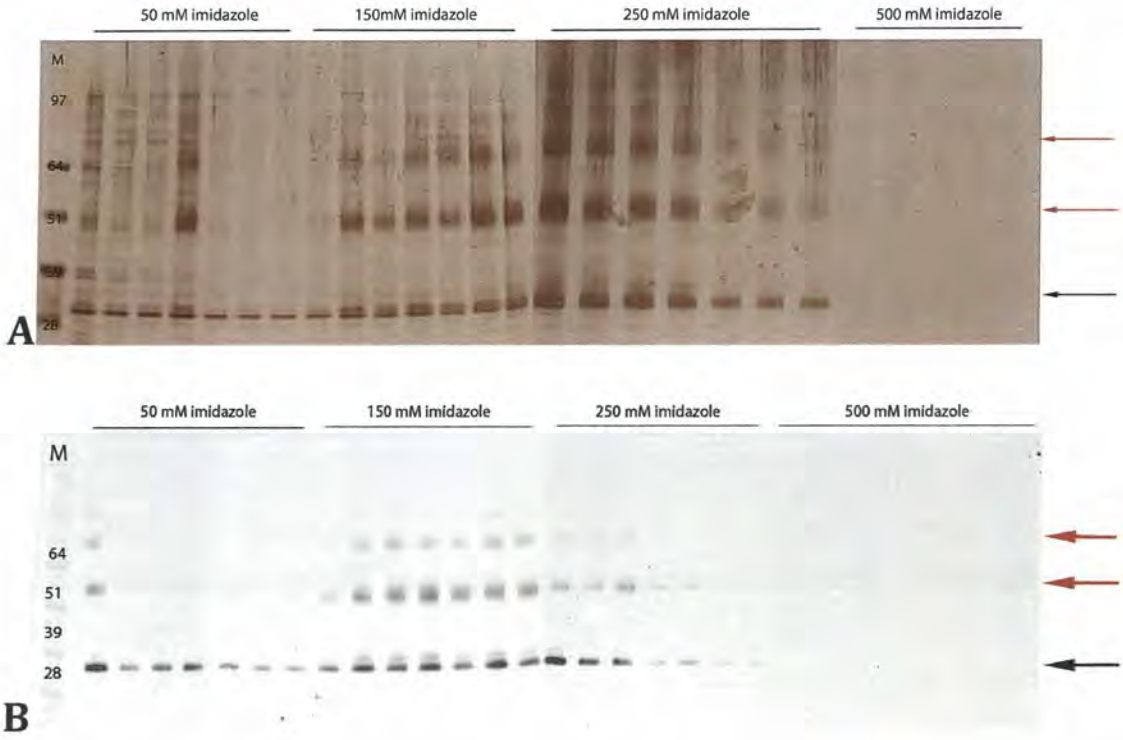

Figure 3-3 Silver-stained gels and Western blots showing purification of GPR41-His_{10} using Talon resin.

GPR41-His_{10} was solubilised with Fos-Choline 12 and run on a Talon resin column and eluted with a step gradient of imidazole (50 mM, 150 mM, 250 mM and 500 mM). The eluted fractions were analysed by SDS-PAGE followed by (A) silver staining and (B) Western blot. Molecular weight marker (M) was run in parallel.

Purification of GPR41-His_{10} - Gel filtration chromatography

Gel filtration chromatography was carried out to separate the monomeric and higher molecular mass species of GPR41-His_{10} observed in IMAC purified samples. However, the chromatograph plot (Figure 3-4) showed several overlapping peaks, which indicates the eluted GPR41-His_{10} was not monodisperse. This was confirmed by silver staining of gel of which different fractions were

analysed (Figure 3-5). The monomer was the major species (in particular in later eluting fractions), however, higher molecular mass species were also present.

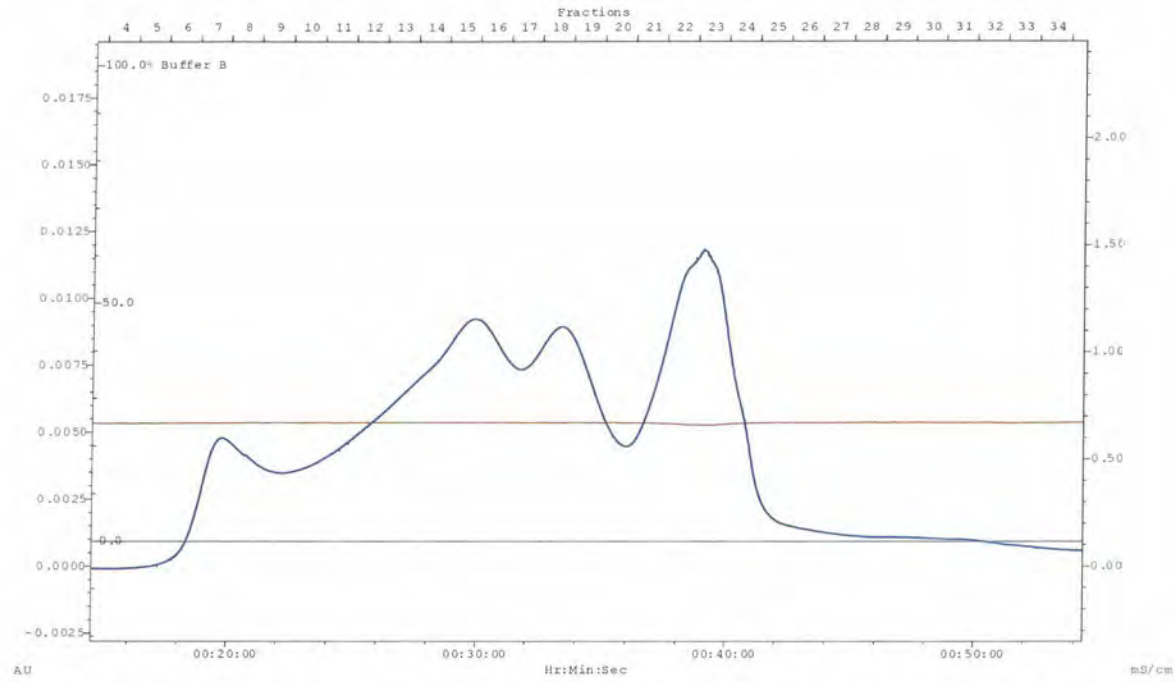

Figure 3-4 Gel filtration chromatography A_{280} profile of concentrated GPR41-His_{10} from IMAC fractions.

The elution was monitored at 280 nm (left y-axis, AU) and conductivity (right y-axis, mS/cm).

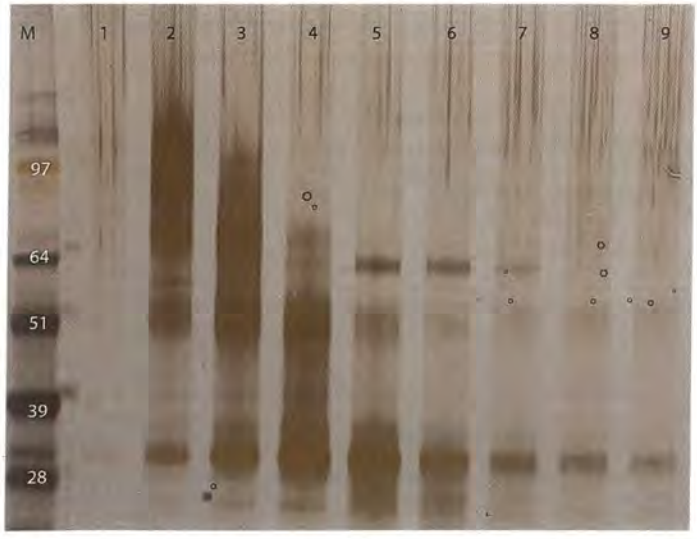

Figure 3-5 Silver-stained gel of samples from Figure 3-4, gel filtration profile.

Lane description: 1 – Fraction 7, 2 – Fraction-13, 3 – Fraction 15, 4 – Fraction 18, 5 – Fraction 20, 6 – Fraction 21, 7 – Fraction 22, 8 – Fraction 23 and 9 – Fraction 24.

Since the size exclusion chromatography did not improve the purity of GPR41-His_{10}, it was eliminated from the purification step. Large-scale purification of GPR41-His_{10} only involved a single step: IMAC with Talon resin. Routinely, IMAC fractions from the 150 and 250 mM imidazole elution were used as they had less contaminating proteins. These fractions were pooled and concentrated to 5 mg/mL. Initially, precipitation was observed during the concentration process. As glycerol and NaCl are known to increase the stability and solubility of membrane proteins, NaCl and glycerol concentrations in the buffer A were increased from 150 mM to 300 mM and 5% to 10% w/v, respectively. This prevented precipitation of the concentrated sample. The yield of GPR41-His_{10} using this method is approximately 250 μg per litre of *Sf9* culture and the final purified GPR41-His_{10} was verified by SDS-PAGE followed by silver staining (Figure 3-6).

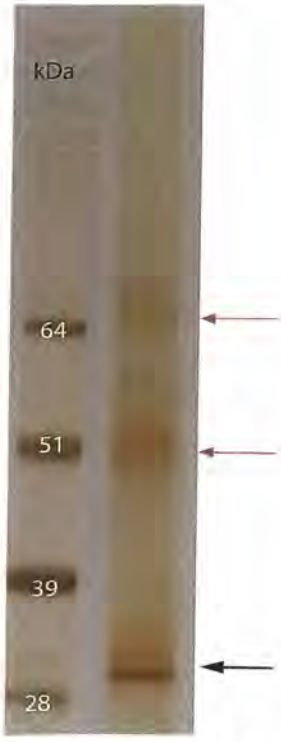

Figure 3-6 Silver-stained gel showing purified and concentrated sample of GPR41-His_{10}

Purified and concentrated GPR41-His_{10} obtained from IMAC. A total of 1.5 μg of concentrated proteins was loaded. The black arrow indicates the monomer and red arrows indicate higher molecular mass species.

3.3.2 Solubilisation and purification of GPR43-His_{10}

A detergent screen for GPR43-His_{10} was carried out with the same selection of detergents used for GPR41-His_{10} in section 3.3.1. Detergent solubilised samples were analysed by SDS-PAGE, followed by Coomassie staining or Western blot. As the extracted GPR43-His_{10} was difficult to visualise by Coomassie stained gel (Figure 3-7A), it was detected by anti-His antibody in a Western blot (Figure 3-7B). Monomeric and higher molecular mass species of GPR43-His_{10} were observed in the Fos-Choline 12 (Lane 5) and digitonin (Lane 10) solubilised samples. No GPR43-His_{10} detected in the other detergent solubilised fractions. Since the intensities of the bands detected in Fos-Choline 12 solubilised sample appeared to be stronger than digitonin, Fos-Choline 12 was used for large-scale solubilisation of GPR43-His_{10}.

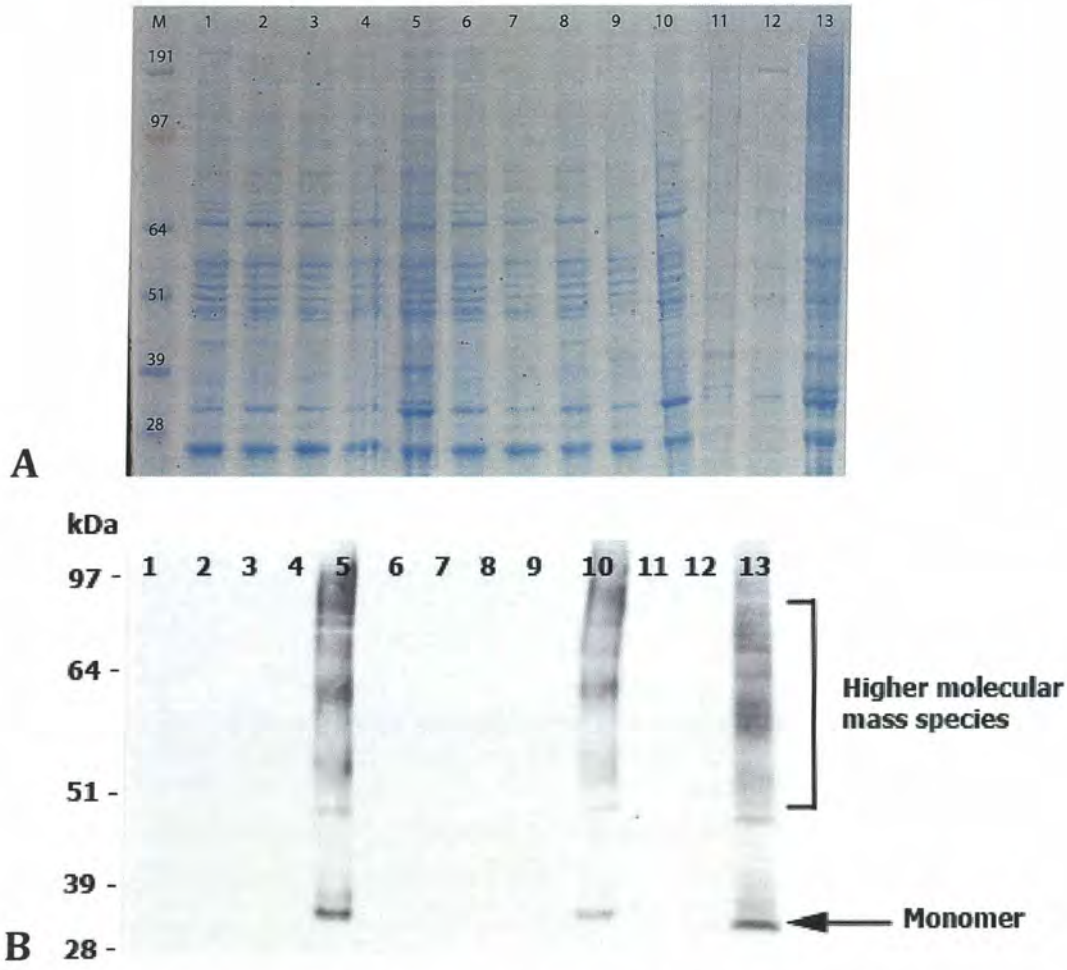

Figure 3-7 Coomassie-stained gel and Western blot of GPR43-His_{10} detergent screen samples.

Detergent solubilised fractions for GPR43-His_{10} were analysed by SDS-PAGE followed by (A) Coomassie-staining or (B) Western Blot. Lane description: 1 – Anzergent 3-12, 2 – n-decyl-β-D maltopyranoside, 3 – n-ocytl- β-D- glucopyranoside, 4 – n-dodecyl-β-D-maltopyranoside, 5 –, Fos-Choline 12, 6 – Cymal 5, 7 – MEGA 10, 8 – HEGA 10, 9 – Dimethyloctyl phosphine oxide, 10 – digitonin, 11 – CHAPS, 12 – n-dodecyl dimethylamine-N-oxide and 13 – untreated GPR43-His_{10} membrane.

Purification of GPR43-His_{10} – IMAC

Similar to GPR41-His_{10}, initial attempts to purify GPR43-His_{10} were carried out using Ni^{2+}-NTA resin. Fractions were collected and analysed by SDS-PAGE, followed by silver staining. As shown in Figure 3-8, the purity of GPR43-His_{10} in imidazole-eluted fractions was unacceptably low. Contaminating proteins were not removed by additional washes with low concentration of imidazole; the contaminants were not present in the final wash with 20 mM imidazole, but they present in fractions eluted with high concentration of imidazole (150 mM to 500 mM).

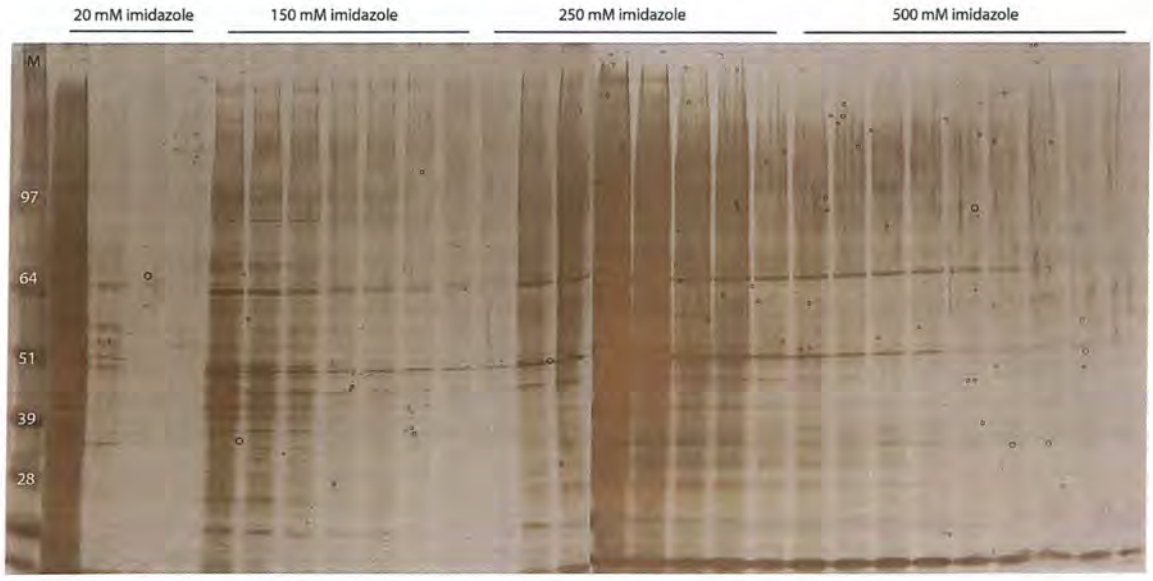

Figure 3-8 Silver-stained gels showing step gradient purification of GPR43-His_{10} using Ni^{2+}-NTA resin.

The Fos-choline 12 detergent solubilised GPR43-$His_{10}$was run on a Ni^{2+}-NTA resin column and eluted with a step gradient of imidazole (20 mM, 150 mM, 250 mM and 500 mM). The eluted samples were analysed by SDS-PAGE followed by silver staining. Molecular weight marker (M) was run in parallel.

As the previous study with GPR41-His_{10} showed the use of Talon resin significantly improved the purity of the receptor, IMAC with Talon resin was also trialled for GPR43-His_{10} purification. Figure 3-9A shows the silver stained gel and Figure 3-9B shows the Western blot of eluted fractions from Talon resin. The

overall purity of GPR43-His_{10} was improved and the amount of receptor in the eluted fractions was found to be higher than the Ni^{2+}-NTA resin eluted fractions. Western blot analysis (Figure 3-9B) showed that GPR43-His_{10} monomer and higher molecular mass species were eluted between 50 mM and 250 mM imidazole. No receptor was detected in the 500 mM imidazole-eluted fractions.

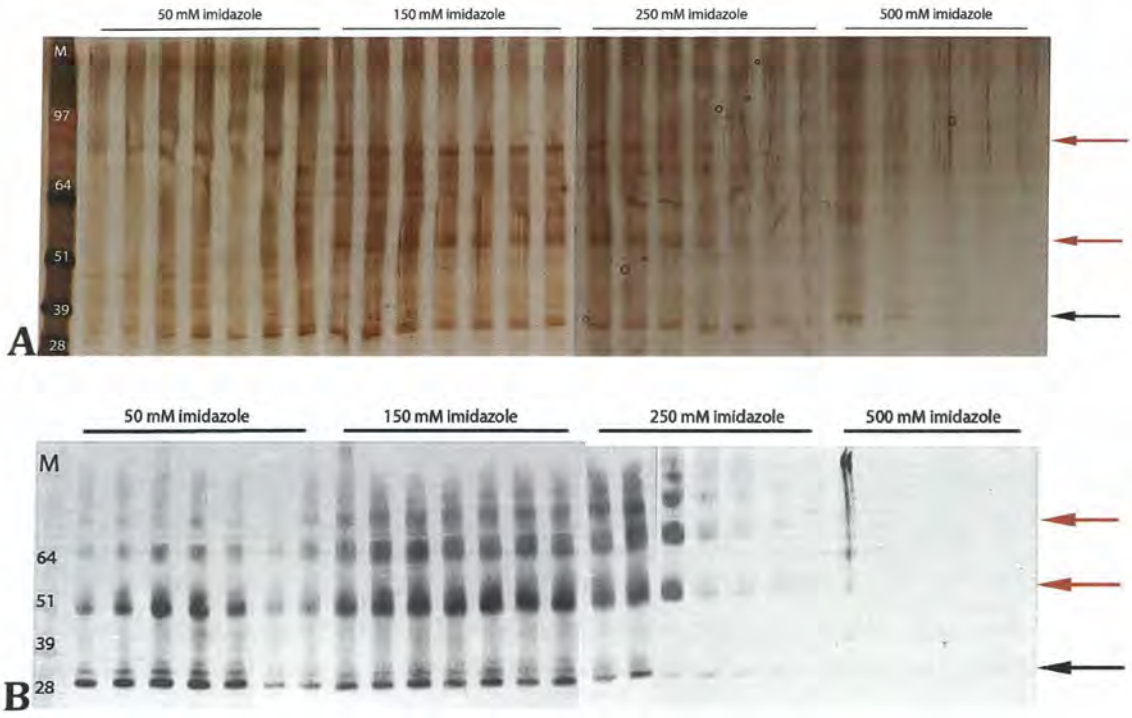

Figure 3-9 Silver-stained gels and Western blots showing step gradient purification of GPR43-His_{10} using Talon resin.

GPR43-His_{10} was solubilised with Fos-Choline 12 and run on a Talon resin column, the eluted fractions were analysed by SDS-PAGE followed by (A) silver staining and (B) Western blot. Black arrow indicates monomeric band and red arrows indicate higher molecular mass species of GPR43-His_{10}.

Purification of GPR43-His_{10} – Gel filtration chromatography

Gel filtration chromatography was carried out to isolate monomer and higher molecular mass species of GPR43-His_{10} present in IMAC fractions. The chromatograph plot showed a large broad peak in Figure 3-10, which indicates that the proteins in the eluted fractions are not monodisperse. This was confirmed by SDS-PAGE and silver staining of the eluted fractions corresponding to this broad

peak (Figure 3-11). The bands shown on the silver stained gel appeared to be thick and smeared, which could be due to an artefact due to silver staining or to additional modifications (for example proteolysis or aggregation occurring during gel electrophoresis). Regardless, the gel filtration chromatography did not improve purity of GPR43-His_{10}.

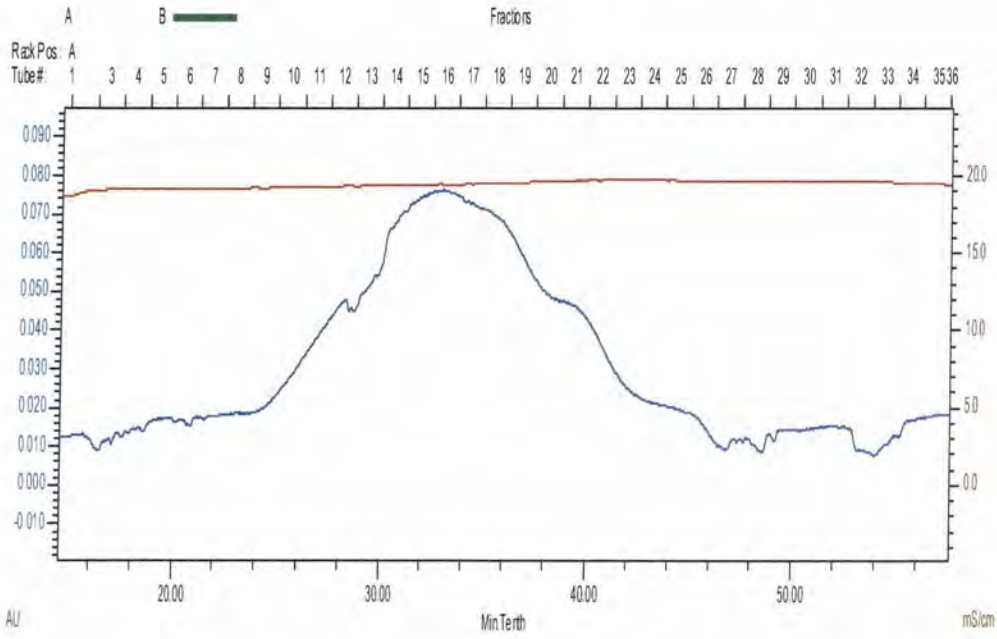

Figure 3-10 Gel filtration chromatography A_{280} profile of concentrated GPR43-His_{10} from IMAC.

The elution was monitored at 280 nm (left y-axis, AU) and conductivity (right y-axis, mS/cm).

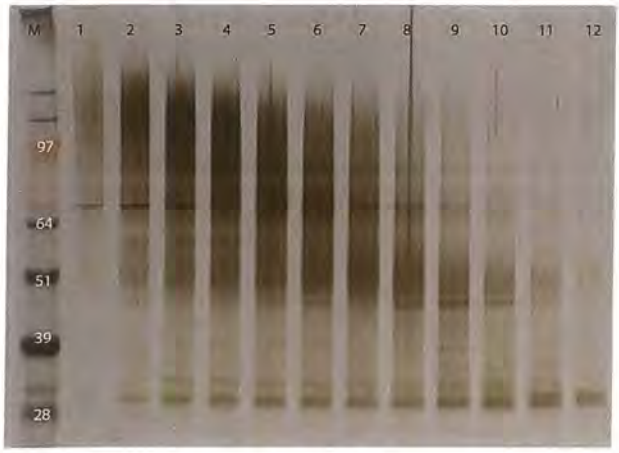

Figure 3-11 Silver-stained gel of samples from Figure 3-10, gel filtration profile.

Lane description: 1- Fraction 12, 2- Fraction 14, 3- Fraction 15, 4- Fraction 16, 5- Fraction 17, 6- Fraction 18, 7- Fraction 19, 8- Fraction 20, 9- Fraction 21, 10- Fraction 22, 11- Fraction 23 and 12- Fraction 24.

Purification of GPR43-His_{10} - Analytical gel filtration chromatography

Analytical gel filtration chromatography was carried out in an attempt to determine if GPR43-His_{10} behaves differently in different detergents. Four detergents were chosen for this study: LDAO, Cymal-5, DDM, Anzergent 3-12, while Fos-Choline 12 was included for comparison.

Figure 3-12 shows that GPR43-His_{10} remained heterogenous in all these detergents. When Fos-Choline 12 was exchanged for Cymal 5 (A), Anzergent 3-12 (B) or DDM (D), a large broad peak was observed in the chromatograph plots, which was similar to results obtained for Fos-Choline 12 (E). Silver-stained gels confirmed the monomer was eluted along with the higher molecular mass species. When Fos-Choline 12 was exchanged for LDAO (Figure 3-13C), a narrower peak on the chromatograph plot was observed, however, the silver stained gel revealed that GPR43-His_{10} remained heterogenous in these fractions.

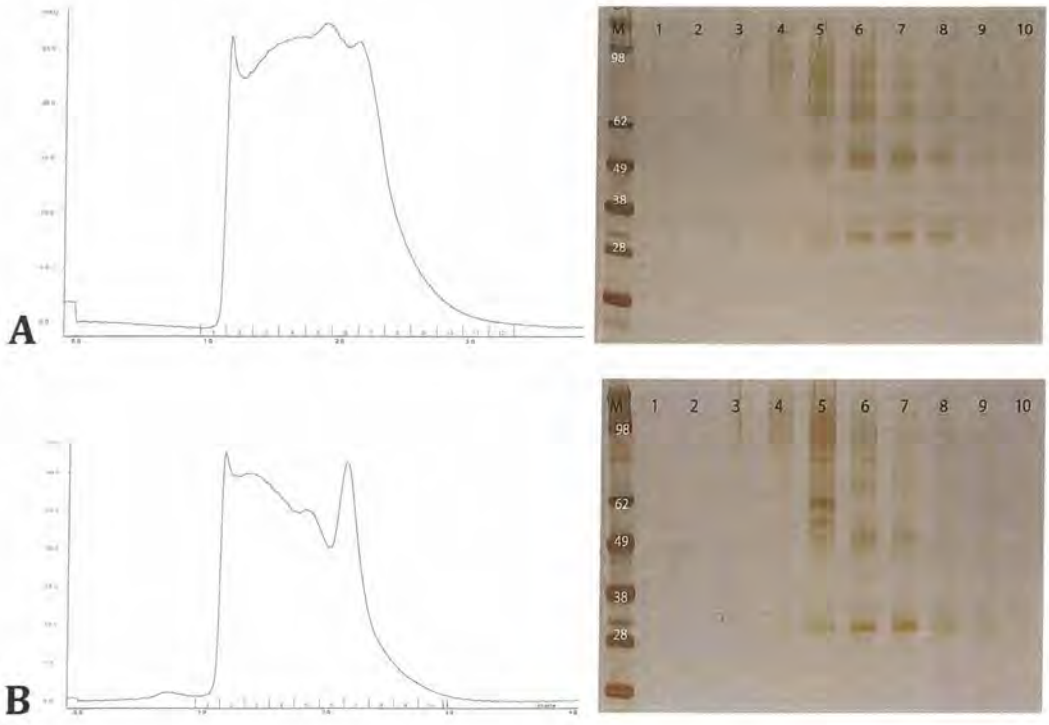

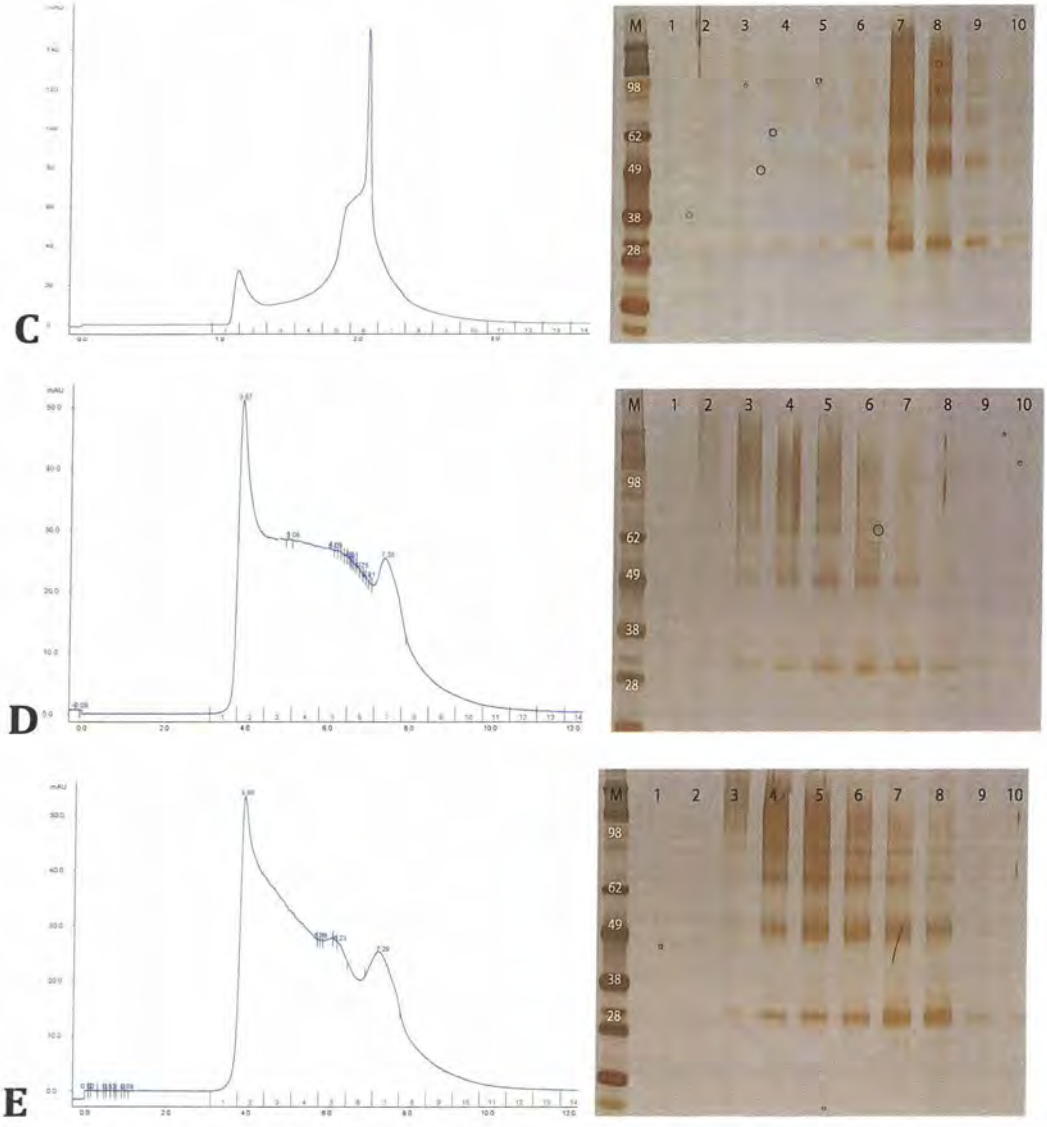

Figure 3-12 Analytical gel filtration chromatography of GPR43-His$_{10}$ for detergent exchange.

Detergent (Fos-Choline 12) was exchanged to (A) Cymal 5, (B) Anzergent 3-12, (C) LDAO, (D) DDM and control (E) Fos-Choline 12. The elution was monitored at 280 nm.

Since size exclusion chromatography and detergent exchange did not decrease the heterogeneity of the IMAC fractions, a single-step protocol purification using Talon resin was carried out for large-scale purification of GPR43-His$_{10}$. IMAC fractions were pooled and concentrated to 5 mg/mL. Similar to GPR41-His$_{10}$, precipitation was also observed during the concentration process; hence NaCl and glycerol concentrations were increased from 150 mM to 300 mM and 5% to 10% w/v, respectively. The yield of GPR43-His$_{10}$ using this method was

approximately 265 μg per litre of *Sf9* culture and the final purified GPR43-His_{10} was verified by SDS-PAGE followed by silver staining Figure 3-13.

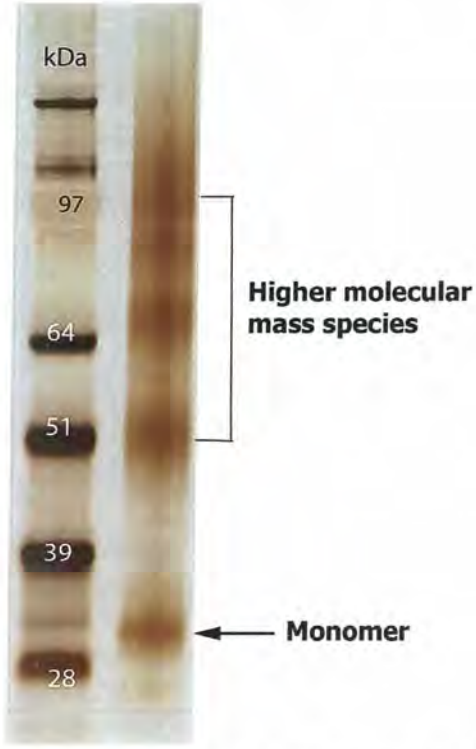

Figure 3-13 Purified and concentrated sample of GPR43-His_{10}

A total of 6.5 μg of concentrated protein was used for SDS-PAGE analysis. Black arrow indicates the monomer band and red arrows indicate the higher molecular mass species of GPR43-His_{10}.

3.4 Discussion

3.4.1 Solubilisation of GPR41-His_{10} and GPR43-His_{10}

A selection of zwitter-ionic and non-ionic detergents was chosen for solubilisation trials of GPR41-His_{10} and GPR43-His_{10}. Although ionic detergents are more efficient in solubilisation, they were not included as they are generally more denaturing and can interfere with IMAC purification.

In recent times, DDM has become the most popular detergent used in GPCR solubilisation. Successful solubilisation of GPCRs with DDM include H1R (Shimamura et al., 2011), human cannabinoid 1 receptor (Zvonok et al., 2010), B2AR (Cherezov et al., 2007), turkey B1AR (Warne et al., 2003) and A2AR (Weiß and Grisshammer, 2002). Therefore, DDM was one of the detergents tested in our study. However, DDM was unable to solubilise either of the receptors in this study. Non-ionic detergents like Cymal 5, HEGA-10 and MEGA-10 were included, as they have been previously shown to solubilise other GPCRs or integral membrane proteins (Hanatani et al., 1984; Mirzabekov et al., 1999; Wetterholm et al., 2008). However, they were likewise unsuccessful in solubilising either receptors of the interest. Detergents that are commonly used for membrane protein solubilisation like OG and DM were also not successful in extracting GPR41-His_{10} and GPR43-His_{10}. One possible explanation for this may be the incompatibility of the detergent with the solubilisation buffer. The presence of some buffer components has been reported to affect the behaviour of detergents; for example NaCl can decrease the critical micellar concentration (CMC) of a non-ionic detergent (Ericsson et al., 2004). Although the selected detergents are classified as mild and non-denaturing, it is possible that these detergents may deactivate the receptor, which in turn can result in aggregation or precipitation of the solubilised receptors, thus leading to inefficient detergent solubilisation. This is supported by a study where OG has been found to deactivate membrane proteins due to its short acyl chain (Lund et al., 1989).

Fos-Choline is a group of recently developed zwitter-ionic detergents used for solubilisation of chemokine receptors (Ren et al., 2009), human olfactory receptors 17-4 (Cook et al., 2009), and other integral membrane proteins (McDevitt et al., 2006). Here, we showed that Fos-Choline 12 is highly efficient in solubilising both GPR41-His_{10} and GPR43-His_{10}. These detergents comprise of a phosphocholine head-group with a hydrophobic alkyl chain length. The solubilisation efficiency of a detergent is dependent on the lipid environment in which the target receptor is expressed. The solubilisation efficiency of Fos-Choline 12 may be due to its resemblance to phosphatidyl choline, which is a major component of native cell membranes.

Anzergent 3-12 has a similar structure to Fos-Choline 12; they have equivalent acyl chain length, a relatively small head-group, and both are zwitter-ionic. However, Anzergent 3-12 does not have a phosphocholine head-group, which may be the reason for the impaired solubilisation efficiency observed for GPR41-His_{10}.

GPR43-His_{10} was also observed in the digitonin solubilised sample, albeit at a lower level than in the Fos-Choline 12 solubilised sample. Digitonin consists of a non-ionic head-group that is larger than the phosphocholine head-group of Fos-Choline 12. In general, non-ionic detergents are milder than zwitter-ionic detergents and detergents with larger head-groups are also milder. Consequently, digitonin may not be as efficient in breaking protein-lipid or lipid-lipid interactions. This may explain the lower solubilisation efficiency of digitonin for GPR43-His_{10}.

For all the reasons outlined above, Fos-Choline 12 was chosen as the detergent to extract GPR41-His_{10} and GPR43-His_{10} from *Sf9* insect cell membranes.

3.4.2 Purification of GPR41-His_{10} and GPR43-His_{10}

GPR41-His_{10} and GPR43-His_{10} bear a His-tag on the C-terminus, which allows the receptors to be purified using IMAC. IMAC is most frequently carried out using Ni^{2+}-NTA resin, however this was proven to be inefficient in this study. Both receptors were eluted with high levels of contaminating proteins and stringent washes with imidazole prior to elution did not remove these contaminating proteins. The result obtained with the Talon resin was significantly better, with a much lower level of contaminating protein present in the eluted fractions. The Talon resin is based on the cobalt ion which only binds to adjacent histidines or histidines with a special arrangement (Smith, 2005). Therefore, non-specific binding is minimised with Talon resin.

Gel filtration chromatography was carried out in an attempt to separate the higher molecular mass species of both GPR41-His_{10} and GPR43-His_{10} observed in the IMAC fractions. Unfortunately, this method was unable to separate different molecular mass species of GPR41-His_{10} or GPR43-His_{10}. This is in contrast with other studies, where the monomer form of the GPCRs was isolated from oligomers by gel filtration chromatography (Ren et al., 2009; Wang et al., 2011). In other studies, the heterogeneity of membrane protein was improved by detergent exchange after the first purification step (Kaiser et al., 2008; Kunji et al., 2008). In this study, detergent exchange was attempted for GPR43-His_{10}, but the heterogeneity was not improved in any of the detergents trialled. Since gel filtration chromatography separates proteins according to their size, our result suggests the formation of higher molecular mass species could be occurring dynamically. Oligomerisation of GPCRs and factors that promote self-association are poorly understood. Oligomerisation has been reported for B2AR and neurotensin NTS1 receptor when they were reconstituted in a model lipid system (White et al., 2007; Fung et al., 2009).

Although, the bands observed with silver-stained gel of purified GPR41-His_{10}/GPR43-His_{10} were at the same molecular weight as detected by anti-His antibody, however, the identities of the protein bands could not be confirmed

without a receptor-specific antibody. In addition, results from Mass Spectrometry and N-terminal sequencing on the protein bands were inconclusive (data not shown). Therefore, we cannot rule out the possibility of other proteins present in the purified sample. If a high affinity ligand is available for the receptor, alternative method for purification may involve in using a ligand affinity column. This would allow specific binding of receptor for purification. For future experiments, it may also be worthwhile to incorporate a FLAG-tag on the N-terminus of the receptor for FLAG-affinity column. In this study, although the homogeneity of GPR41-His_{10} and GPR43-His_{10} could not be improved with gel filtration chromatography, the purity obtained from IMAC with Talon resin was considered adequate for further experiments.

3.5 Conclusion

In conclusion, Fos-Choline 12 was found to be the most efficient detergent for solubilisation of GPR41-His_{10} and GPR43-His_{10}. The receptors were purified using IMAC with Talon resin bypassing the gel filtration chromatography step, as it proved unsuccessful in improving the purity and homogeneity of the receptors.

4 Cubic phase characterisation

4.1 Introduction

In meso crystallisation is an emerging technique used for crystallising membrane proteins. This method has proven successful for several membrane proteins resulting in the growth of diffraction-quality crystals (Cherezov et al., 2007; Jaakola et al., 2008; Chien et al., 2010; Wu et al., 2010; Shimamura et al., 2011; Haga et al., 2012). To date, monoolein (MO) and its derivatives are the only host lipids used for *in meso* crystallisation, however, the exact mechanism of crystal growth in the cubic phase is not well understood. It has been hypothesised that upon mixing lipid with membrane proteins, the membrane protein will be incorporated within the cubic phase of lipids (Caffrey and Cherezov, 2009). The cubic phase consists of two interpenetrating but unconnected water channels. The highly curved lipid bilayer with its bicontinuous water channel is proposed to mimic aspects of the biological membrane bilayer where membrane protein is expressed. Therefore, this system provides stability for the purified membrane proteins allowing the addition of precipitant to induce crystal nucleation.

Under different conditions (temperature, pressure, solvent), lipid in aqueous solution can form various phases, including bicontinuous cubic phases (diamond, gyroid and primitive), lamellar phase, inverse hexagonal phase and fluid isotropic (Figure 4-1). Although it has been shown that the cubic phase for pure MO is formed under the condition of a lipid:aqueous ratio of 60:40 (Qiu and Caffrey, 2000), components in the crystallisation screen or the membrane protein itself could potentially destabilise the cubic phase. Additives of salt, detergents, glycerol and changes in pH are commonly used during the purification to increase the stability of membrane proteins. The effects of these on the cubic phase of MO have been studied by other groups (Ericsson et al., 1983; Cherezov et al., 2001; Li et al., 2001; Misquitta and Caffrey, 2003; Ericsson et al., 2004; Abe and Takahashi,

2007; Darmanin et al., 2012; Joseph et al., 2011). For example, cholesterol is found in the natural membrane bilayer and it is important for modulating the fluidity of cell membranes (Yeagle, 1985). Recently solved GPCR structures using *in meso* crystallisation were carried out in the presence of cholesterol, which was implicated in an increase in the stability of GPCRs in the cubic phase (Cherezov et al., 2007; Jaakola et al., 2008; Chien et al., 2010; Wu et al., 2010; Shimamura et al., 2011; Haga et al., 2012). The swelling effect of cholesterol on MO cubic phase has also been reported (Cherezov et al., 2006). As the cubic phase is required for crystal growth of membrane proteins, it is crucial to determine the initial phase of the lipid upon the addition of membrane protein and the crystallisation mix. This is to avoid wastage of precious purified membrane proteins as well as time consumed on conditions that are not favourable.

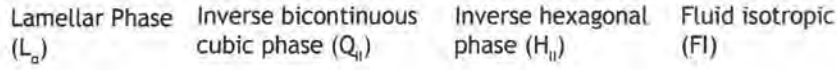

Figure 4-1 Different phases of lipid

From left to right, lipids can form lamellar phase, inverse bicontinuous cubic phases (diamond, gyroid and primitive), inverse hexagonal phase and fluid isotropic phase, depending on the environment they are in. Diagram modified from Mulet et al. (2010).

In this chapter, X-ray diffraction is used to characterize the lipid phase in the presence of purified protein and crystallisation screens. X-ray diffraction is a method to determine distances between repetitive materials. As an X-ray beam hits a crystalline sample, the electron in the atoms from the sample causes the X-ray to scatter/diffract (Figure 4-2). The diffraction pattern of X-ray scattered from crystalline samples can be explained by Bragg's law (Equation 4), where n is the order of reflection, λ is the wavelength of the X-ray beam, θ is the angle at which the X-ray hit the lattice plane and d_{hkl} is the distance between a set of lattice planes defined by Miller indices, h, k and l (Figure 4-2).

$$n\lambda = 2d_{hkl}\sin\theta$$

Equation 4 Bragg's law

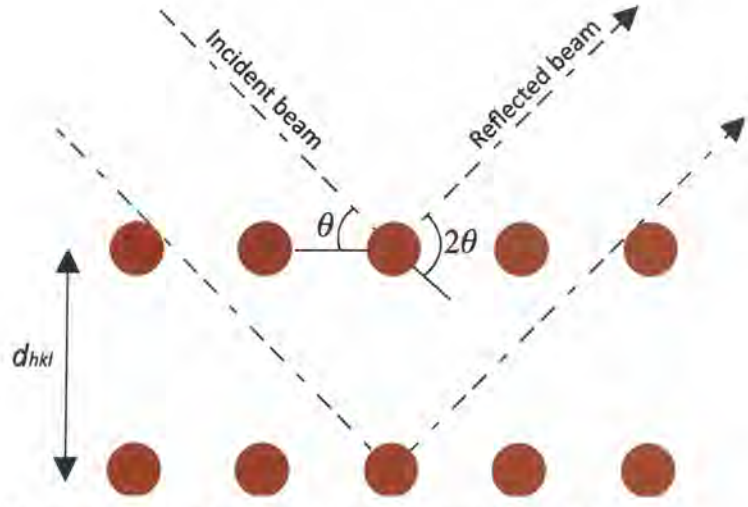

Figure 4-2 Bragg's description of X-ray diffraction.

When X-ray incident on a set of parallel planes at angle $\boldsymbol{\theta}$, the X-ray is reflected from the plane at the same angle. Red spheres represent atoms in a set of parallel planes.

A crystal consists of an orderly arrangement of unit cells in three-dimensional form. The unit cell (Figure 4-3A) is defined by the edge of the unit cell (a, b and c) and the angles between them (α, β and γ) (Rhodes, 1993). The length of a, b and c is known as the lattice parameter of the unit cell. Miller indices are used to describe the orientation of a set of planes in relation to the unit cell.

Examples of different orientation of lattice planes intersecting at axes *x*, *y* and *z* are shown in Figure 4-3B. Miller indices are the reciprocal of the respective positions along axes *x*, *y* and *z* and they are written as (*hkl*) in brackets. If the plane is parallel to one axis, the Miller index for that axis will be written as 0. For example, if a lattice plane do not intercept at y and z axes, the Miller indices would be written as (100), when a lattice plane intercepts at ½ at all 3 axes, the Miller indices is (222) and is equivalent to (111) (Figure 4-3B).

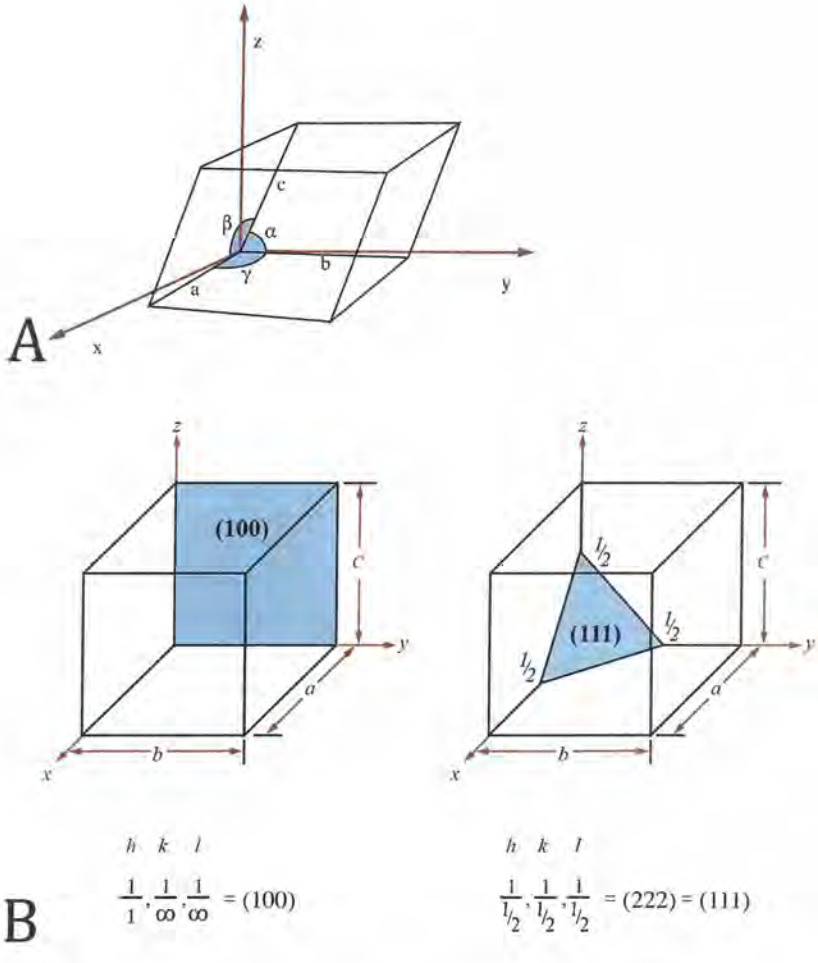

Figure 4-3 Schematic diagram of a unit cell and lattice planes

Diagram showing (A) a unit cell is defined by the edges (*a*, *b* and *c*) and the angles between them (α, β and γ). (B) Different lattice planes and their Miller indices. For a lattice plane that do not intercept at y and z axes, the Miller indices would be (100) (left), where the lattice plane intercepts ½ at all 3 axes, the Miller indices are (222), which is equivalent to (111) (right).

In X-ray diffraction, the position of the detector can be varied to examine different diffracting angles and distances. Small angle X-ray scattering (SAXS) is a technique where the detector is located further from the incident beam to detect X-ray scattering at smaller angles ($2\theta<0.1$ radian). X-ray diffraction from a uniformly oriented crystal is detected as spots. However, cubic phase lipid exists in a liquid crystalline phase, which consists of local domains of randomly oriented repeat units; similar to a sample consists of many tiny crystals. Hence, the scattered X-rays are recorded as powder diffraction rings (also known as Debye rings).

The 2D SAXS diffraction image is transformed into a 1D plot of scattering intensity *(I) vs* the scattering vector q, where q is the reciprocal of d_{hkl} and expressed as:

$$q = 4\pi sin\theta/\lambda = 2\pi/d_{hkl}$$

Equation 5

Each ring presents in the powder diffraction yields a sharp peak (known as Bragg's peak) in the 1D plot. The positions of the peaks depend on the lattice parameter and the intensity of peak depends on the type of atom present. Each peak represents a particular lattice plane and they are annotated using Miller indices. The position of peaks in q_{hkl} can be calculated using lattice parameter (a) and Miller indices (hkl). The peak positions of cubic phase can be calculated by:

$$q_{hkl} = \frac{2\pi\sqrt{h^2 + k^2 + l^2}}{a}$$

Equation 6

As lamellar phase only exist in one dimension, the equation is given as:

$$q_h = \frac{2\pi h}{a}$$

Equation 7

Lattice planes in hexagonal phase are in two dimension (Miller indices h and k) and the equation is given as:

$$q_{hk} = \frac{4\pi\sqrt{(h^2 + hk + k^2)}}{a\sqrt{3}}$$

Equation 8

Each lipid phase (shown in Figure 4-1) has unique structural arrangement, which give rise to a specific SAXS diffraction pattern. Examples SAXS diffraction patterns from different lipid phases are shown in Figure 4-4. Based on the characteristic of how the diffraction peaks are spaced, the phase in which the lipid exists can then be determined. The lipid phases relevant in this study, along with their corresponding spacing ratio and Miller indices are presented in Table 4-1. Once the lipid phase has been identified, the d_{hkl} of each phase can be calculated from q_{hkl} using Equation 5.

The aim of this chapter was to determine which conditions are suitable for initiating crystallisation trials for GPR41-His_{10} and GPR43-His_{10} by identifying the initial phase using SAXS. We aimed to answer the following questions: Is MO, the commonly used lipid, suitable for these receptors? If so, what is the maximum receptor concentration the lipid can withstand whilst remaining in the cubic phase? How do different concentrations of cholesterol affect the protein and lipid system? In parallel, we investigated the suitability of an alternative lipid, phytantriol. We investigated the compatibility of the two lipids with two crystallisation screens: the PACT suite and the PEG/Ion screen.

Figure 4-4 Examples of diffraction pattern for liquid crystalline phases.

Expected diffractions of (A) gyroid Q_{II}^{G} (Ia3d) phase, (B) diamond Q_{II}^{D} (Pn3m) phase, (C) primitive Q_{II}^{P} (Im3m) phase, (D) inverse hexagonal (H_{II}) phase and (E) lamellar (Lα) phase. Diagram adapted from Joseph et al. (2011).

Table 4-1 Spacing ratios and Miller indices (*hkl*) of Braggs peaks position of different lipid phases (International Tables for Crystallography, 2006).

4.2 Materials and methods

4.2.1 Materials

Purified GPR41-His_{10} and GPR43-His_{10} were obtained as described in Chapter 3. SD-2 96-well crystallisation plates were purchased from IDEX corp, California. 3, 7, 11, 15-tetramethyl-1, 2, 3-hexadecanetriol (Phytantriol) was provided by DSM Nutritional Products, Germany. Unless otherwise stated, all buffers were purchased from Sigma Aldrich.

4.2.2 Methods

4.2.2.1 Sample preparations for cubic phase characterisation

Sample preparation for SAXS was carried out according to Darmanin et al., 2012. Briefly, the lipid (MO or phytantriol) and cholesterol were weighed and dissolved in chloroform at the appropriate ratio, and left to dry in a fume hood for 2 days until all chloroform had evaporated. The dried lipid/cholesterol mixture was then re-suspended in absolute ethanol and 210 μg of lipid was dispensed into SD-2 96-well crystallisation plates using a Mosquito® robot (TTP Labtech, Melbourn, UK). The plates were dried in an oven overnight (40 °C and 0.21 MPa) and then allowed to dry in a fume hood for a further day before the protein was added. The ethanol was evaporated resulting in a film of dry lipid.

To determine the effect of purification buffer on the cubic phase, 0.14 μL of water or the buffer was dispensed onto a film of dry lipid to give a ratio of 60:40 (w/v) of lipid:aqueous solution. The cubic phase forms spontaneously *in situ*. GPR41-His_{10} and GPR43-His_{10} from Chapter 3 were diluted to varying concentrations in purification buffer and were also added to the lipid at the same lipid:aqueous solution ratio. For crystallisation screen experiments, an equal ratio of screen:protein was dispensed on top of the cubic phase. A further 20 μL of

crystallisation screen or water was added into each reservoir well to ensure the cubic phase did not dry out during data collection. The plates were sealed and samples were left to equilibrate for 24 hrs prior to data collection. Crystallisation screens used in this study are PACT Suite screen (QIAGEN), PEG/Ion and PEG/Ion2 screens (Hampton Research). Cholesterol concentration used in this study was calculated in mol% based on the total mass of cholesterol and lipid. The concentrations of cholesterol used with MO were 2.9 mol%, 10.4 mol% and 13.9 mol%; with phytantriol, the cholesterol concentrations were 0.8 mol%, 2.2 mol% and 5.6 mol%.

4.2.2.2 Small angle X-ray scattering (SAXS) measurement at Australian Synchrotron

The structure of mesophases was determined using SAXS. All the data were collected at the SAXS/WAXS beamline at the Australian Synchrotron. A beam wavelength of 1.033Å (12.0keV) with X-rays at a typical flux of 5 x 10^{12} photos/s were used for all experiments. 2-D diffraction images were recorded on a Pilatus 1M detector. A custom-designed plate-holder, as described in Conn et al., 2012 allowed high-throughput data collections. The plates were mounted directly in the beam for *in situ* SAXS analysis. All images were analysed using AXcess, a custom-built SAXS analysis program (Seddon et al., 2006). The q-axis of the 1-dimensional (1D) diffraction patterns was calibrated using silver behenate as standard.

4.3 Results

2D images collected from SAXS were converted to 1D plots using a custom-built SAXS analysis program, AXcess (Seddon et al., 2006). The peaks in the 1D plot are fitted individually and program calculates the lattice parameter of the phase based on the positions of the peaks in the 1D plot. Each type of lipid phase has a unique SAXS pattern, examples of some of the phases identified in this study is shown in Figure 4-5. The results presented in this chapter are average lattice parameters calculated from data obtained from two sub-wells. Raw data (lattice parameter and phase) for Table 4-2 to Table 4-5 and Figure 4-6 to Figure 4-13 are presented in Appendix section. On occasions where one sub-well had no diffraction, results of the other sub-well were presented. With samples where both sub-wells had no diffraction, the samples were recorded as no diffraction. Samples where each sub-well produced different phases were considered to be non-reproducible and are labelled as N/A.

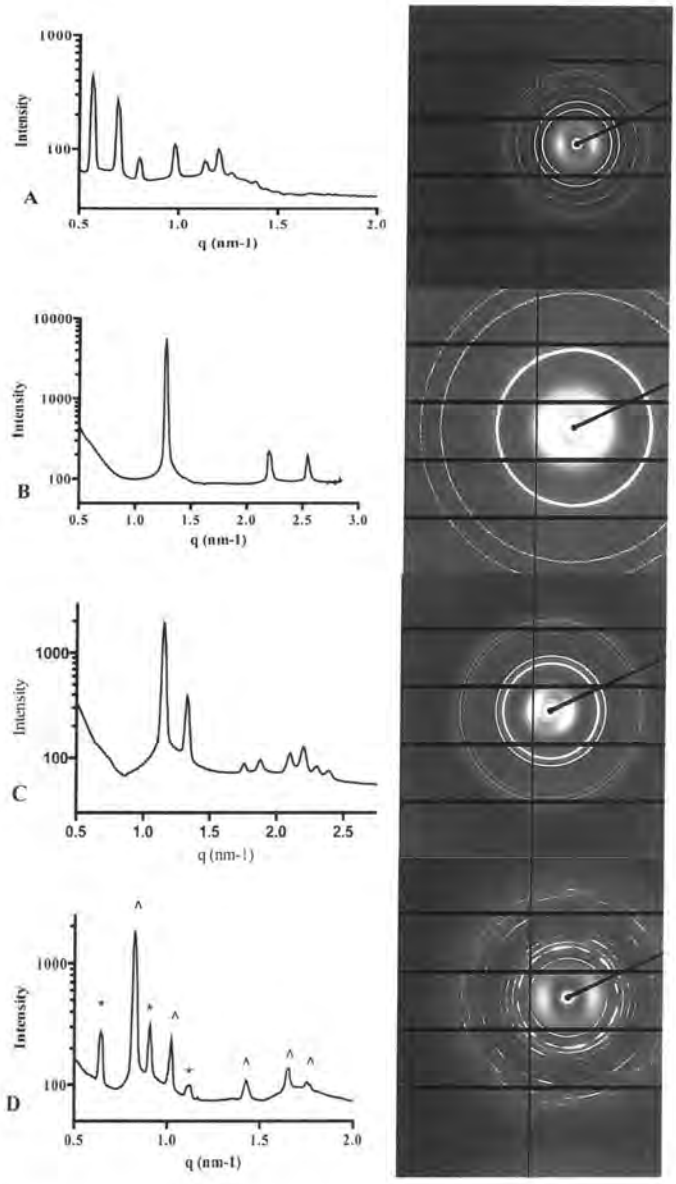

Figure 4-5 Representative 2D images and 1D diffraction plots of intensity vs q.

(A) Q_{II}^{D} (diamond) cubic phase, the √2, √3, √4, √6, √8 and √9 reflections are indicated. (B) H_{II} (inverse hexagonal) phase, the √1, √3 and √4 reflections are indicated. (C) Q_{II}^{G} (gyroid) cubic phase, the √6, √8, √14, √16, √20, √22, √24 and √26 reflections are indicated. (D) Co-existing phases of Q_{II}^{P} and Q_{II}^{D} phases, reflections ^ represent √2, √3, √6, √8 and √9 of Q_{II}^{D} phase and reflections * represent √2, √4 and √6 of Q_{II}^{P} phase.

4.3.1 Effects of purification buffer on lipids

The phase identified and the lattice parameter of MO with water or purification buffer in the presence of a range of cholesterol concentration is presented in Table 4-2. The cubic phase and lattice parameter identified for MO

4.3.1 Effects of purification buffer on lipids

The phase identified and the lattice parameter of MO with water or purification buffer in the presence of a range of cholesterol concentration is presented in Table 4-2. The cubic phase and lattice parameter identified for MO and water is in agreement with a previous study (Qiu and Caffrey, 2000). A slight increase in lattice parameter was observed with buffer and MO. The diamond cubic phase was retained in the presence of a range of cholesterols, and an increase in the lattice parameter was observed with increasing concentrations of cholesterol up to 13.9 mol%. This finding is consistent with a previous study where cholesterol was shown to swell the diamond cubic phase formed by MO (Cherezov et al., 2002).

Table 4-2 Phase adopted and lattice parameter of MO as a function of buffer, water and cholesterol concentration

Sample	Lattice Parameter (Å)			
	Cholesterol (mol%)			
	0	2.9	10.4	13.9
MO (water)	99.7[a]	99.4[a]	102.7[a]	104.1[a]
MO (buffer)	103.2[a]	103.5[a]	103.9[a]	105.7[a]

[a] - Q_{II}^{D} diamond cubic phase

*** Experiments were carried out in duplicate and the average readings are presented in the table.**

The phase and lattice parameter identified for phytantriol with water or purification buffer in the presence of a range of cholesterol concentrations are shown in Table 4-3. Phytantriol made up with water adopted a diamond cubic phase for all conditions and this is in agreement with a previous study (Barauskas and Landh, 2003). The addition of cholesterol to phytantriol led to a slight decrease in the lattice parameter, while retaining the diamond cubic phase. In contrast to MO, the purification buffer did not have any significant effect on the lattice parameter and phase behaviour of phytantriol.

Table 4-3 Phase adopted and lattice parameter of phytantriol as a function of buffer, water and cholesterol concentration

Sample	Lattice Parameter (Å)			
	Cholesterol (mol%)			
	0	0.8	2.2	5.6
Phytantriol (water)	67.7[a]	67.3[a]	66.9[a]	66.5[a]
Phytantriol (buffer)	67.4[a]	67.5[a]	67.2[a]	66.4[a]

[a] - Q_{II}^{D} diamond cubic phase

* Experiments were carried out in duplicate and the average readings are presented in the table.

4.3.2 Incorporation of GPR41-His_{10} and $GPR43_{10}$ within monoolein (MO) and cholesterol mix

The effects GPR41-His_{10} or GPR43-His_{10} on phase behaviour and the lattice parameter of MO are summarised in Table 4-4. Results of the control samples, which consist of purification buffer and MO, are also presented in the table for comparison. Any additional changes above the controls are attributed to the incorporation of the receptor.

MO samples mixed with purified GPR41-His_{10} showed an increase in the lattice parameter with increasing concentrations of receptor up to 3.05 mg/mL. The lattice parameter was increased by up to 41.4% in the absence of cholesterol. The largest increase in the lattice parameter of the diamond cubic phase was 61.3% in the presence of 10.4 mol% cholesterol. At 3.05 mg/mL of GPR41-His_{10} and 13.9 mol% of cholesterol, one sample adopted the diamond cubic phase and the other adopted co-existing phases of diamond and primitive cubic phase. Since the lattice parameters of the diamond cubic phase in both samples are close enough, the results are presented for comparison. This could be due to an equilibrium issue, where the sample is still undergoing phase transition. At 5 mg/mL, the diamond cubic phase in the presence of cholesterol gave way to FI phase.

Incorporation of GPR43-His_{10} showed a diamond cubic phase for all samples made up with MO. An increase in the lattice parameter of the diamond cubic phase that did not appear to be affected by cholesterol concentration was observed with increasing concentrations of GPR43-His_{10}. The lattice parameter was increased by up to 21.1% in the presence of 10.4 mol% cholesterol and 5.77 mg/mL of GPR43-His_{10}.

Table 4-4 SAXS data showing phase adopted and lattice parameter of MO as a function of buffer, water, and concentration of cholesterol, GPR41-His_{10} and GPR43-His_{10}.

Sample	Lattice Parameter (Å) Cholesterol (mol%)			
	0	2.9	10.4	13.9
Buffer	103.2[a]	103.5[a]	103.9[a]	105.7[a]
GPR41-His_{10} (0.81mg/ml)	111.3[a] (7.8)	108.2[a] (4.5)	109.4[a] (5.3)	111.8[a] (5.8)
GPR41-His_{10} (1.63mg/ml)	121.2[a] (17.4)	123.4[a] (19.2)	No D	122.8[a] (16.2)
GPR41-His_{10} (3.05mg/ml)	145.9[a] (41.4)	164.1[a] (58.6)	167.6[a] (61.3)	202.8[b], 158.8[a] 156.9[a]
GPR41-His_{10} (5mg/ml)	N/A	FI	No D	FI
GPR43-His_{10} (0.81mg/ml)	107.2[a] (3.9)	106.9[a] (3.2)	108.1[a] (4.0)	109.1[a] (3.2)
GPR43-His_{10} (1.63mg/ml)	109.8[a] (6.4)	111.3[a] (7.5)	112.4[a] (8.1)	113.8[a] (7.7)
GPR43-His_{10} (3.05mg/ml)	114.0[a] (10.5)	115.4[a] (11.5)	116.4[a] (12.0)	116.3[a] (10.0)
GPR43-His_{10} (4.88mg/ml)	116.8[a] (13.1)	120.1[a] (16)	121.6[a] (17.0)	123.9[a] (17.2)
GPR43-His_{10} (5.77mg/ml)	N/A	124.9[a] (20.7)	125.8[a] (21.1)	125.9[a] (19.1)

[a] – Q_{II}^D diamond cubic phase

[b] – Q_{II}^P primitive cubic phase

FI- fluid isotropic phase

N/A – inconsistent between subwells

No D – No diffractions

*** Percentage of increment with reference to buffer is presented in brackets.**

*** Experiments were carried out in duplicate and the average readings are presented in the table.**

4.3.3 Incorporation of GPR41-His_{10} and GPR43-His_{10} within phytantriol and cholesterol mix

The effects of GPR41-His_{10} and GPR43-His_{10} on phytantriol are presented in Table 4-5. The results for control samples made up with buffer are included in the table for comparison. The cholesterol concentrations were modified to 0.8, 2.2 and 5.6 mol%. A previous study carried out by our group determined that the cubic phase of phytantriol was retained at these concentrations.

In this study, experiments carried out with GPR41-His_{10} with phytantriol doped with cholesterol resulted in a few inconsistent readings. A number of samples containing low concentrations of GPR41-His_{10} were unable to generate reproducible results. Hence, the effects of GPR41-His_{10} at low concentrations were unable to be determined. The reason for this is explained in section 4.4.1. In the absence of cholesterol, the diamond cubic phase of phytantriol was retained in the presence of GPR41-His_{10} concentration up to 3.05 mg/mL. A general trend of an increase in the lattice parameters of the diamond cubic phase was observed with increasing concentrations of GPR41-His_{10}, suggesting the diamond cubic phase had swelled to incorporate the receptor. Further incremental increases of the concentration to 5 mg/mL resulted in the diamond cubic phase giving way to an H_{II} phase. In the presence of all concentrations of cholesterol, 5 mg/mL of GPR41-His_{10} resulted in a FI phase. Co-existing cubic phases were observed with samples made up with 3.05 mg/mL of GPR41-His_{10} and cholesterol.

Similar to MO, the diamond cubic phase of phytantriol was retained at all concentrations of GPR43-His_{10}. An increase in the lattice parameter was observed with increasing concentrations of GPR43-His_{10}, while the diamond cubic phase lattice parameter increased by up to 28.9%.

Table 4-5 SAXS data showing phase adopted and lattice parameter of phytantriol as a function of buffer, water, and concentration of cholesterol, GPR41-His_{10} and GPR43-His_{10}.

Sample	Lattice Parameter (Å)			
	Cholesterol (mol%)			
	0	0.8	2.2	5.6
Buffer	67.4[a]	67.5	67.2	66.4[a]
GPR41-His_{10} (0.81mg/ml)	71.7[a] (6.4)	N/A	74.7[a] (11.2)	(No D)
GPR41-His_{10} (1.63mg/ml)	75.2[a] (11.6)	N/A	N/A	80.35[a] (21.0)
GPR41-His_{10} (3.05mg/ml)	87.5[a] (29.8)	139.5[b], 108.6[a]	142.5[b], 78.2[c]	N/A
GPR41-His_{10} (5mg/ml)	75.3[c]	FI	FI	FI
GPR43-His_{10} (0.81mg/ml)	71.8[a] (6.5)	No D	71.1[a] (5.8)	No D
GPR43-His_{10} (1.63mg/ml)	70.4[a] (4.5)	73.8[a] (9.3)	74.6[a] (11.0)	71.6[a] (7.8)
GPR43-His_{10} (3.05mg/ml)	72.4[a] (7.4)	78.2[a] (15.9)	78.2[a] (16.4)	78.2[a] (17.8)
GPR43-His_{10} (4.88mg/ml)	74.2[a] (10.1)	83.4[a] (23.6)	83.4[a] (24.1)	85.1[a] (28.2)
GPR43-His_{10} (5.77mg/ml)	75.5[a] (12)	N/A	86.6[a] (28.9)	80.2(20.8)

[a] – Q_{II}^{D} diamond cubic phase

[b] – Q_{II}^{P} primitive cubic phase

[c] – H_{II} inverted hexagonal phase

FI- fluid isotropic phase

N/A – inconsistent between subwells

No D – No diffractions

*** Percentage of increment with reference to buffer is presented in brackets.**

*** Experiments were carried out in duplicate and the average readings are presented in the table.**

4.3.4 Effects of PACT crystallisation screen on MO in the presence of GPR41-His_{10} and GPR43-His_{10}

Dr. Charlotte Conn carried out a study on the effect of PACT screens on phase behaviour of MO and the results are included in this section by way of comparison. The phase behaviour of MO in the presence of PACT screens is shown in Figure 4-6. In the presence of PACT screens, the cubic phase was retained in the majority of the wells. To investigate the effect of GPR41-His_{10} or GPR43-His_{10} on MO in the presence of PACT screens, we incorporated 1.63 mg/mL of GPR41-His_{10} or GPR43-His_{10} into MO, followed by overlaying a PACT crystallisation screen on top of the lipid/protein mix. This protein concentration was chosen because protein precipitations in the presence of crystallisation screens were observed with higher protein concentrations at 3.05 mg/mL (refer to Chapter 5).

Incorporation of 1.63 mg/mL of GPR41-His_{10} into MO/PACT have resulted in phase transitions from cubic to lamellar or co-existing phases of lamellar and gyroid cubic phase, shown in Figure 4-7. We were only able to determine the phases for 74% of the samples. The reason for this is discussed in section 4.4.1.

Incorporation of 1.63 mg/mL of GPR43-His_{10} into MO/PACT resulted in the retention of the overall cubic phases observed in the absence of proteins, as shown in Figure 4-8. This set of results obtained was fairly consistent, except for two wells, which were not reproducible, while approximately 10% of the wells had no diffraction. The lattice parameters of the gyroid cubic phase fell in the range from 133.4 Å to 148.2 Å and the lattice parameters of diamond cubic phase were within 84.5 Å and 103.4 Å. The lattice parameters of the gyroid cubic phase and the diamond cubic phase in the absence of protein were in the range of 118 Å to 134.1 Å and 83.9 Å to 90.8 Å, respectively. This suggests that GPR43-His_{10} was incorporated into the cubic phase of MO, whereby the cubic phase swelled to accommodate the receptor. It was noted that GPR43-His_{10} caused phase transition of lamellar to cubic phase in wells B9, D2, E11, G9, G12, H5, H6 and H7. In a few samples it was also observed that the incorporation of GPR43-His_{10}

resulted in a phase transition from the gyroid cubic phase to the diamond cubic phase (wells G1, H1, G11 and H11).

4.3.5 Effects of PACT crystallisation screen on phytantriol in the presence of GPR41-His_{10} and GPR43-His_{10}

Dr. Charlotte Conn carried out a study on the effect of PACT screens on the phase behaviour of phytantriol and the results are included in this section by way of comparison. Figure 4-9 shows the phases obtained with samples made up with phytantriol and PACT screens. In contrast to MO (Figure 4-6), the PACT screens resulted in phytantriol forming lamellar phase in a majority of the wells. The effects of GPR41-His_{10} or GPR43-His_{10} in phytantriol/PACT were studied and samples were set up as described in Section 4.3.4. The results obtained are summarised as a schematic diagram in Figure 4-10 for GPR41-His_{10} and Figure 4-11 for GPR43-His_{10}.

GPR41-His_{10} has a significant influence on the phase behaviour of phytantriol in the PACT crystallisation screen, which resulted in phase transition of lamellar to cubic phase across the entire plate. The results obtained for this study were fairly consistent; reproducibility of this plate was achieved at 98%. GPR43-His_{10} also resulted in cubic phase formation across the whole plate and the results were fairly consistent at 89% reproducibility. Because most of the sample transitioned from lamellar phase to cubic phase, we were unable to make a direct comparison on the lattice parameter. The effects of phase transition may have resulted from incorporation of the receptors. This is further discussed in 4.4.3

Figure 4-6 SAXS characterisation of PACT screen and MO.

SAXS data analysis showing distribution of phases across the crystallisation plates is shown as a schematic. For top and bottom sub-wells that were not reproducible in terms of phase adopted, the well is coded N/A. White wells represent samples with no diffraction. Data obtained from Dr. Charlotte Conn.

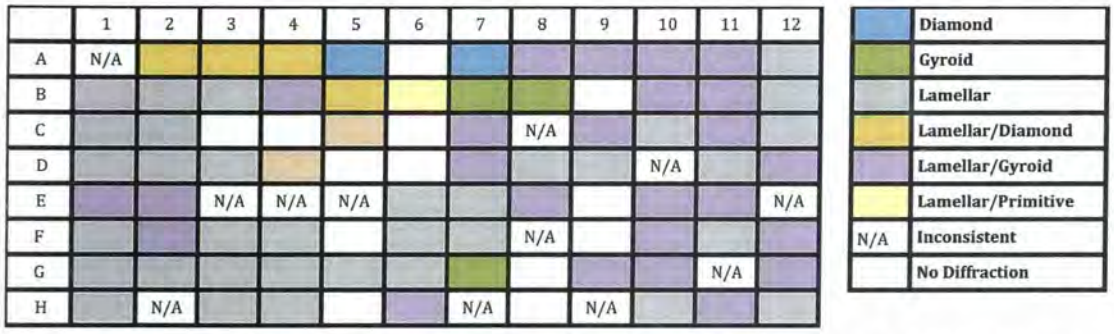

Figure 4-7 SAXS characterisation of PACT screen and MO in the presence of GPR41-His_{10}.

GPR41-His_{10} (1.63 mg/mL) was set up with MO and PACT screen. SAXS data analysis showing distribution of phases across the crystallisation plates is shown as a schematic. For top and bottom sub-wells that were not reproducible in terms of phase adopted, the well is coded N/A. White wells represent samples with no diffraction.

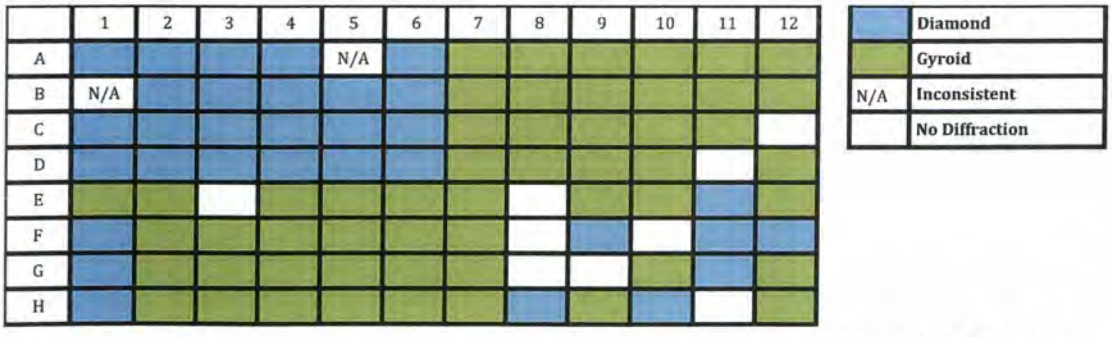

Figure 4-8 SAXS characterisation of PACT screen and MO in the presence of GPR43-His_{10}.

GPR43-His_{10} (1.63 mg/mL) was set up with MO and PACT screen. SAXS data analysis showing distribution of phases across the crystallisation plates is shown as a schematic. For top and bottom sub-wells that were not reproducible in terms of phase adopted, the well is coded N/A. White wells represent samples with no diffraction.

Figure 4-9 SAXS characterisation of PACT screen and phytantriol.

SAXS data analysis showing distribution of phases across the crystallisation plates is shown as a schematic. For top and bottom sub-wells that were not reproducible in terms of phase adopted, the well is coded N/A. White wells represent samples with no diffraction. Data obtained from Dr. Charlotte Conn.

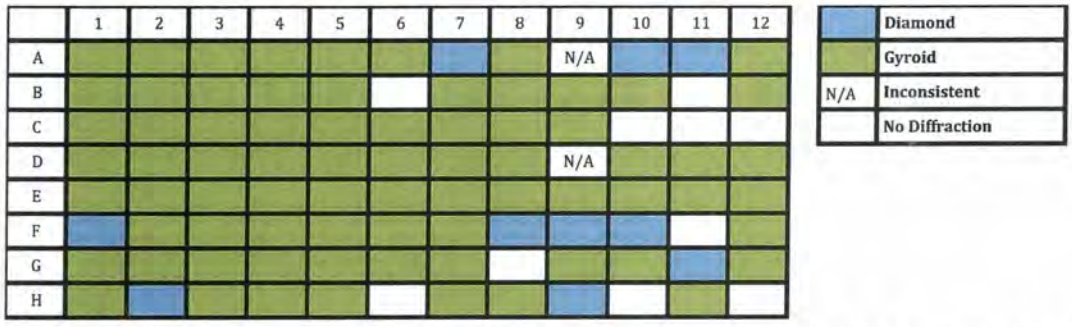

Figure 4-10 SAXS characterisation of PACT screen and phytantriol in the presence of GPR41-His_{10}.

GPR41-His_{10} (1.63 mg/mL) was set up with phytantriol and PACT screen. SAXS data analysis showing distribution of phases across the crystallisation plates is shown as a schematic. For top and bottom sub-wells that were not reproducible in terms of phase adopted, the well is coded N/A. White wells represent samples with no diffraction.

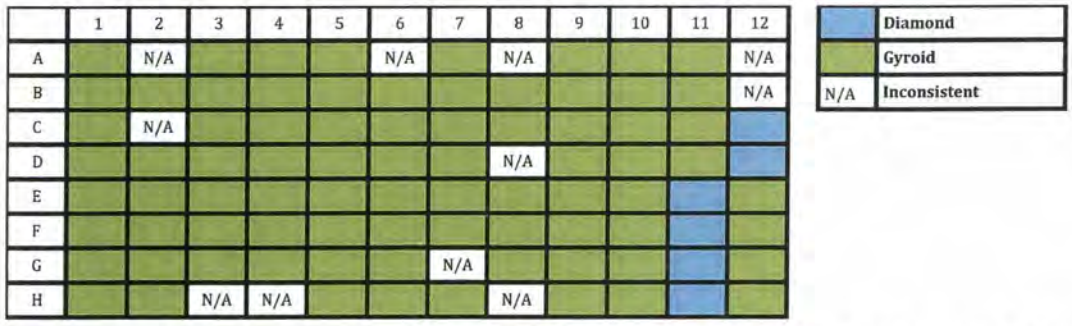

Figure 4-11 SAXS characterisation of PACT screen and phytantriol in the presence of GPR43-His_{10}.

GPR43-His_{10} (1.63 mg/mL) was set up with phytantriol and PACT screen. SAXS data analysis showing distribution of phases across the crystallisation plates is shown as a schematic. For top and bottom sub-wells that are not reproducible in terms of phase adopted, the well is coded N/A.

4.3.6 Effects of GPR43-His_{10} on MO in the presence of PEG/Ion and PEG/Ion2 screens

Dr. Charlotte Conn carried out a study on the effect of PEG/Ion screens on phase behaviour of MO and the results are included in this section by way of comparison. The phases adopted in the presence of PEG/Ion and PEG/Ion2 screens are presented in Figure 4-12. The effect of GPR43-His_{10} in these systems was studied.

Incorporation of GPR43-His_{10} did not result in any significant changes in phase behaviour of MO, shown in Figure 4-13. The reproducibility was approximately 85% for this set of data. The gyroid cubic phase was observed across the entire plate. In particular, wells C12, D2, E10 and E12, were observed to be in the lamellar phase in the absence of receptors (Figure 4-12). Addition of GPR43-His_{10} resulted in gyroid cubic phase in these wells. Lattice parameters of the gyroid cubic phase observed in this data set ranged from 143.5 Å to 168.8 Å. Comparison with the lattice parameters (117 Å to 142.5 Å) observed in the absence of proteins suggests that GPR43-His_{10} was incorporated into the gyroid cubic phase of MO.

Figure 4-12 SAXS characterisation of PEG/Ion screens and MO.

SAXS data analysis showing distribution of phases across the crystallisation plates is shown as a schematic. For top and bottom sub-wells that were not reproducible in terms of phase adopted, the well is coded N/A. White wells represent samples with no diffraction. Data obtained from Dr. Charlotte Conn.

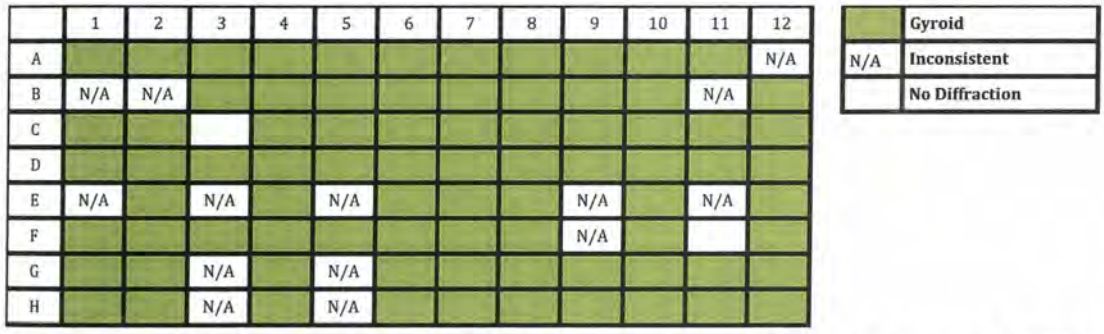

Figure 4-13 SAXS characterisation of PEG/Ion screens and MO in the presence of GPR43-His_{10}.

GPR43-His_{10} (1.63 mg/mL) was set up with MO and PEG/Ion screens. SAXS data analysis showing distribution of phases across the crystallisation plates is shown as a schematic. For top and bottom sub-wells that were not reproducible in terms of phase adopted, the well is coded N/A. White wells represent samples with no diffraction.

4.4 Discussion

Phase characterisation prior to crystallisation trials is an important step to minimise wastage of time and precious protein samples. It has been hypothesised that cubic phase is required for *in meso* crystallisation and formation of 3D crystals (Caffrey and Cherezov, 2009), hence, it is important to have the lipid in the cubic phase after the incorporation of the target protein. In crystallisation, the driving force for nucleation is generally stronger with higher protein concentration. Therefore, the common approach in crystallisation is to use the highest possible protein concentration for crystallisation trials. However, this may not be suitable for *in meso* crystallisation as indicated by our results where a phase change in the lipid was observed at low protein concentrations. This is discussed in more detail in the following sections.

4.4.1 Reproducibility of samples

Samples were set up as duplicates in 96-well crystallisation plates. Reproducibility of the plates ranged from 74% to 97.9%. Several wells had no diffraction during analysis and these wells were confirmed to have no lipid by light microscope examination. On several occasions during plate setups, the Mosquito® robot was problematic and inconsistent in drawing up solution to all tips, leaving some wells without lipids. This issue was later resolved and found to be a manufacturer problem. Once this was fixed, the reproducibility of the setup was improved. Some samples were observed with different phases adopted in each sub-well and are considered to be non-reproducible. As the samples set up in this study were only equilibrated for 1 day, it is possible that the inconsistencies of some wells may have resulted from equilibration issues. The difference in phases between sub-wells could also be due to the delay in dispensing samples to the bottom sub-wells. A recent report on high throughput phase characterisation studies using an automated system has shown that samples that were dispensed earlier were observed with smaller lattice parameters due to dehydration of the sample, although no differences in phases were observed (Joseph et al., 2011).

This may be due to the sample setup in that study, where the lipid was pre-mixed with water prior to dispensing and overlaying with the crystallisation screen, being different to the setup we used. In this study, protein and crystallisation screens were added to a dry film of lipid and hence it is possible that the dehydration effect was greater in our setup, resulting in different phases being adopted between sub-wells.

4.4.2 Effects of GPR41-His_{10} and GPR43-His_{10} incorporation within cubic phase of MO and phytantriol cholesterol mix.

Initially, phase characterisation was carried out with lipid and receptors in the absence of crystallisation screens. In addition, the effect on cholesterol concentration was also investigated. A phase transition was found when the protein concentration in the lipid was increased. GPR41-His_{10} resulted in a phase transition from diamond cubic to FI phase as the protein concentration increased to 5 mg/mL. Cubic phase was retained at a lower concentration of GPR41-His_{10} at 3.05 mg/mL in both systems. It was also noted for GPR41-His_{10} samples in both lipids that the FI phase was only observed in the presence of cholesterol. Although it was hypothesised that cholesterol would have a beneficial effect on crystallisation, our results on GPR41-His_{10} suggest that cholesterol had a significant effect on the phase boundary of both MO and phytantriol, potentially destabilising the cubic phase and causing it to form FI phase as the concentration of GPR41-His_{10} was increased.

As opposed to GPR41-His_{10}, cubic phase was retained at all concentrations of GPR43-His_{10} in both systems, with the highest concentration studied being 5.77 mg/mL. Higher concentrations were not attempted because at 3.05 mg/mL, protein precipitations of both GPR41-His_{10} and GPR43-His_{10} were observed in the presence of crystallisation screens (Results in Chapter 5). Therefore, 1.63 mg/mL of protein concentration was used for subsequent studies with crystallisation screens. Successful *in meso* crystallisation of GPCRs ranges from 20 mg/mL to 70

mg/mL (Cherezov et al., 2007; Chien et al., 2010; Wu et al., 2010; Shimamura et al., 2011), however, a much lower concentration (2.5 mg/mL) was shown to be successful for obtaining membrane protein crystals of photosynthetic reaction centre from *Rhodobacter sphaeroides* (RC) (Wallace et al., 2011). They demonstrated that upon addition of RC to MO, the protein spontaneously incorporates within the lipid without mechanical mixing and is followed by enrichment of RC within the lipid matrix, suggesting *in meso* crystallisation with low protein concentration could still be feasible.

Our results clearly show that GPR41-His_{10} and GPR43-His_{10} have different effects on lipids. The effect of proteins on lipid structure and organization is attributed to several factors: the hydrophobic and hydrophilic domains of the proteins, the degree of protein penetration into the membrane bilayer, and the ability to alter the curvature of the membrane (Yaghmur et al., 2007). Given that GPR41-His_{10} and GPR43-His_{10} have the same molecular weight (37kDa and 38kDa, respectively), similar inter-helical loops and predicted TM and hydrophilic regions (secondary structures), it is unlikely that the lipid behaviour can be attributed to size or the secondary structure of the receptors. In addition both receptors were in the same buffer composition, ruling out buffer components affecting phase change.

The likely explanation is that the results observed may be due to the differences in amino acid composition of the receptors. A sequence alignment of GPR41 and GPR43 revealed that these two receptors only have 52% similarity in amino acid composition. The majority of differences were found to be in the inter-helical cytoplasmic loops. Given that the head-groups of both lipids are uncharged, we can therefore rule out the possibility of electrostatic interaction between charged residues and lipid head-groups. Other possible explanations include: i) The polar amino acid residues located close to the apolar/polar interface form hydrogen bonds with the lipid head-group, thereby altering the curvature of the lipid or ii) A negative mean curvature of the bicontinuous cubic phase causes the lipid to curve towards the water channel (Killian and Nyholm, 2006). Electrostatic repulsion between the charged residues present in the inter-helical loops of the

protein could increase the distance between proteins, resulting in the lipid curving away from the water channel and producing a positive mean curvature. As GPR41 has slightly more positive residues in the first intracellular cytoplasmic loop (ICL1), ICL3 and ECL2 loops, this could potentially destabilise the cubic phase. iii) The length of the TM region may affect phase transitions of lipids as has been shown with studies of TM peptide (Morein et al., 2000; Siegel et al., 2006). This is known as hydrophobic mismatch, whereby the thickness of the membrane bilayer is greater than the TM region of protein, resulting in a disordering of the lipid acyl chains (Killian and Nyholm, 2006). Although the lengths of TM helices for both receptors could not be accurately calculated, differences in the number of residues present in TM1 and TM6 of GPR41 and GPR43 were noted. TM1 of GPR41 was found to be three residues longer than GPR43, and TM6 of GPR41 was found to be four residues shorter than GPR43. Although these differences are minor, they could have a significant effect on lipid organisation.

4.4.3 Comparison of effects exerted by GPR41-His_{10} and GPR43-His_{10} on MO and phytantriol in the presence of crystallisation screens

Crystals of GPCRs with known structures were crystallised in the presence of polyethylene glycols (PEGs). PEGs are known to have a water-withdrawing effect and are commonly included in crystallisation screens. The water-withdrawing effect results in supersaturation of protein concentration, which will subsequently favour crystal nucleation (Wiener, 2004). The PACT screen consists of various molecular weights of PEGs ranging from PEG 1500 to PEG 6000 and is commonly used for protein crystallisation (Newman et al., 2005). A previous study by Dr. Charlotte Conn found that PACT screen resulted in MO forming mostly cubic phases. Diamond cubic phase was observed with low molecular weight PEGs (1500), while a few wells formed the lamellar phase and the remaining wells consisting of higher molecular weight PEGs (3500 and 6000) were observed with gyroid cubic phase. This is expected as higher molecular weight PEGs have a greater water-withdrawing effect and the gyroid cubic phase is found at low water content on the MO/water phase diagram (Figure 1-14). The effects of other

components in this screen have been discussed in detail elsewhere (Conn et al., 2012). Whilst PACT screens consist of varying molecular weights of PEGs, the PEG/Ion screens are only comprised of PEG 3350 with a variety of anions, cations and organic acids. As it was also found that PEG/Ion screens resulted in mostly gyroid cubic phase across the plate, with a few wells observed with lamellar phase, we began by using crystallisation screens that produced the desired phases in the lipids for our experiments.

In this study, GPR41-His_{10} and GPR43-His_{10} were shown to have exerted different effects in this multi-component system. The incorporation of GPR41-His_{10} destabilised the cubic phase formed by MO; only a very small number of cubic phases remained with the vast majority being either pure lamellar or co-existing lamellar and cubic phases in the presence of PACT screen. The mechanism of *in meso* crystallisation occurs within the cubic phase and nucleation is accompanied by co-localisation of the lamellar phase (Nollert et al., 2001; Qutub et al., 2004; Caffrey and Cherezov, 2009), however, the nucleation process usually occurs several days after setting up. Given that the sample was set up only one day prior to SAXS measurement, it is unlikely that the nucleation process had taken place to induce co-localised lamellar formation. This is also supported by the fact that crystallisation trials were set up for this condition (1.63 mg/mL of GPR41-His_{10} in MO with PACT screen) and no crystals were observed under these conditions (Refer to Chapter 5). This suggests that the destabilising effect of GPR41-His_{10} on the cubic phase of MO was amplified by the PACT screen components. Therefore, it is suggested that MO and PACT screen are unsuitable for crystallisation trials of GPR41-His_{10}.

By contrast, the presence of GPR43-His_{10} did not have a significant effect on the phase behaviour of MO in the presence of PACT screens with a majority of the samples remaining in cubic phase (gyroid and diamond). The incorporation of GPR43-His_{10} to MO in the presence of PEG/Ion screens was observed with only gyroid cubic phase, which is favourable for crystallisation. The increase in the lattice parameter of cubic phase shows that GPR43-His_{10} was incorporated within

the lipid matrix. Consequently, MO with PACT and PEG/Ion screens were used in crystallisation trials for GPR43-His_{10} (refer to Chapter 5).

In the presence of the PACT screen, phytantriol was previously observed with mainly lamellar phase across the entire plate with some gyroid cubic phase (results were provided by Dr. Charlotte Conn). With the addition of GPR41-His_{10} or GPR43-His_{10} to this system, the result was unexpectedly reversed and the majority of the wells were observed with gyroid cubic phase and some diamond cubic phase. A possible explanation for this might be the receptors themselves had stabilised the cubic phase of phytantriol, thereby preventing the water-withdrawing effect caused by the PACT screen. In addition, the acyl chain of phytantriol is shorter than MO, with smaller bilayer thickness and lattice parameters. Therefore, it is possible that both GPR41-His_{10} and GPR43-His_{10} are more stable in this condition compared to MO. These results suggest that phytantriol may be a better lipid host for crystallisation of GPR41-His_{10} and GPR43-His_{10} and that PACT screen is suitable for crystallisation trials with phytantriol for the two receptors. Therefore, these crystallisation trials were set up and are discussed in Chapter 5.

Although there have been several studies on the effects of crystallisation screens (Hampton screen and PEG 400/citrate screen) on cubic phase lipids, they were carried out in the absence of membrane protein (Cherezov et al., 2001; Joseph et al., 2011). We have demonstrated GPR41 and GPR43 exert different effects on the cubic phase lipids in the presence of crystallisation screens. In addition, our results also show that commonly used PACT screens may not be suitable for crystallisation trials with certain lipids and membrane proteins. Results presented in this Chapter may provide a useful comparison reference for future studies employing different crystallisation screens.

4.5 Conclusion

We have shown that in the absence of crystallisation screens, the cubic phase of MO was retained in the presence of 3.05 mg/mL of GPR41-His_{10} with 10.4 mol% of cholesterol and 5.77 mg/mL of GPR43-His_{10} with 13.9 mol% of cholesterol. As for phytantriol, the cubic phase was stable in the presence of 3.05 mg/mL of GPR41-His_{10} without cholesterol and 5.77 mg/mL of GPR43-His_{10} with 5.6mol% of cholesterol.

In this study, the PACT screen in phytantriol was found to be suitable for crystallisation trials of GPR41-His_{10} and GPR43-His_{10} at 1.63 mg/mL. PACT screen and PEG/Ion screens were found to be compatible for GPR43-His_{10} (1.63 mg/mL) with MO as the host lipid.

The interactions between lipids and proteins have raised great interest, particularly in the field of *in meso* crystallisation of membrane proteins. Many studies have been carried out to investigate the effects of crystallisation screen components or short TM peptides on lipid behaviour. However, phase characterisation studies with target protein prior to crystallisation are not routinely carried out, as is reflected by the number of publications on phase characterisation studies in the presence of membrane proteins. Results reported in this chapter clearly demonstrate the effects of membrane proteins on cubic phase lipids under different conditions and the importance of identifying these conditions before initiating crystallisation trials.

5 *In meso* crystallisation trials of GPR41-His_{10} and GPR43-His_{10}

5.1 Introduction

3D crystallisation and structure determination of GPCRs remain as major challenges due to the hydrophobic nature and the highly flexible cytoplasmic region of this class of receptor. The traditional vapour diffusion method of attempting to crystallise membrane proteins from detergent micelles has not led to much success. New technologies in GPCR engineering have enhanced the crystallisation process and a novel method, *in meso* crystallisation, has resulted in a number of new GPCR structures (Cherezov et al., 2007; Jaakola et al., 2008; Chien et al., 2010; Wu et al., 2010; Shimamura et al., 2011; Haga et al., 2012). This method involves incorporation of the membrane protein into a highly curved lipid bilayer of bicontinuous cubic phase to mimic the native environment of cell membranes and thus provide stability. Addition of a wide range of components available in crystallisation screens is then used to promote crystal nucleation (Caffrey and Cherezov, 2009). As discussed in Chapter 4, the components present in the crystallisation screens, as well as the target protein itself have effects on the phase behaviour of cubic phase lipids. The appropriate crystallisation conditions (protein and cholesterol concentrations, soluble screen components) that would be compatible with GPR41-His_{10} and GPR43-His_{10} *in meso* crystallisation were determined as described in Chapter 4. This chapter describes attempts to use those conditions for crystallisation trials of the receptors in MO and phytantriol.

5.2 Materials and methods

5.2.1 Materials

SD-2 96-well crystallisation plates were purchased from IDEX corp, California. All buffers and lipids were purchased from Sigma Aldrich, unless otherwise stated. 3, 7, 11, 15-tetramethyl-1, 2, 3-hexadecanetriol (Phytantriol) was provided by DSM Nutritional Products, Germany.

5.2.2 Methods

5.2.2.1 3D *in-meso* crystallisation

All crystallisation plates were set up as sitting drop vapour diffusion experiments. The lipid preparation for the plates was set up as described in section 4.3.1. Briefly, the lipid (MO or phytantriol) was weighed out and dissolved in chloroform at the appropriate ratio and left to dry in the fume hood for 2 days until all chloroform had evaporated. The dried lipid/cholesterol mixture was then re-suspended in absolute ethanol and 210 μg of lipid was dispensed into SD-2 96-well crystallisation plates using a Mosquito® robot (TTP Labtech, Melbourn, UK). The plates were dried in an oven overnight (40 °C and 0.21 Mpa) and then allowed to dry in a fume hood for a further day before the protein was added. After evaporation of the ethanol, 0.14 μL of the protein solution was dispensed onto a film of dry lipid to give a ratio of 60:40 (w/v) of lipid:aqueous solution. 0.14 μL of crystallisation screen was dispensed onto the lipid:protein mix and a further 20 μL of crystallisation screen was added into each reservoir well. After the plates were set up, they were immediately sealed and incubated at 20 degrees for up to 2 months. During the incubation period, each well was photographed by Rigaku Minstrel Imager using the routine inspection time and images were made available for download from the Rigaku Crystaltrak database (C3 facility, Parkville).

Minstrel Imager using the routine inspection time and images were made available for download from the Rigaku Crystaltrak database (C3 facility, Parkville).

The crystallisation screens tested were PEG/Ion, PEG/Ion2 screen (Hampton Research), PACT suite screen (QIAGEN), Index screen (Hampton Research), JCSG+ suite and JCSG Core Suite IV (QIAGEN), CP Custom IV (Axygen), Cubic screen (Emerald Biosystems) and Memgold (Molecular Dimension). Two cubic phase lipids (MO and phytantriol) were used for crystallisation trials for the two receptors. Some of the trials were set up with cholesterol and the cholesterol concentration used in this study was calculated in mol% based on the total mass of cholesterol and lipid. Optimal cholesterol concentrations were determined in Chapter 4 and were used in these trials: they were 10.4 mol% for MO and 5.6 mol% for phytantriol.

5.3 Results

5.3.1 *In meso* crystallisation

In meso crystallisation trials for GPR41-His_{10} and GPR43-His_{10} were performed using several commercially available crystallisation screens. The conditions that were trialled for *in meso* crystallisation of GPR41-His_{10} and GPR43-His_{10} are summarised in Table 5-1.

Initially, crystallisation trials were set up with 3.05 mg/mL of purified receptors with MO or phytantriol. This concentration was previously shown to be compatible with the retention of the cubic phase of both lipids in the absence of the crystallisation screen components by SAXS analysis (refer to Chapter 4). However, upon addition of the crystallisation screen components (Table 5-2) to this system, precipitation was observed in the majority of the wells within 1 day after set up. Examples of wells with protein precipitations are shown in Figure 5-1 and Figure 5-2. The concentrations of the receptors were therefore lowered to 1.63 mg/mL (which was the next highest concentration that had retained the cubic phase studied in Chapter 4) for subsequent crystallisation trials. The appearance of aggregates within MO was significantly reduced, as shown in Figure 5-3; similar results were obtained for samples set up with phytantriol (results not shown).

The effects of cholesterol on the two lipids in the presence of the receptors were studied in Chapter 4. Based on these results, 10.4 mol% and 5.6 mol% of cholesterol was added to MO and phytantriol, respectively for crystallisation trials. No crystals were grown from the trials with protein concentration at 1.63 mg/mL or from the various screens that were tested.

Table 5-1 Conditions used to set up *in meso* crystallisation trials for GPR41-His$_{10}$ and GPR43-His$_{10}$

Screens	GPR41-His$_{10}$				GPR43-His$_{10}$			
	MO		Phytantriol		MO		Phytantriol	
	0 mol% cholesterol	10.4 mol% cholesterol	0 mol% cholesterol	5.6 mol% cholesterol	0 mol% cholesterol	10.4mol% cholesterol	0 mol% cholesterol	5.6 mol% cholesterol
PEG	✓	✶	✓	✶	✓	✶	✓	✶
PACT	✓	✶	✓	✶	✓	✶	✓	✶
Index Screen	✓	✶	✓	✶	✓	✶	✓	✶
JCSG + Suite	✓	✶	✓	✶	✓	✶	✓	✶
JCSG Core Suite IV	✓	✶	✓	✶	✓	✶	✓	✶
CP Custom IV	✓	✶	✓	✶	✓	✶	✓	✶
Cubic Screen	✓	✶	✓	✶	✓	✶	✓	✶
Memgold Screen	✶	N/A	✶	N/A	✶	N/A	✶	N/A

✓ - Conditions were carried out with 3.05 mg/mL and 1.63 mg/mL of purified receptors

✶ - Conditions were only carried out with 1.63 mg/mL of purified receptors

N/A – Not attempted

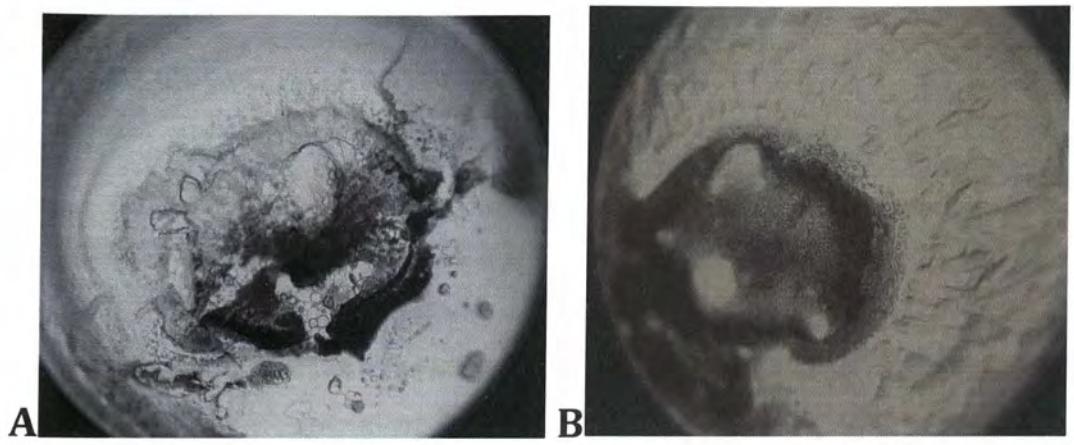

Figure 5-1 GPR41-His_{10} in (A) MO and (B) phytantriol at 3.05 mg/mL

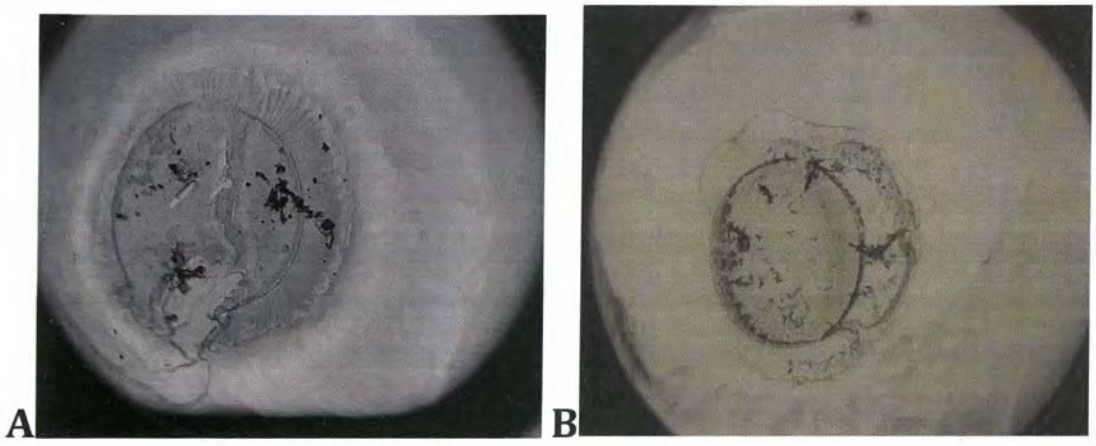

Figure 5-2 GPR43-His_{10} in (A) MO and (B) phytantriol at 3.05 mg/mL

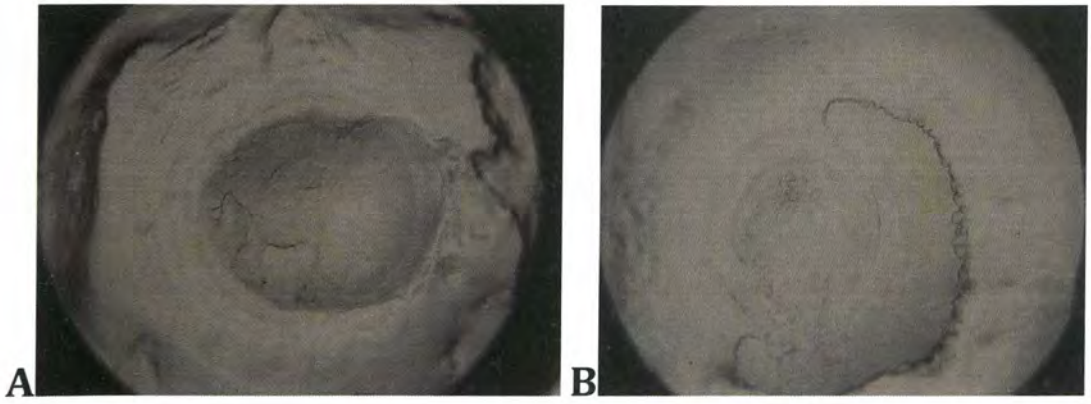

Figure 5-3 (A) GPR41-His_{10} and (B) GPR43-His_{10} in MO at 1.63 mg/mL

5.4 Discussion

5.4.1 *In meso* crystallisation

Full-length GPR41 and GPR43 protein C-terminally His-tagged were subjected to *in meso* crystallisation trials in an attempt to obtain 3D crystals. This method utilises cubic phase lipids, which provide an environment closer to that of the native cell membrane than is the case for detergent micelles. Approximately 4416 conditions were trialled for each receptor. Two different cubic phase lipids, 2 concentrations of cholesterol, 2 different protein concentrations and 8 crystallisation screens were trialled.

Although crystallising GPCR in its native and unaltered form is preferable, for the known GPCR whose structures have been successfully solved to date have proved that alterations, including deletions, mutations or insertions are required for successful crystallisation. B2AR, A2AR, D3R, CXCR4, H1R and M2R crystal structures were obtained by replacing the ICL3 with the highly soluble T4-lysozyme (Cherezov et al., 2007; Jaakola et al., 2008; Chien et al., 2010; Wu et al., 2010; Shimamura et al., 2011; Haga et al., 2012). The structures of B1AR and A2AR-agonist were solved only after point mutations were introduced and the C-terminus was truncated to generate thermo-stabilised constructs (Warne et al., 2008; Lebon et al., 2011). None of these alterations were performed on GPR41-His_{10} or GPR43-His_{10} in this study, although a 10 His-tag was added to the C-terminus. Bioinformatics tools used to predict the TM and cytoplasmic regions of GPR41 and GPR43 (Figure S1 in appendix), revealed that the overall sizes, as well as the ICL3 regions of the two receptors, are relatively small. It was thus decided to attempt to determine the structures of these receptors in their unaltered forms. However, from the limited number of crystallisation trials initiated, no crystals were grown and further trials are required.

Successful attempts of crystallisation of known GPCR were performed at concentration ranging from 20 mg/mL to 120 mg/mL (Chien et al., 2010; Wu et al., 2010; Rasmussen et al., 2011b). In this study, crystallisation trials were carried

out at 3.05 mg/mL protein because SAXS results (refer to Chapter 4) showed that the cubic phase was retained at this protein concentration. However, high levels of protein precipitation were observed in both lipids upon addition of the crystallisation screen components (for GPR41 and GPR43). This suggests that the destabilising effect of GPR41-His_{10} or GPR43-His_{10} on the cubic phase was amplified by the presence of the crystallisation screen components. The incorporation of the protein into the lipid phase was likely prevented by the absence of the cubic phase, thus resulting in protein precipitation. The protein concentration was thereafter lowered to 1.63 mg/mL for further crystallisation trials and protein precipitation was reduced. However, 1.63 mg/mL of protein might be too low to drive the nucleation process as nucleation occurs under conditions where the protein concentration is supersaturated (Asherie, 2004).

Although, MO has been used in all GPCR crystal structures obtained by *in meso* crystallisation, the fact that the protein precipitates even at low concentrations (3.05 mg/mL) suggests that MO may not be compatible with GPR41-His_{10} or GPR43-His_{10}. Another lipid system may be more able to accommodate higher amounts of the receptors. Our study shows that there is a need to develop additional cubic phase lipids that can accommodate a wider variety of GPCRs and membrane proteins. More research into phase behaviour of cubic phase lipids is also required to achieve a better understanding of *in meso* crystallisation.

To date, there is no known natural or synthetic antagonist available for either GPR41-His_{10} or GPR43-His_{10}. A weak agonist, propionic acid was added to the purification buffer in an attempt to stabilise the receptors in the active (R*) state; however, it is known that GPCR in the R* state in a non-native environment is often unstable. Most previously solved GPCR structures involved proteins crystallised with a bound antagonist or inverse agonist. Only last year, structures of B1AR, B2AR and A2AR bound with agonist were solved to a high resolution (Lebon et al., 2011; Warne et al., 2011; Rasmussen et al., 2011a). Much effort has been put into obtaining these receptor structures in the R* state. In particular with B2AR, the R* conformation was stabilised by a nano-body specifically bound to the

G protein binding site or co-crystallised with G protein heterotrimer (Rasmussen et al., 2011a; 2011b). Currently, there is no specific GPR41 or GPR43 antibody that could have been included for co-crystallisation trials. The presence of G proteins with the GPCR may help stabilising the conformation in a state suitable for growing crystals. G proteins could not be included in the co-crystallisation studies described here because purified G proteins were not available (discussed in Chapter 2).

Wallace et al. showed that the length of incubation of the membrane protein with MO prior to the addition of crystallisation screens, could affect the quantity of crystals. They observed an increase in the number of crystals at longer incubation times (Wallace et al., 2011). However, the set up reported was different to this study in that they dispensed the RC onto hydrated MO, whereas we dispensed the protein onto a dry thin film of lipid. Although the set up was different, we demonstrated that incorporation of protein within the lipid occurs within 24 hrs and Darmanin et al. also showed that Br crystals can be obtained using the procedure performed in this study (Darmanin et al., 2012). Nevertheless, the incubation time may be another parameter to investigate.

In order to increase the likelihood of obtaining GPR41 and GPR43 crystals and solving the crystal structure, I would, if time permitted, generate G protein virus constructs and obtain purified G proteins for co-crystallisation, and generate constructs to stabilise the conformations of the receptors. In addition, the development of new cubic phase lipids would also be beneficial. However, these further avenues of research are beyond the scope of this PhD project.

5.5 Conclusion

In summary, GPR41-His_{10} and GPR43-His_{10} were used for *in meso* and 2D site-oriented crystallisation trials. High-throughput screening for *in meso* crystallisation failed to identify viable starting conditions for further optimisation, suggesting the constructs for the receptors may require some modification in order to stabilise the conformation to allow crystal packing to occur. The absence of any crystal in all the crystallisation screens may also be attributable to the heterogeneity and low concentration of the purified samples. The presence of protein precipitation observed with samples set up with higher concentration of protein suggesting the lipid systems may not be compatible with proteins. Therefore, different lipid systems will need to be trialled to increase the protein concentration in the crystallisation trials.

6 Final conclusion

Solving the structure of a membrane protein is a challenging task as evidenced by the small number (<300) of unique membrane protein structures that have been deposited in the PDB (Raman et al., 2006). Despite the importance in drug development, the progress in GPCR structural biology has been slow, hindered by difficulties in obtaining sufficient amounts of purified proteins and in stabilising the receptor in a soluble form for crystallisation. Although structural biology of GPCRs is a massive challenge, some progress was made towards the crystallisation of two GPCRs. This chapter summarises the findings of this project along with areas, which could be further optimised.

GPR41 and GPR43 have been expressed in baculovirus expression system. The optimal conditions for expression of the receptors were found to be with an M.O.I of 1 at 48 hrs post infection. Expression of the receptors was detected using an antibody recognising the His-tag and functionality of the receptors was determined using [^{35}S] GTPγS assay. Agonist-induced [^{35}S] GTPγS binding was observed when the receptor was co-expressed with G proteins in insect cells.

The receptors expressed in insect cells were efficiently extracted using detergent, Fos-Choline 12. A single step IMAC purification was sufficient to obtain purified receptors in different species (monomeric and higher molecular mass). The yields of GPR41-His_{10} and GPR43-His_{10} in one litre of cell culture were approximately 250 μg and 265 μg, respectively. The observation of higher molecular mass species being eluted along with the monomeric form in gel filtration chromatography suggests the receptors may oligomerise dynamically in detergent solution. GPR41 and GPR43 expressed in mammalian cells have shown to form homo-oligomers and hetero-oligomers (Stoddart, 2007). Further research into the ability of GPR41 and GPR43 to form oligomers using fluorescence

resonance energy transfer (FRET) or bioluminescence resonance energy transfer (BRET) technique is warranted.

In meso crystallisation is a promising new method generating crystals that are suitable for structure determination of GPCRs. Although MO has been proven useful as a host lipid for crystallising GPCRs, the underlying molecular basis for the crystallisation process is still not well understood. Therefore, as part of this study, cubic phase lipids were studied in regard to their phase behaviour in the presence of additives and target receptors. In this study, cubic phase of MO and phytantriol were destabilised in the presence of low concentration of GPR41 (5 mg/mL). As this is far below the supersaturated concentration required for crystallisation, this important result demonstrates that MO may not be suitable for crystallising all GPCRs. In addition, we have showed that compatibilities of crystallisation screens vary with host lipid and target receptors. PEG/Ion and PACT screens are suitable for GPR43- His_{10} with MO as the host lipid, and PACT screen is suitable for GPR41-His_{10} and GPR43-His_{10} with phytantriol as the host lipid. These results highlight the importance of identifying the initial conditions that retain cubic phase and the strong need to develop new cubic phase lipids for membrane protein crystallisation. In conclusion, results from this project form a good basis for further studies of GPR41 and GPR43.

7 Appendix

A

B

Figure S 1 Predicted TM and cytoplasmic regions of (A) GPR41 and (B) GPR43.

Protein diagram of GPR41 and GPR43 drawn following TMHMM prediction, using TMRPres2D software (Sonnhammer et al., 1998).

Table S1 Phases and lattice parameters for GPR41-His_{10} in MO and cholesterol

Conditions		Phases			
GPR41 (mg/mL)	**Cholesterol (mol%)**	**Diamond**	**Gyroid**	**FI**	**Comments**
0.81	0	111.8			
		110.7			
1.63	0	125.7			
		116.6			
3.05	0	149			
		142.8			
5	0	95.8			
					No diffraction
0.81	2.9	107.1			
		109.2			
1.63	2.9	122.4			
		124.4			
3.05	2.9	161.6			
		166.5			
5	2.9				No diffraction
				FI	
0.81	10.4	108.9			
		109.9			
1.63	10.4				No diffraction
					No diffraction
3.05	10.4	167.6			
		167.5			
5	10.4				No diffraction
					No diffraction
0.81	13.9	111.4			
		112.1			
1.63	13.9	122.9			
		122.7			
3.05	13.9	158.8	202.8		
		156.9			
5	13.9			FI	
				FI	

Table S2 Phases and lattice parameters for GPR43-His_{10} in MO and cholesterol

Conditions		Phases			
GPR43 (mg/mL)	Cholesterol (mol%)	Diamond	Gyroid	FI	Comments
		108			
0.81	0	106.4			
		111.2			
1.63	0	108.4			
		114.9			
3.05	0	113.1			
		116.9			
4.88	0	116.6			
			179.2		
5.77	0	118.9			
		106.5			
0.81	2.9	107.2			
		111.1			
1.63	2.9	111.5			
		115.5			
3.05	2.9	115.3			
		119.2			
4.88	2.9	120.9			
		121.2			
5.77	2.9	128.6			
		108.2			
0.81	10.4	108			
		112.6			
1.63	10.4	112.1			
		117.3			
3.05	10.4	115.4			
		120.2			
4.88	10.4	122.9			
		125.5			
5.77	10.4	126.1			
		108.9			
0.81	13.9	109.2			
		114.2			
1.63	13.9	113.5			
		117.4			
3.05	13.9	115.2			
		122.5			
4.88	13.9	125.3			
		127.2			
5.77	13.9	124.5			

Table S3 Phases and lattice parameters for GPR41-His_{10} in phytantriol and cholesterol

Conditions		Phases				
GPR41 (mg/mL)	**Cholesterol (mol%)**	**Diamond**	**Primitive**	**FI**	**H_{II}**	**Comments**
		71.8				
0.81	0	71.6				
		75.9				
1.63	0	74.4				
		88.77				
3.05	0	86.2				
					75.9	1 peak undefined
5	0				74.7	
			144.6			
0.81	0.8	89.3				
		91.4				
1.63	0.8				55.3	
		109.8	141.5			
3.05	0.8	107.4	138.4			
				FI		
5	0.8			FI		
		75.6				
0.81	2.2	73.7				
		95.3				
1.63	2.2	78.8				
			144.3		79.1	
3.05	2.2		140.6		77.2	
				FI		
5	2.2			FI		
						No diffraction
0.81	5.6					No diffraction
		82.3				
1.63	5.6	78.4				
			149.1			
3.05	5.6	104.7				
				FI		
5	5.6					No diffraction

Table S4 Phases and lattice parameters for GPR43-His_{10} in phytantriol and cholesterol

Conditions		Phases		
GPR43 (mg/mL)	**Cholesterol (mol%)**	**Diamond**	**Primitive**	**Comments**
0.81	0	74.2		
		69.4		
1.63	0	70.4		
		70.3		
3.05	0	72.5		
		72.3		
4.88	0	74.4		
		74		
5.77	0	75.7		
		74.4		
0.81	0.8			No diffraction
				No diffraction
1.63	0.8	74.3		
		73.2		
3.05	0.8	77.8		
		78.5		
4.88	0.8	82.4		
		79.7		
5.77	0.8	103.5	133.3	
		85.6		
0.81	2.2	71.3		
		70.8		
1.63	2.2	76.3		
		72.9		
3.05	2.2	79.2		
		78.2		
4.88	2.2	82.8		
		83.9		
5.77	2.2	85		
		88.2		
0.81	5.6			No diffraction
				No diffraction
1.63	5.6	71		
		72.2		
3.05	5.6	79.6		
		76.7		
4.88	5.6	81.9		
		88.2		
5.77	5.6	85.6		
		74.8		

Table S5 Phases and lattice parameters for MO in PACT screen

Screen number	Phases			Comments
	Diamond	Gyroid	Lamellar	
A1	83.6			
		127.7		
A2	85.9			
				No diffraction
A3	88.4			
	89.6			
A4	89.8			
	90.5			
A5	89.6			
				No diffraction
A6	87.1			
				No diffraction
A7		118.2		
				No diffraction
A8		125.6		
				No diffraction
A9		120.9		
				No diffraction
A10		119.6		
				No diffraction
A11		120.1		
				No diffraction
A12		122.8		
				No diffraction
B1	83.5			
				No diffraction
B2	87.2			
				No diffraction
B3	88.4			
				No diffraction
B4	88.7			
				No diffraction
B5	89.1			
				No diffraction
B6	86.1			
				No diffraction
B7		119.3		
				No diffraction
B8		124		
				No diffraction
B9			42.2	
				No diffraction
B10		118.5		
				No diffraction
B11		119.5		
				No diffraction
B12		124.2		
				No diffraction

Screen number	Phases			Comments
	Diamond	Gyroid	Lamellar	
C1	88.4			
	88.3			
C2	89.2			
	88.3			
C3	88.2			
	88.9			
C4	88.7			
	90			
C5	89.9			
	90.8			
C6	83.9			
	88.4			
C7		127.4		
		129.1		
C8		129.5		
		129.6		
C9			42.5	
		128.4		
C10		127.3		
		128.2		
C11			42.1	
		128.7		
C12			43.6	
				No diffraction
D1	84.8			
				No diffraction
D2			42.4	
				No diffraction
D3	87.6			
	87.8			
D4	86.8			
	88			
D5	90.1			
	90.2			
D6	82.8			
	87.3			
D7		118		
		123.5		
D8		118.2		
				No diffraction
D9		125.5		
		128.4		
D10		125.3		
		128.5		
D11		124.5		
		128.2		
D12		119.8		
				No diffraction
E1		121.1		
				No diffraction

Screen number	Phases			Comments
	Diamond	Gyroid	Lamellar	
E2		125		
				No diffraction
E3		131.6		
				No diffraction
E4		135.2		
				No diffraction
E5		129.6		
				No diffraction
E6		126.6		
				No diffraction
E7		129.9		
		130.1		
E8		132.4		
		132.5		
E9		131.9		
				No diffraction
E10		124.8		
				No diffraction
E11		126.8		
				No diffraction
E12				No diffraction
				No diffraction
F1		120.6		
				No diffraction
F2		118.3		
				No diffraction
F3		129.1		
				No diffraction
F4		133.6		
				No diffraction
F5		129.4		
				No diffraction
F6		123.2		
				No diffraction
F7		128.5		
		130.4		
F8		133.7		
		133.9		
F9		133.1		
		133.4		
F10		133.2		
		133.8		
F11			40.9	
				No diffraction
F12		125.2		
				No diffraction
G1		123.1		
				No diffraction

Screen number	Phases			Comments
	Diamond	Gyroid	Lamellar	
G2		120.4		
				No diffraction
G3		128.9		
				No diffraction
G4		134.1		
				No diffraction
G5		130.1		
				No diffraction
G6		129.6		
				No diffraction
G7				No diffraction
		130.2		
G8		133.3		
		133.6		
G9			42.2	
				No diffraction
G10			41.5	
				No diffraction
G11		128.3		
				No diffraction
G12			41.4	
				No diffraction
H1		118.7		
				No diffraction
H2		120.2		
				No diffraction
H3		129.9		
				No diffraction
H4		122.2		
				No diffraction
H5			43.5	
				No diffraction
H6			41.8	
				No diffraction
H7			41.8	
				No diffraction
H8			41.3	
				No diffraction
H9			42.4	
				No diffraction
H10		125.7		
				No diffraction
H11		132.6		
				No diffraction
H12			41.5	
		121.6		

Table S6 Phases and lattice parameters for GPR41-His_{10} in MO and PACT screen

Screen number	Phases				Comments
	Diamond	Gyroid	Primitive	Lamellar	
A1					No diffraction
					No diffraction
A2	98.3			46.9	
					No diffraction
A3	117.1			48.4	
					No diffraction
A4	107.8			49.2	
	94.5			46.2	
A5	95.9				
	95.7				
A6	97.2			47.3	
				47.9	lamellar 1 peak
A7					No diffraction
	87.9				
A8		163.5		51.9	
		137.9		48.6	
A9		141.6		48.9	
		136.9		48	
A10		139.1		48.8	
		142.1		49.6	
A11		138.4		48.5	
		143.4		50.1	lamellar 1 peak
A12				49.4	lamellar 1 peak
				47.9	
B1				46.3	
				46.5	
B2				48.3	
				48.1	lamellar 1 peak
B3				47.2	
				47.7	lamellar 1 peak
B4		139.2		47.4	
					No diffraction
B5	93.6			46.4	
	93.7			46.7	
B6			124.8	46.9	
					No diffraction
B7					No diffraction
		132.6			
B8		132.8			
					No diffraction
B9		138.5		48.5	
		132.6			
B10		140.6		49.6	
		147.3		49.9	

Screen number	Phases				Comments
	Diamond	Gyroid	Primitive	Lamellar	
B11		140.1		49.1	
					No diffraction
B12				48.7	
				48.5	
C1				47	
				46.9	
C2					No diffraction
				47.2	
C3				48	
	94.4			46.6	
C4	96.9			47.6	
				46.9	
C5	96			46.9	
					No diffraction
C6				47.1	lamellar 1 peak
					No diffraction
C7		142.8		49.4	
					No diffraction
C8					No diffraction
					No diffraction
C9		144.1		48.7	
					No diffraction
C10				50.2	lamellar 1 peak
				49.8	
C11		139.1		48.1	
					No diffraction
C12				48.1	
					No diffraction
D1					No diffraction
				47.7	
D2				47.1	
				46.4	
D3				46	
				47	
D4	96.8			47.2	
	88.6			63.1	1 peak
D5	95.6			46.7	
				46.8	
D6	93.8				
				47.3	1 peak
D7		142.6		49.9	
		137.5		48.9	
D8				50.2	
					No diffraction
D9				49.6	
					No diffraction
D10					No diffraction
					No diffraction

Screen number	Phases				Comments
	Diamond	Gyroid	Primitive	Lamellar	
D11				50.2	
				50.7	
D12					No diffraction
		132.5		46.8	
E1		148.3		49.6	
					No diffraction
E2		161.8		52.9	
		136.9		48.1	
E3					No diffraction
					No diffraction
E4					No diffraction
					No diffraction
E5					No diffraction
					No diffraction
E6				48.9	
					No diffraction
E7				47.5	lamellar 1 peak
					No diffraction
E8		158.3		50.5	
		159.5		49.6	
E9		155			
				51.8	
E10		154.6		50.5	
		153.1		49.9	
E11		175.4		50.6	
		178.4		51.4	
E12					No diffraction
					No diffraction
F1				49.7	lamellar 1 peak
				50.2	lamellar 1 peak
F2					No diffraction
		139.2		49.3	
F3				49.6	
				50.9	
F4				50.4	lamellar 1 peak
				49.9	
F5		140		49.5	
				49.5	
F6				49.2	
					No diffraction
F7				49.9	lamellar 1 peak
				49.9	
F8					No diffraction
					No diffraction
F9		160.1			
				51.9	lamellar 1 peak
F10					No diffraction
		164.6		49.2	
F11					No diffraction
		174.3			

Screen number	Phases				Comments
	Diamond	Gyroid	Primitive	Lamellar	
F12		158.4		49	
		157.8		49.1	
G1				52.8	lamellar 1 peak
				49.1	lamellar 1 peak
G2				49.9	
				50	
G3				50.1	
				49.2	
G4				50	lamellar 1 peak
				51.1	lamellar 1 peak
G5				49.2	
					No diffraction
G6					No diffraction
				48.4	
G7					No diffraction
		139.3			
G8				51.9	
		165.3		49.8	
G9					No diffraction
		156.5		51.7	
G10					No diffraction
		168.9		49.1	
G11					No diffraction
					No diffraction
G12		156.1		49.9	
		155.2		49.3	
H1				50	
				49.6	
H2					No diffraction
					No diffraction
H3				51.7	
				49.6	
H4				51.1	
				49.6	
H5		136.5		47.9	
				48.8	
H6		143.5		49.3	
					No diffraction
H7					No diffraction
					No diffraction
H8		161.9		49.9	
		152.8			
H9					No diffraction
					No diffraction
H10				49.6	lamellar 1 peak
				50.6	lamellar 1 peak
H11		181.4		51.5	
					No diffraction
H12					No diffraction
				50.6	lamellar 1 peak

Table S7 Phases and lattice parameters for GPR43-His_{10} in MO and PACT screen

Screen number	Phases				Comments
	Diamond	Gyroid	Primitive	Lamellar	
A1	100.6				
	97.18				
A2	99.2				
	99.8				
A3	100.4				
	93.7				
A4	97.7				
					No diffraction
A5					No diffraction
					No diffraction
A6	103.4				
					No diffraction
A7		159.1			
					No diffraction
A8		152.7			
					No diffraction
A9		147.5			
		147.4			
A10					No diffraction
		143.3			
A11		161.1			
					No diffraction
A12		148.2			
		148.7			
B1					No diffraction
					No diffraction
B2	95.6				
					No diffraction
B3	96.7				
	95				
B4	94				
	92.3				
B5	91.8				
					No diffraction
B6	91				
					No diffraction
B7		145.9			
					No diffraction
B8		144.7			
					No diffraction
B9		139.6			
		139.4			
B10		146.6			
		143.2			
B11		144.8			
					No diffraction
B12		141.4			
					No diffraction

Screen number	Phases				Comments
	Diamond	Gyroid	Primitive	Lamellar	
C1	95.3				
	94.7				
C2	95.3				
	94.2				
C3	95.3				
	94.4				
C4	94.3				
	94.9				
C5	93.6				
	94.3				
C6	90.7				
	91.2				
C7		147.1			
		142			
C8		144.7			
		141			
C9		139.5			
		137.2			
C10		142.9			
		141.5			
C11		154.2			
					No diffraction
C12		136.8			
		136.9			
D1	94.1				
	94.1				
D2	91.7				
	93.5				
D3	92.2				
	90.3				
D4	92				
	93				
D5	94.1				
	93.2				
D6	90.5				
	89.2				
D7		144.8			
		137.5			
D8		137.4			
		136.3			
D9		139.7			
		136.8			
D10		140.7			
		138.4			
D11		141			
					No diffraction
D12		137.5			
		135.4			
E1		146.6			
					No diffraction

Screen number	Phases				Comments
	Diamond	Gyroid	Primitive	Lamellar	
E2		139.7			
					No diffraction
E3		141.9			
		137.8			
E4		144.5			
		144.2			
E5		138.5			
		140.4			
E6		140.6			
		140.4			
E7		141.1			
		138.7			
E8		140.4			
	89.2				
E9		144			
		143.1			
E10		150.5			
		148.8			
E11	87.8				
	86.4				
E12		141.1			
		143.8			
F1	101.1				
	100.3				
F2		142.4			
		142.3			
F3		137.1			
		144.5			
F4		145.4			
		144.5			
F5		142.1			
		140.9			
F6		142.8			
		142.1			
F7		87.6?			
		141.8			
F8	87.4				
	90				
F9	87.4				
	87.1				
F10		153.9			
		143.3	90		
F11	89.1				
					No diffraction
F12	86.6				
	87.1				
G1	102.5				
					No diffraction
G2		141.4			
					No diffraction

Screen number	Phases				Comments
	Diamond	Gyroid	Primitive	Lamellar	
G3		141.4			
		138.8			
G4		145.9			
		143.5			
G5		140.2			
		139.2			
G6		141.8			
		141.8			
G7					No diffraction
		141.8			
G8		142.8	87.6		
		139.9			
G9	85.4				
		137.1?			
G10		144.9			
		144.2			
G11		88.6			
		88.6			
G12		143.5			
		142.3			
H1		94.8			
					No diffraction
H2		133.9			
					No diffraction
H3		139.4			
		135.8			
H4		143.7			
		142.3			
H5		137.3			
					No diffraction
H6		133.4			
					No diffraction
H7		138.5			
		139.2			
H8	84.5				
	84.2				
H9		143.1			
		144			
H10	88.1				
		146.1			
H11		140.2			
	87.8				
H12		140.2			
		129.8			

Table S8 Phases and lattice parameters for phytantriol in PACT screen

Screen number	Phases			Comments
	Gyroid	FI	Lamellar	
A1			33.9	
			33.9	
A2			33.9	
			33.8	
A3			34	
			34	
A4			33.9	
			33.9	
A5			33.9	
			34	
A6			33.9	
			34	
A7	94.5			
	94.8			
A8			35	
			35.1	
A9			34.9	
			35	
A10			34.7	
			34.9	
A11			34.9	
			35	
A12			34.8	
			34.8	
B1			34	
			34	
B2			33.8	
			33.9	
B3			33.9	
			33.9	
B4			34	
			34	
B5			34.1	
			34.1	
B6			34.1	
			34.2	
B7			34.8	
			34.8	
B8			34.9	
			34.9	
B9			34.7	
			34.8	
B10			34.8	
			34.8	
B11			34.8	
			34.9	
B12			34.9	
			34.9	

Screen number	Phases			Comments
	Gyroid	FI	Lamellar	
C1			33.7	
			33.7	
C2			33.9	
			33.9	
C3			33.9	
			33.9	
C4			33.9	
			34	
C5			34.1	
			34.1	
C6			33.9	
			33.9	
C7			34.7	
			34.8	
C8			34.8	
			34.8	
C9	93.8		34.8	
	94		34.8	
C10				No diffraction
	94			
C11			34.8	
			34.8	
C12				
			34.7	
D1			33.9	
			33.9	
D2			33.4	
			33.7	
D3			33.9	
			33.9	
D4			33.8	
			33.9	
D5			33.8	
			33.9	
D6			33.9	
			34	
D7			35	
			35.1	
D8			35	
			35.1	
D9			35	
				No diffraction
D10	94.6			
	94.5			
D11			35.1	
			35.1	
D12			35.2	
			35.3	
E1			34.9	
			34.9	

Screen number	Phases			Comments
	Gyroid	FI	Lamellar	
E2			35	
			35	
E3			35.1	
			35.2	
E4			35.5	
			35.6	
E5			34.9	
			35	
E6			34.9	
			34.9	
E7			34.7	
			34.7	
E8	94.8		34.8	
	95			
E9	95		34.8	
	95.3			
E10	94.9			
	95.2			
E11		FI		
		FI		
E12				
			34.7	
F1			34.7	
			34.7	
F2			34.6	
			34.7	
F3			34.7	
			34.9	
F4			35	
			35.1	
F5			34.7	
			34.8	
F6			34.7	
			34.1	
F7			34.8	
			34.8	
F8			34.3	
		FI		
F9			34.4	
		FI		
F10			33	
	94.4			
F11			32.3	
			32.2	
F12		FI		
		FI		
G1			34.8	
			34.8	
G2			34.8	
			34.8	

Screen number	Phases			Comments
	Gyroid	FI	Lamellar	
G3			34.9	
			34.9	
G4			35.2	
			35.3	
G5			34.8	
			34.9	
G6			34.8	
			34.9	
G7				No diffraction
			34.8	
G8		FI		
		FI		
G9			32.5	
			32.6	
G10			32.9	
			33	
G11		FI		
			32.6	
G12			32.4	
			32.7	
H1			33	
			34.9	
H2			34.7	
			34.8	
H3			34.9	
			35	
H4			33.6	
			33.6	
H5			33.2	
			33.3	
H6			33.2	
			33.3	
H7			33	
			33.1	
H8			32.8	
		FI		
H9			32.6	
			32.7	
H10				No diffraction
			33	
H11				No diffraction
			33	
H12			32.6	
		FI		

Table S9 Phases and lattice parameters for GPR41-His_{10} in phytantriol and PACT screen

Screen number	Phases			Comments
	Diamond	Gyroid	Lamellar	
A1				
		113.3		
A2		110.3		
		106.1		
A3		123.2		
		103.6		
A4		118.8		
		108.9		
A5		109.4		
		116.5		
A6		119.5		
		114		
A7	107.8			
				No diffraction
A8		127.2		
				No diffraction
A9				lamellar 1 peak
				No diffraction
A10	81.5			
	69.7			
A11	86.4			
				No diffraction
A12		145.9		
				No diffraction
B1		109.4		
		108.9		
B2		104.9		
		101.9		
B3		105.8		
		108.6		
B4		111.9		
		109.8		
B5		112.7		
		108.9		
B6			49.5	
		112.4		
B7		130.9		
		126.9		
B8		119.5		
		117.6		
B9		121.5		
		121.6		
B10		118.3		
		117.5		
B11	79.3			
		115.9		

Screen number	Phases			Comments
	Diamond	Gyroid	Lamellar	
B12		121.1		
		118.7		
C1		132.6		
		100.4		
C2		107.5		
		104.7		
C3		114		
		108.6		
C4		107.7		
		107.4		
C5		108.8		
				Weak diffraction
C6		109.7		
		109.9		
C7		118.5		
		123		
C8		118.8		
		118.4		
C9		157.7		
				No diffraction
C10	74.2			
		124.4		
C11	84			
		117.4		
C12	83.9			
		116.2		
D1		112		
		99.7		
D2		108.4		
		108.1		
D3		110.8		
		110.8		
D4		114.1		
		108.2		
D5		111.2		
		109.7		
D6		105.9		
		105.2		
D7		122.5		
		113.9		
D8		124.7		
		121.9		
D9				Weak diffraction
				Weak diffraction
D10		123.3		
		118.2		
D11				No diffraction
		118.4		
D12		129.2		
		126.8		

Screen number	Phases			Comments
	Diamond	Gyroid	Lamellar	
E1		120.5		
		115.4		
E2		115.7		
		112.7		
E3		119.9		
		118.8		
E4		119.3		
		126.14		
E5		118.1		
		115.4		
E6		116.2		
		111.8		
E7		115.4		
		118.1		
E8		119.1		
		119.6		
E9		117.7		
		120.2		
E10		118.5		
		119.9		
E11		139.7		
		131.1		
E12				No diffraction
		136.2		
F1	81.1			
	77.4			
F2		110.4		
		115.8		
F3		112.8		
		111.8		
F4		118.4		
		118.4		
F5		109.9		
		106.9		
F6		111.7		
		112.1		
F7		109.36		
		114.8		
F8	68.8			
	71			
F9				No diffraction
	69.7			
F10	70.4			
				No diffraction
F11		124.7		
	67.3			
F12		123.5		
		122.1		
G1		130.5		
				No diffraction

Screen number	Phases			Comments
	Diamond	Gyroid	Lamellar	
G2				No diffraction
		112.4		
G3		110.9		
		116		
G4		116.2		
		115.5		
G5		118.4		
		111.3		
G6		115.6		
		114.4		
G7				No diffraction
		113.6		
G8		118.2		
	71.5			
G9		116.5		
		116.9		
G10		118.2		
		118		
G11	61.5			
	61.7			
G12				No diffraction
		129.8		
H1		129.9		
				No diffraction
H2	77			
				No diffraction
H3		116.5		
				No diffraction
H4		111.2		
				No diffraction
H5		117.9		
				No diffraction
H6		116.7		
			47.7	
H7		114.3		
				No diffraction
H8		114.7		
				No diffraction
H9	78			
				No diffraction
H10	71.1			
			49.2	
H11		127.7		
				No diffraction
H12		129.6		
			50	

Table S10 Phases and lattice parameters for GPR43-His_{10} in phytantriol and PACT screen

Screen number	Phases			Comments
	Diamond	Gyroid	H_{II}	
A1		105		
		104.6		
A2			49	
		103.7		
A3		104.9		
		104.5		
A4		100.9		
		101.5		
A5		101.5		
		101.5		
A6				No diffraction
		102.3		
A7		103.9		
		104.1		
A8			48.9	
				No diffraction
A9		104.4		
		104.1		
A10		103.8		
		104.6		
A11		103.5		
		104.7		
A12			49.3	
	69.3			
B1		104.2		
		104.9		
B2		98.1		
		105		
B3		99.6?		
		104.9		
B4		101.4?		
		104.6		
B5		102.2		
		101.9		
B6		102.6		
		103.5		
B7		107		
		106.8		
B8		106.7		
		106.7		
B9		108.3		
		106.6		
B10		104.7		
		106.4		
B11		104.4		
		107.4		

Screen number	Phases			Comments
	Diamond	Gyroid	H_{II}	
B12	68.9			
		111.3		
C1		103.5		
		104.2		
C2				No diffraction
		101.2		
C3		101.9		
		101.9		
C4		101.9		
		105.4		
C5		102.7		
		103.9		
C6		102.5		
		104.6		
C7		105.3		
		108.1		
C8		107.4		
		109.8		
C9		105.8		
		107.6		
C10		107.7		
		108.5		
C11		105.2		
		108.4		
C12	69.5			
	71.2			
D1		106.5		
		107.7		
D2		101.5		
		104.1		
D3		102.2		
		104.7		
D4		101.8		
		102.3		
D5		102.8		
		103.9		
D6		103.7		
		102.4		
D7		107.6		
		109.2		
D8	68.5			
		108.5		
D9		105.6		
		108.6		
D10		106.9		
		107.2		
D11		105.6		
		108.9		
D12	70.9			
	69.9			

Screen number	Phases			Comments
	Diamond	Gyroid	H_{II}	
E1		109.3		
		108.1		
E2		107.5		
		108.7		
E3		109.7		
		109		
E4		111.1		
		110.6		
E5		111.9		
		109.2		
E6		106.4		
		107.6		
E7		105.8		
		108.2		
E8		107.7		
		105.7		
E9		106.2		
		106.1		
E10		106.9		
		106.8		
E11	65.9			
	67.2			
E12		111.2		
		106.2		
F1		106.6		
		108.5		
F2		105.8		
		106.4		
F3		109.5		
		109.2		
F4		109.9		
		110.7		
F5		111.3		
		109.7		
F6		111.2		
		111.3		
F7		110.7		
		107.3		
F8		111.3		
		106.4		
F9		108.6		
		105.8		
F10		106.3		
		105.6		
F11	66.1			
	67.2			
F12		110.5		
		107.6		
G1		105.8		
		108.9		

Screen number	Phases			Comments
	Diamond	Gyroid	H_{II}	
G2		108.9		
		108.7		
G4		112.6		
		111		
G5		112		
		108.2		
G6		110.5		
		108.3		
G7				No diffraction
		107.4		
G8		109.6		
		106.4		
G9		109.4		
		107.7		
G10		110.3		
		108.4		
G11	68.2			
	67.2			
G12		110		
		108.2		
H1		106.8		
		91.8		
H2		107.9		
		91.7		
H3		111.2		
				1 peak
H4		112.6		
				No diffraction
H5		109.1		
		91.3		
H6		105.9		
		91.1		
H7		107.6		
		93.8		
H8		106.3		
		142.1?		
H9		107.6		
		116.9		
H10		109.3		
		108.2		
H11	66.9			
	67.3			
H12		108.9		
		114.5		

Table S11 Phases and lattice parameters for MO in PEG/Ion and PEG/Ion2 screens

Screen number	Phases		Comments
	Gyroid	Lamellar	
A1	123		
			No diffraction
A2	123.8		
			No diffraction
A3	130.5		
	133.5		
A4	129.9		
			No diffraction
A5	119.4		
			No diffraction
A6	118.8		
			No diffraction
A7	120.9		
	124.1		
A8	122		
			No diffraction
A9	130.4		
			No diffraction
A10	140.1		
			No diffraction
A11	132.8		
			No diffraction
A12	129.6		
			No diffraction
B1	131.2		
	135.9		
B2	134.7		
	137.4		
B3	130.8		
	133.2		
B4	122.1		
	125.7		
B5	132		
	132.5		
B6	132.3		
	132.7		
B7	129.9		
			No diffraction
B8	128.7		
	130.4		
B9		43.7	
	130.3		
B10	119.8		
	122.2		
B11	118.4		
			No diffraction
B12	123.6		
			No diffraction

Screen number	Phases		Comments
	Gyroid	Lamellar	
C1	127		
	128.3		
C2	124.9		
	129.3		
C3	122.2		
	125.5		
C4	122.6		
	126.4		
C5	131.5		
	132.7		
C6	132.3		
	133		
C7	128.9		
	129.9		
C8	134.6		
	135.4		
C9	134.8		
	135.7		
C10	128.9		
	134.8		
C11	121.3		
		42.3	
C12		42.3	
		42.4	
D1	132.7		
	134.6		
D2		42.3	
		42.5	
D3	122.5		
	125.2		
D4	124.9		
	126.5		
D5	124.8		
	126.1		
D6	132.3		
	135.6		
D7	124.6		
	126.7		
D8	133.8		
	134.7		
D9	131.8		
	133.7		
D10	131.6		
	137.4		
D11	128.4		
	135.6		
D12	122.4		
	125.8		
E1	141.4		
	142.5		

Screen number	Phases		Comments
	Gyroid	Lamellar	
E2	124		
	125.7		
E3	139		
	140.2		
E4	125.1		
	126.4		
E5	142.1		
	143		
E6	133.7		
	134.4		
E7	143		
	143.4		
E8	129.9		
	133.2		
E9	141.9		
	143		
E10		43.4	
	131		
E11	125.7		
	142.1		
E12		42.1	
		42.3	
F1	140.8		
	141.8		
F2	123.7		
	125.3		
F3	141.8		
	142		
F4	134.8		
	135.3		
F5	141.6		
	143		
F6	133.6		
	134.3		
F7	142.7		
	144.4		
F8	133		
	135.1		
F9	144		
	145.3		
F10	117		
	134.2		
F11	131.3		
	143.5		
F12	125.8		
	127.2		
G1	144		
			No diffraction
G2	122.2		
			No diffraction

Screen number	Phases		Comments
	Gyroid	Lamellar	
G3	142		
	143		
G4	131.5		
	132.1		
G5	143		
	143.9		
G6	132.5		
	133.2		
G7			No diffraction
	137.1		
G8	136.5		
	136.9		
G9	132.2		
	132.5		
G10		48.4	
	132.5		
G11	133.9		
	134.2		
G12	125.9		
	133.7		
H1	136.4		
			No diffraction
H2	134.3		
			No diffraction
H3	131.5		
	131.9		
H4	123.8		
	130.4		
H5	135.2		
			No diffraction
H6	132.1		
			No diffraction
H7	131.3		
	131.9		
H8	131.9		
	132		
H9	130.8		
	136.6		
H10	125.2		
	130.3		
H11	133.9		
	140.5		
H12		44.1	
	130.7		

Table S12 Phases and lattice parameters for GPR43-His_{10} in MO and PEG/Ion and PEG/Ion2 screens

Screen number	Phases			Comments
	Pn3m	Ia3d	Lamellar	
A1		165.4		
		163.4		
A2		163.9		
		162.2		
A3		160.6		
		153.7		
A4		160.6		
		146.1		
A5		160.9		
		152.9		
A6		163.1		
		147.7		
A7		164.8		
		163.2		
A8		160.1		
		149.6		
A9		163.4		
		145.2		
A10		168.8		
		146.9		
A11		166.7		
		148.9		
A12		165.4		
			48.2	
B1	114.5			
				1 peak
B2	110.9			
				1 peak
B3		165.7		
		153.7		
B4		164.5		
		155.7		
B5		165.7		
		151.3		
B6		152.8		
		149.9		
B7		162.4		
				1 peak
B8		159.9		
		163.7		
B9		165.2		
		148.8		
B10		165.2		
		148.8		
B11				No diffraction
		143.9		

Screen number	Phases			Comments
	Pn3m	Ia3d	Lamellar	
B12		167.4		
		143.5		
C1				No diffraction
		160.5		
C2		164.8		
		163.6		
C3				No diffraction
				No diffraction
C4		159.5		
		152.3		
C5		166.7		
		148.7		
C6				No diffraction
		147.2		
C7		161.6		
		165.5		
C8		164.9		
		156.9		
C9		159.2		
		160.6		
C10		153.8?		
		158.4		
C11		164.5		
		152		
C12				No diffraction
		157.3		
D1				No diffraction
		158.9		
D2		159.9		
				No diffraction
D3		164.4		
		156.8		
D4		163.9		
		161.7		
D5		167.7		
		157.8		
D6		165.2		
		158.9		
D7		156.3		
		151.6		
D8		162.2		
		154.1		
D9		156.9		
		160.9		
D10		161.7		
		162.2		
D11		162.9		
		152.8		
D12		166.2		
		135.6		

Screen number	Phases			Comments
	Diamond	Gyroid	Lamellar	
E1	109.3			
				No diffraction
E2		162.9		
		151.9		
E3	107.4			
				No diffraction
E4		161.9		
				No diffraction
E5				1 peak
		164.6		
E6		160.9		
		161.5		
E7		167.3		
		163.4		
E8		158.4		
		156.2		
E9				1 peak
				No diffraction
E10		163.3		
		151.6		
E11				No diffraction
				1 peak
E12				1 peak
		143.1		
F1		161.1		
		162.9		
F2		157.7		
				No diffraction
F3		168		
		164.5		
F4		158.1		
		161.5		
F5		189		
		161.2		
F6		161.4		
		160.4		
F7		164.2		
		162.9?		
F8		159.8		
		160.5		
F9	106.9			
		159.5		
F10		157.6		
		154.6		
F11				No diffraction
				No diffraction
F12		150		
		150.1		
G1		162.9		
				No diffraction

Screen number	Phases			Comments
	Diamond	Gyroid	Lamellar	
G2		160		
		160.7		
G3	106.9			
		164		
G4		162.3		
		151.2		
G5	103.1			
		160.7		
G6		163.9		
		163.2		
G7				No diffraction
		157.4		
G8		162		
		162		
G9		163.4		
		149.1		
G10		163.2		
		163.5		
G11		160.7		
		147.3		
G12		160.8		
		157.7		
H1		168.1		
		158.9		
H2		166.5		
		166.5		
H3	104.7			
				1 peak
H4		162.6		
		143.1		
H5				No diffraction
				1 peak
H6		167.4		
		151.3		
H7		159.7		
		144.6		
H8		163.6		
		145.1		
H9		168.2		
		155		
H10		165.5		
		146.4		
H11		164.9		
		164.5		
H12		155.9		
		147.6		

8 References

Abe, S., and Takahashi, H. (2007). A comparative study of the effects of dimethylsulfoxide and glycerol on the bicontinuous cubic structure of hydrated monoolein and its phase behavior. Chemistry and Physics of Lipids *147*, 59–68.

Ai, X., and Caffrey, M. (2000). Membrane protein crystallization in lipidic mesophases: Detergent effects. Biophysical Journal *79*, 394–405.

Akermoun, M., Koglin, M., Zvalova-Iooss, D., Folschweiller, N., Dowell, S.J., and Gearing, K.L. (2005). Characterization of 16 human G protein-coupled receptors expressed in baculovirus-infected insect cells. Protein Expression and Purification *44*, 65–74.

Amar, F. G. (2010). Crystal lattices. Retrieved December 19, 2011, from http://chemistry.umeche.maine.edu/~amar/spring2010/crystal.html

Arun Kumar, S., Winfried, H., Christoph, R., and Hartmut, M. (2006). Functional overexpression and characterization of human bradykinin subtype 2 receptor in insect cells using the baculovirus system. Journal of Cellular Biochemistry *99*, 868–877.

Asherie, N. (2004). Protein crystallization and phase diagrams. Methods *34*, 266–272.

Attrill, H., Harding, P.J., Smith, E., Ross, S., and Watts, A. (2009). Improved yield of a ligand-binding GPCR expressed in E. coli for structural studies. Protein Expression and Purification *64*, 32–38.

Bane, S.E., Velasquez, J.E., and Robinson, A.S. (2007). Expression and purification of milligram levels of inactive G protein coupled receptors in E. coli. Protein Expression and Purification *52*, 348–355.

Barauskas, J., and Landh, T. (2003). Phase behavior of the phytantriol/water system. Langmuir *19*, 9562–9565.

Benians, A., Nobles, M., Hosny, S., and Tinker, A. (2005). Regulators of G protein signaling form a quaternary complex with the agonist, receptor, and G protein. A novel explanation for the acceleration of signaling activation kinetics. Journal of Biological Chemistry *280*, 13383–13394.

Bernard, A., Payton, M., and Radford, K.R. (2001). Current Protocols in Protein Science (Hoboken, NJ, USA: John Wiley & Sons, Inc.).

Betz, U.A.K. (2005). How many genomics targets can a portfolio afford? Drug Discovery Today *10*, 1057–1063.

Briscoe, C.P., Tadayyon, M., Andrews, J.L., Benson, W.G., Chambers, J.K., Eilert, M.M., Ellis, C., Elshourbagy, N.A., Goetz, A.S., Minnick, D.T., et al. (2003). The orphan G protein-coupled receptor GPR40 is activated by medium and long chain fatty acids. Journal of Biological Chemistry *278*, 11303–11311.

Brown, A.J., Goldsworthy, S.M., Barnes, A.A., Eilert, M.M., Tcheang, L., Daniels, D., Muir, A.I., Wigglesworth, M.J., Kinghorn, I., Fraser, N.J., et al. (2003). The orphan G protein-coupled receptors GPR41 and GPR43 are activated by propionate and other short chain carboxylic acids. Journal of Biological Chemistry *278*, 11312–11319.

Brown, A.J., Jupe, S., and Briscoe, C.P. (2005). A family of fatty acid binding receptors. DNA and Cell Biology *24*, 54–61.

Caffrey, M., and Cherezov, V. (2009). Crystallizing membrane proteins using lipidic mesophases. Nature Protocols *4*, 706–731.

Cameron, W., Doyle, K., and Rocklin, R.E. (1986). Histamine type I (H1) receptor radioligand binding studies on normal T cell subsets, B cells, and monocytes. Journal of Immunology *136*, 2116–2120.

Carter, C.C., McNamara, L.A., Onafuwa-Nuga, A., Shackleton, M., Riddell, J., Bixby, D., Savona, M.R., Morrison, S.J., and Collins, K.L. (2011). HIV-1 utilizes the CXCR4 chemokine receptor to infect multipotent hematopoietic stem and progenitor cells. Cell Host & Microbe *9*, 223–234.

Cherezov, V., Clogston, J., Misquitta, Y., Abdel-Gawad, W., and Caffrey, M. (2002). Membrane protein crystallization in meso: Lipid type-tailoring of the cubic phase. Biophysical Journal *83*, 3393–3407.

Cherezov, V., Clogston, J., Papiz, M.Z., and Caffrey, M. (2006). Room to move: Crystallizing membrane proteins in swollen lipidic mesophases. Journal of Molecular Biology *357*, 1605–1618.

Cherezov, V., Fersi, H., and Caffrey, M. (2001). Crystallization screens: Compatibility with the lipidic cubic phase for in meso crystallization of membrane proteins. Biophysical Journal *81*, 225–242.

Cherezov, V., Rosenbaum, D.M., Hanson, M.A., Rasmussen, S.G.F., Thian, F.S., Kobilka, T.S., Choi, H.-J., Kuhn, P., Weis, W.I., Kobilka, B.K., et al. (2007). High-resolution crystal structure of an engineered human beta2-adrenergic G protein coupled receptor. Science *318*, 1258–1265.

Chien, E.Y.T., Liu, W., Zhao, Q., Katritch, V., Won Han, G., Hanson, M.A., Shi, L., Newman, A.H., Javitch, J.A., Cherezov, V., et al. (2010). Structure of the human dopamine D3 receptor in complex with a D2/D3 selective antagonist. Science *330*, 1091–1095.

Cho, D., Min, C., Jung, K., Cheong, S., Zheng, M., Cheong, S., Oak, M., Cheong, J., Lee, B., and Kim, K. (2011). N-terminal region of dopamine D(2) receptor, a rhodopsin family GPCR, regulates proper integration into plasma membrane and endocytic routes. British Journal of Pharmacology *166*, 659-675

Choe, H.-W., Kim, Y.J., Park, J.H., Morizumi, T., Pai, E.F., Krauss, N., Hofmann, K.P., Scheerer, P., and Ernst, O.P. (2011). Crystal structure of metarhodopsin II. Nature *471*, 651–655.

Chupin, V., Killian, J.A., and de Kruijff, B. (2003). Effect of phospholipids and a transmembrane peptide on the stability of the cubic phase of monoolein: Implication for protein crystalization from a cubic phase. Biophysical Journal *84*, 2373–2381.

Ciccarone, V.C., Polayes, D.A., and Luckow, V.A. (1997). Generation of recombinant baculovirus DNA in E.coli using a baculovirus shuttle vector. Methods in Molecular Medicine *13*, 213–235.

Conn, C.E., Darmanin, C., Mulet, X., Le Cann, S., Kirby, N., and Drummond, C.J. (2012). High-throughput analysis of the structural evolution of the monoolein cubic phase in situ under crystallogenesis conditions. Soft Matter *8*, 2310–2321.

Conn, C.E., Darmanin, C., Sagnella, S.M., Mulet, X., Greaves, T.L., Varghese, J.N., and Drummond, C.J. (2010a). Incorporation of the dopamine D2L receptor and bacteriorhodopsin within bicontinuous cubic lipid phases. 1. Relevance to in meso crystallization of integral membrane proteins in monoolein systems. Soft Matter *6*, 4828–4837.

Conn, C.E., Darmanin, C., Sagnella, S.M., Mulet, X., Greaves, T.L., Varghese, J.N., and Drummond, C.J. (2010b). Incorporation of the dopamine D2L receptor and bacteriorhodopsin within bicontinuous cubic lipid phases. 2. Relevance to in meso crystallization of integral membrane proteins in monoolein systems. Soft Matter *6*, 4838–4846.

Cook, B.L., Steuerwald, D., Kaiser, L., Graveland-Bikker, J., Vanberghem, M., Berke, A.P., Herlihy, K., Pick, H., Vogel, H., and Zhang, S. (2009). Large-scale production and study of a synthetic G protein-coupled receptor: human olfactory receptor 17-4. Proceedings of the National Academy of Sciences of the United States of America *106*, 11925–11930.

Cook, S. (1998). Review article: short chain fatty acids in health and disease. Alimentary Pharmacology & Therapeutics *12*, 499–507.

Cooper, M.A. (2002). Optical biosensors in drug discovery. Nature Reviews. Drug Discovery *1*, 515–528.

Cooper, T., McMurchie, E.J., and Leifert, W.R. (2009). [35S]GTPgammaS binding in G protein-coupled receptor assays. Methods in Molecular Biology *552*, 143–151.

Costedio, M.M., Hyman, N., and Mawe, G.M. (2007). Serotonin and its role in colonic function and in gastrointestinal disorders. Diseases of the Colon and Rectum *50*, 376–388.

Darmanin, C., Conn, C.E., Newman, J., Mulet, X., Seabrook, S.A., Liang, Y.-L., Hawley, A., Kirby, N., Varghese, J.N., and Drummond, C.J. (2012). High-throughput production and structural characterization of libraries of self-assembly lipidic cubic phase materials. ACS Combinatorial Science. doi: 10.1021/co2001718

Dorsam, R.T., and Gutkind, J.S. (2007). G protein-coupled receptors and cancer. Nature Reviews. Cancer *7*, 79–94.

Dreele, Von, R.B. (2003). Protein crystal structure analysis from high-resolution X-ray powder-diffraction data. Methods in Enzymology *368*, 254–67.

Du, A.T., Onan, D., Dinh, D.T., Lew, M.J., Ziogas, J., Aguilar, M.-I., Pattenden, L.K., and Thomas, W.G. (2010). Ligand-supported purification of the urotensin-II receptor. Molecular Pharmacology *78*, 639–647.

Dubuquoy, L., Rousseaux, C., Thuru, X., Peyrin-Biroulet, L., Romano, O., Chavatte, P., Chamaillard, M., and Desreumaux, P. (2006). PPARgamma as a new therapeutic target in inflammatory bowel diseases. Gut *55*, 1341–1349.

Dupré, D.J., Robitaille, M., Rebois, R.V., and Hébert, T.E. (2009). The role of Gbetagamma subunits in the organization, assembly, and function of GPCR signaling complexes. Annual Review of Pharmacology and Toxicology *49*, 31–56.

Eglen, R.M.(2005). Muscarinic receptor subtype pharmacology and physiology. In Progress in Medicinal Chemistry *43*, 105–136.

Engel, A., Hoenger, A., Hefti, A., Henn, C., Ford, R.C., Kistler, J., and Zulauf, M. (1992). Assembly of 2-D membrane protein crystals: Dynamics, crystal order, and fidelity of structure analysis by electron microscopy. Journal of Structural Biology *109*, 219–234.

Erbes, J., Czeslik, C., Hahn, W., Winter, R., Rappolt, M., and Rapp, G. (1994). On the Existence of Bicontinuous Cubic Phases in Dioleoylphosphatidylethanolamine. Berichte Der Bunsengesellschaft *98*, 1287–1293.

Ericsson, B., Larsson, K., and Fontell, K. (1983). A cubic protein-monoolein-water phase. Biochimica Et Biophysica Acta (BBA) - Biomembranes *729*, 23–27.

Ericsson, C.A., Söderman, O., Garamus, V.M., Bergström, M., and Ulvenlund, S. (2004). Effects of temperature, salt, and deuterium oxide on the self-aggregation of alkylglycosides in dilute solution. 1. n-nonyl-beta-D-glucoside. Langmuir *20*, 1401–1408.

Forward, N.A., Furlong, S.J., Yang, Y., Lin, T.-J., and Hoskin, D.W. (2009). Mast cells down-regulate CD4+CD25+ T regulatory cell suppressor function via histamine H1 receptor interaction. Journal of Immunology *183*, 3014–3022.

Fredriksson, R., Lagerstrom, M.C., Lundin, L.-G., and Schiöth, H.B. (2003). The G protein-coupled receptors in the human genome form five main families. Phylogenetic Analysis, Paralogon Groups, and Fingerprints. Molecular Pharmacology *63*, 1256–1272.

Fung, J.J., Deupi, X., Pardo, L., Yao, X.J., Velez-Ruiz, G.A., Devree, B.T., Sunahara, R.K., and Kobilka, B.K. (2009). Ligand-regulated oligomerization of [beta]2-adrenoceptors in a model lipid bilayer. EMBO Journal *28*, 3315–3328.

Gan, L., Alexander, J.M., Wittelsberger, A., Thomas, B., and Rosenblatt, M. (2006). Large-scale purification and characterization of human parathyroid hormone-1 receptor stably expressed in HEK293S GnTI- cells. Protein Expression and Purification *47*, 296–302.

Ge, H., Li, X., Weiszmann, J., Wang, P., Baribault, H., Chen, J.-L., Tian, H., and Li, Y. (2008). Activation of G protein-coupled receptor 43 in adipocytes leads to inhibition of lipolysis and suppression of plasma free fatty acids. Endocrinology *149*, 4519–4526.

Guo, W., Urizar, E., Kralikova, M., Mobarec, J.C., Shi, L., Filizola, M., and Javitch, J.A. (2008). Dopamine D2 receptors form higher order oligomers at physiological expression levels. EMBO Journal *27*, 2293–2304.

Gutzmer, R., Langer, K., Lisewski, M., Mommert, S., Rieckborn, D., Kapp, A., and Werfel, T. (2002). Expression and function of histamine receptors 1 and 2 on human monocyte-derived dendritic cells. Journal of Allergy and Clinical Immunology *109*, 524–531.

Hacker, M., Bachmann, K., and Messer, W. (2009). Pharmacology Principle and Practice (Academic Press).

Haga, K., Kruse, A.C., Asada, H., Yurugi-Kobayashi, T., Shiroishi, M., Zhang, C., Weis, W.I., Okada, T., Kobilka, B.K., Haga, T., et al. (2012). Structure of the human M2 muscarinic acetylcholine receptor bound to an antagonist. Nature *482*, 547-551.

Hanatani, M., Nishifuji, K., Futai, M., and Tsuchiya, T. (1984). Solubilization and reconstitution of membrane proteins of escherichia coli using alkanoyl-N-methylglucamides. Journal of Biological Chemistry *95*, 1349–1353.

Hahn, T. (2006). International Tables for Crystallography, Volume A. Space-group symmetry (John Wiley & Sons, Inc).

Hanson, M.A., Cherezov, V., Griffith, M.T., Roth, C.B., Jaakola, V.-P., Chien, E.Y.T., Velasquez, J., Kuhn, P., and Stevens, R.C. (2008). A specific cholesterol binding site is established by the 2.8 A structure of the human beta2-adrenergic receptor. Structure *16*, 897–905.

Hara, T., Hirasawa, A., Sun, Q., Koshimizu, T.-A., Itsubo, C., Sadakane, K., Awaji, T., and Tsujimoto, G. (2009). Flow cytometry-based binding assay for GPR40 (FFAR1; Free Fatty Acid Receptor 1). Molecular Pharmacology *75*, 85–91.

Harrison, C., and Traynor, J.R. (2003). The [35S]GTPgammaS binding assay: approaches and applications in pharmacology. Life Sciences *74*, 489–508.

Hatanaka, H., Tsukui, M., Takada, S., Kurashina, K., Choi, Y.L., Soda, M., Yamashita, Y., Haruta, H., Hamada, T., Ueno, T., et al. (2010). Identification of transforming activity of free fatty acid receptor 2 by retroviral expression screening. Cancer Science *101*, 54–59.

Hayashi, M.K., and Haga, T. (1996). Purification and functional reconstitution with GTP-binding regulatory proteins of hexahistidine-tagged muscarinic acetyicholine receptors (m2 Subtype). Journal of Biochemistry *120*, 1232–1238.

Heitz, F., McClue, S.J., Harris, B.A., and Guenet, C. (1995). Expression of human M2 muscarinic receptors in SF9 cells: Characterisation and reconstitution with G proteins. Journal of Receptors and Signal Transduction *15*, 55–70.

Hill, S.J. (1990). Distribution, properties, and functional characteristics of three classes of histamine receptor. Pharmacological Reviews *42*, 45–83.

Holst, J.J. (2007). The physiology of glucagon-like peptide 1. Physiological Reviews *87*, 1409–39.

Hong, Y.-H., Nishimura, Y., Hishikawa, D., Tsuzuki, H., Miyahara, H., Gotoh, C., Choi, K.-C., Feng, D.D., Chen, C., Lee, H.-G., et al. (2005). Acetate and propionate short chain fatty acids stimulate adipogenesis via GPCR43. Endocrinology *146*, 5092–5099.

Inan, M.S., Rasoulpour, R.J., Yin, L., Hubbard, A.K., Rosenberg, D.W., and Giardina, C. (2000). The luminal short-chain fatty acid butyrate modulates NF-kappaB activity in a human colonic epithelial cell line. Gastroenterology *118*, 724–734.

Invitrogen (2004). Bac-to-Bac Baculovirus Expression System: An efficient site-specific transposition system to generate baculovirus for high-level expression of recombinant proteins.

Issafras, H., Angers, S., Bulenger, S., Blanpain, C., Parmentier, M., Labbé-Jullié, C., Bouvier, M., and Marullo, S. (2002). Constitutive agonist-independent CCR5 oligomerization and antibody-mediated clustering occurring at physiological levels of receptors. Journal of Biological Chemistry *277*, 34666–34673.

Jaakola, V.-P., Griffith, M.T., Hanson, M.A., Cherezov, V., Chien, E.Y.T., Lane, J.R., Ijzerman, A.P., and Stevens, R.C. (2008). The 2.6 angstrom crystal structure of a human A2A adenosine receptor bound to an antagonist. Science *322*, 1211–1217.

Jobin, C., and Sartor, R.B. (2000). The Ikappa B/NF-kappa B system: a key determinant of mucosal inflammation and protection. American Journal of Physiology Cell Physiology *278*, C451–462.

Jockers, R., and Kamal, M. (2011). Biological significance of GPCR heteromerization in the neuro-endocrine system. Frontiers in Endocrinology *2*. doi: 10.3389/fendo.2011.00002

Johnston, C.A., and Siderovski, D.P. (2007). Receptor-mediated activation of heterotrimeric G proteins: Current structural insights. Molecular Pharmacology *72*, 219–230.

Joseph, J.S., Liu, W., Kunken, J., Weiss, T.M., Tsuruta, H., and Cherezov, V. (2011). Characterization of lipid matrices for membrane protein crystallization by high-throughput small angle X-ray scattering. Methods *55*, 342–349.

Kaiser, L., Graveland-Bikker, J., Steuerwald, D., Vanberghem, M., Herlihy, K., and Zhang, S. (2008). Efficient cell-free production of olfactory receptors: detergent optimization, structure, and ligand binding analyses. Proceedings of the National Academy of Sciences of the United States of America *105*, 15726–15731.

Karaki, S.-I., Mitsui, R., Hayashi, H., Kato, I., Sugiya, H., Iwanaga, T., Furness, J., and Kuwahara, A. (2006). Short-chain fatty acid receptor, GPR43, is expressed by enteroendocrine cells and mucosal mast cells in rat intestine. Cell and Tissue Research *324*, 353–360.

Karra, E., Chandarana, K., and Batterham, R.L. (2009). The role of peptide YY in appetite regulation and obesity. Journal of Physiology *587*, 19–25.

Keen, M. (1998). Receptor binding techniques (New Jersey: Humana Press).

Killian, J.A., and Nyholm, T.K.M. (2006). Peptides in lipid bilayers: the power of simple models. Current Opinion in Structural Biology *16*, 473–479.

Kino, T., Tiulpakov, A., Ichijo, T., Chheng, L., Kozasa, T., and Chrousos, G.P. (2005). G protein beta interacts with the glucocorticoid receptor and suppresses its transcriptional activity in the nucleus. The Journal of Cell Biology *169*, 885–896.

Kinoshita, M., Suzuki, Y., and Saito, Y. (2002). Butyrate reduces colonic paracellular permeability by enhancing PPARgamma activation. Biochemical and Biophysical Research Communications *293*, 827–831.

Klampfer, L., Huang, J., Sasazuki, T., Shirasawa, S., and Augenlicht, L. (2003). Inhibition of interferon gamma signaling by the short chain fatty acid butyrate. Molecular Cancer Research *1*, 855–862.

Koch, M.H.J. (2006). X-ray scattering of non-crystalline biological systems using synchrotron radiation. Chemical Society Reviews *35*, 123–133.

Kolakowski, L.F. (1994). GCRDb: a G protein-coupled receptor database. Receptors Channel 1–7.

Kornberg, R.D., and Darst, S.A. (1991). Two-dimensional crystals of proteins on lipid layers. Current Opinion in Structural Biology *1*, 642–646.

Krebs, A., Edwards, P.C., Villa, C., Li, J., and Schertler, G.F.X. (2003). The three-dimensional structure of bovine rhodopsin determined by electron cryomicroscopy. Journal of Biological Chemistry *278*, 50217–50225.

Kuang, Y., Wu, Y., Jiang, H., and Wu, D. (1996). Selective G protein coupling by C-C chemokine receptors. Journal of Biological Chemistry *271*, 3975–3978.

Kunji, E.R.S., Harding, M., Butler, P.J.G., and Akamine, P. (2008). Determination of the molecular mass and dimensions of membrane proteins by size exclusion chromatography. Methods *46*, 62–72.

Laemmli, U.K. (1970). Cleavage of structural proteins during the assembly of the head of bacteriophage T4. Nature *227*, 680–685.

Landau, E.M., and Rosenbusch, J.P. (1996). Lipidic cubic phases: A novel concept for the crystallization of membrane proteins. Proceedings of the National Academy of Sciences of the United States of America *93*, 14532–14535.

le Maire, M., Champeil, P., and MÃ ller, J.V. (2000). Interaction of membrane proteins and lipids with solubilizing detergents. Biochimica Et Biophysica Acta (BBA) - Biomembranes *1508*, 86–111.

Le Poul, E., Loison, C., Struyf, S., Springael, J.-Y., Lannoy, V., Decobecq, M.-E., Brezillon, S., Dupriez, V., Vassart, G., Van Damme, J., et al. (2003). Functional characterization of human receptors for short chain fatty acids and their role in polymorphonuclear cell activation. Journal of Biological Chemistry *278*, 25481–25489.

Lebon, G., Warne, T., Edwards, P.C., Bennett, K., Langmead, C.J., Leslie, A.G.W., and Tate, C.G. (2011). Agonist-bound adenosine A2A receptor structures reveal common features of GPCR activation. Nature *474*, 521–525.

Lee, T., Schwandner, R., Swaminath, G., Weiszmann, J., Cardozo, M., Greenberg, J., Jaeckel, P., Ge, H., Wang, Y., Jiao, X., et al. (2008). Identification and functional characterization of allosteric agonists for the G protein-coupled receptor FFA2. Molecular Pharmacology *74*, 1599–1609.

Lefkowitz, R.J., Sun, J.-P., and Shukla, A.K. (2008). A crystal clear view of the beta2-adrenergic receptor. Nature Biotechnology *26*, 189–191.

Li, S.J., Yamashita, Y., and Yamazaki, M. (2001). Effect of electrostatic interactions on phase stability of cubic phases of membranes of monoolein/dioleoylphosphatidic acid mixtures. Biophysical Journal *81*, 983–993.

Littman, D.R. (1998). Chemokine receptors: keys to AIDS pathogenesis? Cell *93*, 677–680.

Lund, S., Orlowski, S., de Foresta, B., Champeil, P., le Maire, M., and Møller, J.V. (1989). Detergent structure and associated lipid as determinants in the stabilization of solubilized Ca2+-ATPase from sarcoplasmic reticulum. Journal of Biological Chemistry *264*, 4907–4915.

Lundstrom, K., Wagner, R., Reinhart, C., Desmyter, A., Cherouati, N., Magnin, T., Zeder-Lutz, G., Courtot, M., Prual, C., André, N., et al. (2006). Structural genomics on membrane proteins: comparison of more than 100 GPCRs in 3 expression systems. Journal of Structural and Functional Genomics *7*, 77–91.

Ma, A.W.S., Pawagi, A.B., and Wells, J.W. (2008). Heterooligomers of the muscarinic receptor and G proteins purified from porcine atria. Biochemical and Biophysical Research Communications *374*, 128–133.

Malbon, C.C. (2005). G proteins in development. Nature Reviews. Molecular Cell Biology *6*, 689–701.

Maslowski, K.M., Vieira, A.T., Ng, A., Kranich, J., Sierro, F., Di, Y., Schilter, H.C., Rolph, M.S., Mackay, F., Artis, D., et al. (2009). Regulation of inflammatory responses by gut microbiota and chemoattractant receptor GPR43. Nature *461*, 1282–1286.

Massotte, D. (2003). G protein-coupled receptor overexpression with the baculovirus-insect cell system: a tool for structural and functional studies. Biochimica Et Biophysica Acta (BBA) - Biomembranes *1610*, 77–89.

McCusker, E.C., Bane, S.E., O'Malley, M.A., and Robinson, A.S. (2007). Heterologous GPCR expression: A bottleneck to obtaining crystal structures. Biotechnology Progress *23*, 540–547.

McDevitt, C.A., Collins, R.F., Conway, M., Modok, S., Storm, J., Kerr, I.D., Ford, R.C., and Callaghan, R. (2006). Purification and 3D structural analysis of oligomeric human multidrug transporter ABCG2. Structure *14*, 1623–1632.

Menzel, T., Melcher, R., Koehler, S., Dusel, G., Backhaus, K., Ott, G., Breithaupt, W., Al-Taie, O., Schauber, J., Gostner, A., et al. (2004). Establishment of a colonic adenoma cell line (GEKI-2): spectral karyotype analysis and functional characterization. International Journal of Colorectal Disease *19*, 12–17.

Michalke, K., Gravière, M.-E., Huyghe, C., Vincentelli, R., Wagner, R., Pattus, F., Schroeder, K., Oschmann, J., Rudolph, R., Cambillau, C., et al. (2009). Mammalian G protein-coupled receptor expression in Escherichia coli: I. High-throughput large-scale production as inclusion bodies. Analytical Biochemistry *386*, 147–155.

Mirzabekov, T., Bannert, N., Farzan, M., Hofmann, W., Kolchinsky, P., Wu, L., Wyatt, R., and Sodroski, J. (1999). Enhanced expression, native purification, and characterization of CCR5, a principal HIV-1 coreceptor. Journal of Biological Chemistry *274*, 28745–28750.

Misquitta, Y., and Caffrey, M. (2003). Detergents destabilize the cubic phase of monoolein: Implications for membrane protein crystallization. Biophysical Journal *85*, 3084–3096.

Missale, C., Nash, S.R., Robinson, S.W., Jaber, M., and Caron, M.G. (1998). Dopamine receptors: From structure to function. Physiological Reviews *78*, 189–225.

Moran, N.C. (1963). Adrenergic receptors within the cardiovascular system. Circulation *28*, 987–993.

Morein, S., Koeppe, R.E., II, Lindblom, G., de Kruijff, B., and Killian, J.A. (2000). The effect of peptide/lipid hydrophobic mismatch on the phase behavior of model membranes mimicking the lipid composition in Escherichia coli membranes. Biophysical Journal *78*, 2475–2485.

Mulet, X., Kennedy, D.F., Conn, C.E., Hawley, A., and Drummond, C.J. (2010). High throughput preparation and characterisation of amphiphilic nanostructured nanoparticulate drug delivery vehicles. International Journal of Pharmaceutics *395*, 290–7.

Nehmé, R., Joubert, O., Bidet, M., Lacombe, B., Polidori, A., Pucci, B., and Mus-Veteau, I. (2010). Stability study of the human G protein coupled receptor, Smoothened. Biochimica Et Biophysica Acta (BBA) - Biomembranes *1798*, 1100–1110.

Newman, J., Egan, D., Walter, T.S., Meged, R., Berry, I., Ben Jelloul, M., Sussman, J.L., Stuart, D.I., and Perrakis, A. (2005). Towards rationalization of crystallization screening for small- to medium-sized academic laboratories: the PACT/JCSG+ strategy. Acta Crystallographica Section D *61*, 1426–1431.

Nilsson, N.E., Kotarsky, K., Owman, C., and Olde, B. (2003). Identification of a free fatty acid receptor, FFA2R, expressed on leukocytes and activated by short-chain fatty acids. Biochemical and Biophysical Research Communications *303*, 1047–1052.

Nishimura, K., Frederick, J., and Kwatra, M.M. (1998). Human substance P receptor expressed in Sf9 cells couples with multiple endogenous G proteins. Journal of Receptor and Signal Transduction *18*, 51–65.

Nollert, P., Qiu, H., Caffrey, M., Rosenbusch, J.P., and Landau, E.M. (2001). Molecular mechanism for the crystallization of bacteriorhodopsin in lipidic cubic phases. FEBS Letters *504*, 179–186.

Oka, T., Miura, K., Inoue, K., Ueki, T., and Yagi, N. (2006). High-resolution powder diffraction study of purple membrane with a large Guinier-type camera. Journal of Synchrotron Radiation *13*, 281–284.

Olah, M.E., and Stiles, G.L. (1995). Adenosine receptor subtypes: characterization and therapeutic regulation. Annual Review of Pharmacology and Toxicology *35*, 581–606.

Oldham, W.M., and Hamm, H.E. (2006). Structural basis of function in heterotrimeric G proteins. Quaterly Reviews of Biophysics *39*, 117–166.

Palczewski, K., Kumasaka, T., Hori, T., Behnke, C.A., Motoshima, H., Fox, B.A., Trong, I.L., Teller, D.C., Okada, T., Stenkamp, R.E., et al. (2000). Crystal structure of rhodopsin: A G protein-coupled receptor. Science *289*, 739–745.

Panetta, R., and Greenwood, M.T. (2008). Physiological relevance of GPCR oligomerization and its impact on drug discovery. Drug Discovery Today *13*, 1059–1066.

Park, J.H., Scheerer, P., Hofmann, K.P., Choe, H.-W., and Ernst, O.P. (2008a). Crystal structure of the ligand-free G protein-coupled receptor opsin. Nature *454*, 183–187.

Park, P., and Wells, J. (2003). Monomers and oligomers of the M2 muscarinic cholinergic receptor purified from Sf9 cells. Biochemistry *42*, 12960–12971.

Park, P., Lodowski, D., and Palczewski, K. (2008b). Activation of G protein coupled receptors: Beyond two-state models and tertiary conformational changes. Annual Review of Pharmacology and Toxicology *48*, 107–141.

Petoukhov, M.V., and Svergun, D.I. (2007). Analysis of X-ray and neutron scattering from biomacromolecular solutions. Current Opinion in Structural Biology *17*, 562–571.

Prashen, C., Philip, J.R., Uttam, L.R., and Khorana, H.G. (2006). The synthesis and high-level expression of a beta(2)adrenergic receptor gene in a tetracycline-inducible stable mammalian cell line. Protein Science *15*, 1433–1440.

Qiu, H., and Caffrey, M. (2000). The phase diagram of the monoolein/water system: metastability and equilibrium aspects. Biomaterials *21*, 223–234.

Qutub, Y., Reviakine, I., Maxwell, C., Navarro, J., Landau, E.M., and Vekilov, P.G. (2004). Crystallization of transmembrane proteins in cubo: mechanisms of crystal growth and defect formation. Journal of Molecular Biology *343*, 1243–1254.

Raman, P., Cherezov, V., and Caffrey, M. (2006). The membrane protein data bank. Cellular and Molecular Life Sciences *63*, 36–51.

Rasmussen, S.G.F., Choi, H.-J., Fung, J.J., Pardon, E., Casarosa, P., Chae, P.S., Devree, B.T., Rosenbaum, D.M., Thian, F.S., Kobilka, T.S., et al. (2011a). Structure of a nanobody-stabilized active state of the β(2) adrenoceptor. Nature *469*, 175–180.

Rasmussen, S.G.F., Choi, H.-J., Rosenbaum, D.M., Kobilka, T.S., Thian, F.S., Edwards, P.C., Burghammer, M., Ratnala, V.R.P., Sanishvili, R., Fischetti, R.F., et al. (2007). Crystal structure of the human beta2 adrenergic G protein-coupled receptor. Nature *450*, 383–387.

Rasmussen, S.G.F., Devree, B.T., Zou, Y., Kruse, A.C., Chung, K.Y., Kobilka, T.S., Thian, F.S., Chae, P.S., Pardon, E., Calinski, D., et al. (2011b). Crystal structure of the β2 adrenergic receptor–Gs protein complex. Nature *477*, 549–555.

Rath, A., Glibowicka, M., Nadeau, V.G., Chen, G., and Deber, C.M. (2009). Detergent binding explains anomalous SDS-PAGE migration of membrane proteins. Proceedings of the National Academy of Sciences of the United States of America *106*, 1760–1765.

Reiländer, H., Boege, F., Vasudevan, S., Maul, G., Hekman, M., Dees, C., Hampe, W., Helmreich, E.J.M., and Michel, H. (1991). Purification and functional characterization of the human [beta]2-adrenergic receptor produced in baculovirus-infected insect cells. FEBS Letters *282*, 441–444.

Reisner, A.H., Nemes, P., and Bucholtz, C. (1975). The use of Coomassie Brilliant Blue G250 perchloric acid solution for staining in electrophoresis and isoelectric focusing on polyacrylamide gels. Analaytical Biochemistry *64*, 509–516.

Ren, H., Yu, D., Ge, B., Cook, B., Xu, Z., and Zhang, S. (2009). High-level production, solubilization and purification of synthetic human GPCR chemokine receptors CCR5, CCR3, CXCR4 and CX3CR1. PLoS ONE *4*, e4509.

Rhodes, G. (1993). Crystallography Made Crystal Clear: A Guide for Users of Macromolecular Models (Elsevier Science).

Richardson, R.M., and Hosey, M.M. (1992). Agonist-induced phosphorylation and desensitization of human m2 muscarinic cholinergic receptors in Sf9 insect cells. Journal of Biological Chemistry *267*, 22249–22255.

Rigaud, J.-L., Chami, M., Lambert, O., Lévy, D., and Ranck, J.-L. (2000). Use of detergents in two-dimensional crystallization of membrane proteins. Biochimica Et Biophysica Acta (BBA) - Biomembranes *1508*, 112–128.

Rigaud, J.-L., Mosser, G., Lacapere, J.-J., Olofsson, A., Lévy, D., and Ranck, J.-L. (1997). Bio-Beads: An efficient strategy for two-dimensional crystallization of membrane proteins. Journal of Structural Biology *118*, 226–235.

Rigaud, J.L. (2002). Membrane proteins: functional and structural studies using reconstituted proteoliposomes and 2-D crystals. Brazilian Journal of Medical and Biological Research *35*, 753–766.

Rinken, A., Kameyama, K., Haga, T., and Engström, L. (1994). Solubilization of muscarinic receptor subtypes from baculovirus infected sf9 insect cells. Biochemical Pharmacology *48*, 1245–1251.

Roberfroid, M.B. (2007). Inulin-type fructans: Functional food ingredients. Journal of Nutrition *137*, 2493S-2502S.

Rosenbaum, D.M., Cherezov, V., Hanson, M.A., Rasmussen, S.G.F., Thian, F.S., Kobilka, T.S., Choi, H.-J., Yao, X.J., Weis, W.I., Stevens, R.C., et al. (2007). GPCR engineering yields high-resolution structural insights into beta2-adrenergic receptor function. Science *318*, 1266-1273.

Roy, C.C., Kien, C.L., Bouthillier, L., and Levy, E. (2006). Short-chain fatty acids: Ready for prime time? Nutrition in Clinical Practice *21*, 351-366.

Ruprecht, J.J., Mielke, T., Vogel, R., Villa, C., and Schertler, G.F.X. (2004). Electron crystallography reveals the structure of metarhodopsin I. The EMBO Journal *23*, 3609-3620.

Salahpour, A., Bonin, H., Bhalla, S., Petäjä-Repo, U., and Bouvier, M. (2003). Biochemical characterization of beta2-adrenergic receptor dimers and oligomers. Biological Chemistry *384*, 117-123.

Salom, D., Lodowski, D.T., Stenkamp, R.E., Le Trong, I., Golczak, M., Jastrzebska, B., Harris, T., Ballesteros, J.A., and Palczewski, K. (2006). Crystal structure of a photoactivated deprotonated intermediate of rhodopsin. Proceedings of the National Academy of Sciences of the United States of America *103*, 16123-16128.

Sawzdargo, M., George, S.R., Nguyen, T., Xu, S., Kolakowski, L.F., and O'Dowd, B.F. (1997). A cluster of four novel human G protein-coupled receptor genes occurring in close proximity to CD22 gene on chromosome 19q13.1. Biochemical and Biophysical Research Communications *239*, 543-547.

Scheerer, P., Park, J.H., Hildebrand, P.W., Kim, Y.J., Krauss, N., Choe, H.-W., Hofmann, K.P., and Ernst, O.P. (2008). Crystal structure of opsin in its G protein-interacting conformation. Nature *455*, 497-502.

Scheppach, W., and Weiler, F. (2004). The butyrate story: old wine in new bottles? Current Opinion in Clinical Nutrition and Metabolic Care *7*, 563-567.

Scheppach, W., Bartram, H.P., and Richter, F. (1995). Role of short-chain fatty acids in the prevention of colorectal cancer. European Journal of Cancer *31A*, 1077-1080.

Scheppach, W., Bartram, P., Richter, A., Richter, F., Liepold, H., Dusel, G., Hofstetter, G., Ruthlein, J., and Kasper, H. (1992). Effect of short-chain fatty acids on the human colonic mucosa in vitro. Journal of Parenteral and Enteral Nutrition *16*, 43-48.

Schiöth, H.B., and Fredriksson, R. (2005). The GRAFS classification system of G protein coupled receptors in comparative perspective. General and Comparative Endocrinology *142*, 94-101.

Schmidt, J., Smith, N.J., Christiansen, E., Tikhonova, I.G., Grundmann, M., Hudson, B.D., Ward, R.J., Drewke, C., Milligan, G., Kostenis, E., et al. (2011). Selective orthosteric free fatty acid receptor 2 (FFA2) agonists: identification of the structural and chemical requirements for selective activation of FFA2 versus FFA3. Journal of Biological Chemistry *286*, 10628-10640.

Schneider, E.H., and Seifert, R. (2010). Sf9 cells: A versatile model system to investigate the pharmacological properties of G protein-coupled receptors. Pharmacology & Therapeutics *128*, 387-418.

Schroder, K., Hertzog, P.J., Ravasi, T., and Hume, D.A. (2004). Interferon-γ: an overview of signals, mechanisms and functions. Journal of Leukocyte Biology *75*, 163-189.

Seddon, A.M., Curnow, P., and Booth, P.J. (2004). Membrane proteins, lipids and detergents: not just a soap opera. Biochimica Et Biophysica Acta (BBA) - Biomembranes *1666*, 105-117.

Seddon, J.M., Squires, A.M., Conn, C.E., Ces, O., Heron, A.J., Mulet, X., Shearman, G.C., and Templer, R.H. (2006). Pressure-jump X-ray studies of liquid crystal transitions in lipids. Philosophical Transactions of the Royal Society a: Mathematical, Physical and Engineering Sciences *364*, 2635–2655.

Segain, J.P., Raingeard de la Blétière, D., Bourreille, A., Leray, V., Gervois, N., Rosales, C., Ferrier, L., Bonnet, C., Blottière, H.M., and Galmiche, J.P. (2000). Butyrate inhibits inflammatory responses through NFkappaB inhibition: implications for Crohn's disease. Gut *47*, 397–403.

Sen, S., Jaakola, V.-P., Heimo, H., Engström, M., Larjomaa, P., Scheinin, M., Lundstrom, K., and Goldman, A. (2003). Functional expression and direct visualization of the human [alpha]2B-adrenergic receptor and [alpha]2B-AR-green fluorescent fusion protein in mammalian cell using Semliki Forest virus vectors. Protein Expression and Purification *32*, 265–275.

Sengupta, S., Muir, J.G., and Gibson, P.R. (2006). Does butyrate protect from colorectal cancer? Journal of Gastroenterology and Hepatology *21*, 209–218.

Shimamura, T., Shiroishi, M., Weyand, S., Tsujimoto, H., Winter, G., Katritch, V., Abagyan, R., Cherezov, V., Liu, W., Han, G.W., et al. (2011). Structure of the human histamine H1 receptor complex with doxepin. Nature *475*, 65–70.

Siegel, D.P., Cherezov, V., Greathouse, D.V., Koeppe, R.E., Killian, J.A., and Caffrey, M. (2006). Transmembrane peptides stabilize inverted cubic phases in a biphasic length-dependent manner: Implications for protein-induced membrane fusion. Biophysical Journal *90*, 200–211.

Smith, C. (2005). Striving for purity: advances in protein purification. Nature Methods *2*, 71–77.

Smith, N.J., Ward, R.J., Stoddart, L.A., Hudson, B.D., Kostenis, E., Ulven, T., Morris, J.C., Tränkle, C., Tikhonova, I.G., Adams, D.R., et al. (2011). Extracellular loop 2 of the free fatty acid receptor 2 mediates allosterism of a phenylacetamide ago-allosteric modulator. Molecular Pharmacology *80*, 163–173.

Smrcka, A.V. (2008). G protein betagamma subunits: central mediators of G protein-coupled receptor signaling. Cellular and Molecular Life Sciences *65*, 2191–2214.

Sokoloff, P., Giros, B., Martres, M.P., Bouthenet, M.L., and Schwartz, J.C. (1990). Molecular cloning and characterization of a novel dopamine receptor (D3) as a target for neuroleptics. Nature *347*, 146–151.

Spector, T. (1977). Refinement of the Coomassie blue method of protein quantitation: A simple and linear spectrophotometric assay for ≤0.5 to 50 μg of protein. Analytical Biochemistry *86*, 142–146.

Steinhart, A.H., Hiruki, T., Brzezinski, A., and Baker, J.P. (1996). Treatment of left-sided ulcerative colitis with butyrate enemas: a controlled trial. Alimentary Pharmacology & Therapeutics *10*, 729–736.

Stoddart, L.A. (2007). Investigation of the function, pharmacology and oligomerisation of GPR40, GPR41 and GPR43. PhD Thesis (University of Glasgow)

Stoddart, L.A., Smith, N.J., Jenkins, L., Brown, A.J., and Milligan, G. (2008). Conserved polar residues in transmembrane domains V, VI, and VII of free fatty acid receptor 2 and free fatty acid receptor 3 are required for the binding and function of short chain fatty acids. Journal of Biological Chemistry *283*, 32913–32924.

Sutton, B.J., and Sohi, M.K. (1993). Crystallization of membrane proteins for X-ray analysis. Biomembrane Protocols *27*, 1–18.

Swaminath, G., Jaeckel, P., Guo, Q., Cardozo, M., Weiszmann, J., Lindberg, R., Wang, Y., Schwandner, R., and Li, Y. (2010). Allosteric rescuing of loss-of-function FFAR2 mutations. FEBS Letters *584*, 4208–4214.

Tanaka, M., Iio, T., and Tabata, T. (1987). Purification and characterization of a carboxylesterase from rabbit liver lysosomes. Journal of Biochemistry *101*, 619–624.

Tang, Y., Chen, Y., Jiang, H., Robbins, G.T., and Nie, D. (2011). G protein-coupled receptor for short-chain fatty acids suppresses colon cancer. International Journal of Cancer *128*, 847–856.

Taylor, I.L. (2008). Peptide YY: The Ileo-Colonic, Gastric, and Pancreatic Inhibitor. Biological Bulletin *177*, 187–191.

Tazoe, H., Otomo, Y., Karaki, S.-I., Kato, I., Fukami, Y., Terasaki, M., and Kuwahara, A. (2009). Expression of short-chain fatty acid receptor GPR41 in the human colon. Biomedical Research *30*, 149–156.

Thess, A., Hutschenreiter, S., Hofmann, M., Tampé, R., Baumeister, W., and Guckenberger, R. (2002). Specific orientation and two-dimensional crystallization of the proteasome at metal-chelating lipid interfaces. Journal of Biological Chemistry *277*, 36321–36328.

Tolhurst, G., Heffron, H., Lam, Y.S., Parker, H.E., Habib, A.M., Diakogiannaki, E., Cameron, J., Grosse, J., Reimann, F., and Gribble, F.M. (2011). Short-chain fatty acids stimulate glucagon-like peptide-1 secretion via the G protein-coupled receptor FFAR2. Diabetes *61*, 364–371.

Topping, D.L., and Clifton, P.M. (2001). Short-chain fatty acids and human colonic function: Roles of resistant starch and nonstarch polysaccharides. Physiological Reviews *81*, 1031–1064.

Triggiani, M., Petraroli, A., Loffredo, S., Frattini, A., Granata, F., Morabito, P., Staiano, R.I., Secondo, A., Annunziato, L., and Marone, G. (2007). Differentiation of monocytes into macrophages induces the upregulation of histamine H1 receptor. Journal of Allergy and Clinical Immunology *119*, 472–481.

US Food and Drug Administration (2011). Is it true FDA is approving fewer new drugs lately.

Venkata, R.P.R., Herman, G.P.S., Jenny, V., Rob, L., Huub, J.M.D., Remko, A.B., Willem, J.D., Ratnala, V.R.P., Swarts, H.G.P., VanOostrum, J., et al. (2004). Large-scale overproduction, functional purification and ligand affinities of the His-tagged human histamine H1 receptor. European Journal of Biochemistry *271*, 2636–2646.

Wacker, D., Fenalti, G., Brown, M.A., Katritch, V., Abagyan, R., Cherezov, V., and Stevens, R.C. (2010). Conserved binding mode of human beta2 adrenergic receptor inverse agonists and antagonist revealed by X-ray crystallography. Journal of the American Chemical Society *132*, 11443–11445.

Wallace, E., Dranow, D., Laible, P.D., Christensen, J., and Nollert, P. (2011). Monoolein lipid phases as incorporation and enrichment materials for membrane protein crystallization. PLoS ONE *6*, e24488

Wang, C.-J., Hsu, S.-H., Hung, W.-T., and Luo, C.-W. (2009). Establishment of a chimeric reporting system for the universal detection and high-throughput screening of G protein-coupled receptors. Biosensors and Bioelectronics *24*, 2298–2304.

Wang, D., Sun, X., Bohn, L.M., and Sadée, W. (2005). Opioid receptor homo- and heterodimerization in living cells by quantitative bioluminescence resonance energy transfer. Molecular Pharmacology *67*, 2173–2184.

Wang, X., Corin, K., Rich, C., and Zhang, S. (2011). Study of two G protein coupled receptor variants of human trace amine-associated receptor 5. Scientific Reports *1*. doi:10.1038/srep00102

Wang, Y., Jiao, X., Kayser, F., Liu, J., Wang, Z., Wanska, M., Greenberg, J., Weiszmann, J., Ge, H., Tian, H., et al. (2010). The first synthetic agonists of FFA2: Discovery and SAR of phenylacetamides as

allosteric modulators. Bioorganic & Medicinal Chemistry Letters *20*, 493–498.

Warne, T., Chirnside, J., and Schertler, G.F.X. (2003). Expression and purification of truncated, non-glycosylated turkey beta-adrenergic receptors for crystallization. Biochimica Et Biophysica Acta (BBA) - Biomembranes *1610*, 133–140.

Warne, T., Moukhametzianov, R., Baker, J.G., Nehmé, R., Edwards, P.C., Leslie, A.G.W., Schertler, G.F.X., and Tate, C.G. (2011). The structural basis for agonist and partial agonist action on a β(1)-adrenergic receptor. Nature *469*, 241–244.

Warne, T., Serrano-Vega, M.J., Baker, J.G., Moukhametzianov, R., Edwards, P.C., Henderson, R., Leslie, A.G.W., Tate, C.G., and Schertler, G.F.X. (2008). Structure of a beta1-adrenergic G protein-coupled receptor. Nature *454*, 486–491.

Wehmeyer, A., and Schulz, R. (1997). Overexpression of delta-opioid receptors in recombinant baculovirus-infected Trichoplusia ni "High 5" insect cells. Journal of Neurochemistry *68*, 1361–1371.

Wei, Q., Zhou, D.H., Shen, Q.X., Chen, J., Chen, L.W., Wang, T.L., Pei, G., and Chi, Z.Q. (2000). Human [mu]-opioid receptor overexpressed in Sf9 insect cells functionally coupled to endogenous Gi/o proteins. Cell Research *10*, 93–102.

Weiß, H.M., and Grisshammer, R. (2002). Purification and characterization of the human adenosine A2a receptor functionally expressed in Escherichia coli. European Journal of Biochemistry *269*, 82–92.

Wetterholm, A., Martinez Molina, D., Nordlund, P., Eshaghi, S., and Haeggström, J.Z. (2008). High-level expression, purification, and crystallization of recombinant rat leukotriene C(4) synthase from the yeast Pichia pastoris. Protein Expression and Purification *60*, 1–6.

White, J.F., Grodnitzky, J., Louis, J.M., Trinh, L.B., Shiloach, J., Gutierrez, J., Northup, J.K., and Grisshammer, R. (2007). Dimerization of the class A G protein-coupled neurotensin receptor NTS1 alters G protein interaction. Proceedings of the National Academy of Sciences of the United States of America *104*, 12199–12204.

Wickham, T.J., and Nemerow, G.R. (2002). Optimization of growth methods and recombinant protein production in BTI-Tn-5B1-4 insect cells using the baculovirus expression system. Biotechnology Progress *9*, 25–30.

Wieland, T., and Seifert, R. (2006). Methods and Principles in Medicinal Chemistry (Weinheim, FRG: Wiley-VCH Verlag GmbH & Co. KGaA).

Wiener, M.C. (2004). A pedestrian guide to membrane protein crystallization. Methods *34*, 364–372.

Williams, E.A., Coxhead, J.M., and Mathers, J.C. (2003). Anti-cancer effects of butyrate: use of micro-array technology to investigate mechanisms. Proceedings of the Nutrition Society *62*, 107–115.

Windh, R.T., and Manning, D.R. (2002). Analysis of G protein activation in Sf9 and mammalian cells by agonist-promoted [35S]GTP gamma S binding. Methods in Enzymology *344*, 3–14.

Wong, J.M.W., de Souza, R., Kendall, C.W.C., Emam, A., and Jenkins, D.J.A. (2006). Colonic health: Fermentation and short chain fatty acids. Journal of Clinical Gastroenterology *40*, 235–243.

Woodard, L.E., and Nimmagadda, S. (2011). CXCR4-based imaging agents. Journal of Nuclear Medicine : Official Publication, Society of Nuclear Medicine *52*, 1665–1669.

Wu, B., Chien, E.Y.T., Mol, C.D., Fenalti, G., Liu, W., Katritch, V., Abagyan, R., Brooun, A., Wells, P., Bi, F.C., et al. (2010). Structures of the CXCR4 chemokine GPCR with small-molecule and cyclic peptide

antagonists. Science *330*, 1066–1071.

Xiong, Y., Miyamoto, N., Shibata, K., Valasek, M.A., Motoike, T., Kedzierski, R.M., and Yanagisawa, M. (2004). Short-chain fatty acids stimulate leptin production in adipocytes through the G protein-coupled receptor GPR41. Proceedings of the National Academy of Sciences of the United States of America *101*, 1045–1050.

Yaghmur, A., Laggner, P., Zhang, S., and Rappolt, M. (2007). Tuning curvature and stability of monoolein bilayers by designer lipid-like peptide surfactants. PLoS ONE *2*, e479.

Yeagle, P. (1985). Cholesterol and the cell membrane. Biochimica Et Biophysica Acta (BBA) - Reviews on Biomembranes *822*, 267–287.

Zaibi, M.S., Stocker, C.J., O'Dowd, J., Davies, A., Bellahcene, M., Cawthorne, M.A., Brown, A.J.H., Smith, D.M., and Arch, J.R.S. (2010). Roles of GPR41 and GPR43 in leptin secretory responses of murine adipocytes to short chain fatty acids. FEBS Letters *584*, 2381–2386.

Zhou, J., Hegsted, M., McCutcheon, K.L., Keenan, M.J., Xi, X., Raggio, A.M., and Martin, R.J. (2006). Peptide YY and proglucagon mRNA expression patterns and regulation in the gut. Obesity *14*, 683–689.

Zvonok, N., Xu, W., Williams, J., Janero, D.R., Krishnan, S.C., and Makriyannis, A. (2010). Mass spectrometry-based GPCR proteomics: comprehensive characterization of the human cannabinoid 1 receptor. Journal of Proteome Research *9*, 1746–1753.